N70-28201
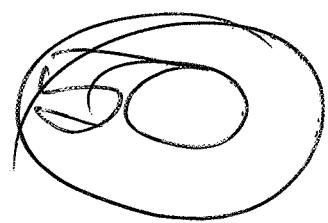
AD706292

EFFICIENT OPTICAL COMMUNICATION IN A TURBULENT ATMOSPHERE

Seppo J. Halme

TECHNICAL REPORT 474

APRIL 1, 1970

CASE FILE COPY

DDC
RECEIVED
JUN 2 1970
E

MASSACHUSETTS INSTITUTE OF TECHNOLOGY

RESEARCH LABORATORY OF ELECTRONICS

CAMBRIDGE, MASSACHUSETTS 02139

MASSACHUSETTS INSTITUTE OF TECHNOLOGY

RESEARCH LABORATORY OF ELECTRONICS

EFFICIENT OPTICAL COMMUNICATION IN A
TURBULENT ATMOSPHERE

Seppo J. Halme

Abstract

    Given a transmitter that radiates an electromagnetic light field, we assume that the resulting field at the plane of the receiver aperture is log-normal with some coherence properties. Various representations of the field are discussed: aperture sampling, plane-wave decomposition, and Karhunen-Loève expansion. The statistical properties of the coefficients in these representations are investigated by analytical, simulation, and experimental methods. Based on these representations the problem of optimum detection of an orthogonal signal set, subject to distortion and noise in the atmosphere, is investigated. The optimum receiver and its performance are evaluated and discussed in the cases of log-normal and Gaussian statistics, classical and quantum models, large and small apertures, and strong, weak or absent background noise.

TABLE OF CONTENTS

CONTENTS

CONTENTS

v

I. INTRODUCTION

1.1 STATEMENT OF THE PROBLEM

A laser produces light with spatial and temporal coherence comparable to that of ordinary radio waves. The short wavelength of optical and infrared radiation makes enormous antenna gains possible even with physically small apertures. Even narrow-band optical signals (for example, 1% bandwidth) are capable of carrying thousands of times more information than microwave radio signals. On the other hand, rain, snow, fog or haze may virtually stop the terrestrial optical communication link from functioning for a period of time. Moreover, the best and most common coherent radio reception method, heterodyning, is very difficult to use. Heterodyning is impaired by spatial incoherence caused by atmospheric turbulence. Thermal background noise may often be a problem, while quantum noise is very significant.

The advent of the laser and communication at optical frequencies was greeted initially with great enthusiasm and high hopes. Soon it was realized that many obstacles had to be overcome before optical communication could even compete with other communication techniques in use, such as microwaves and coaxial cables. Serious doubts arose about the usefulness of optical communication for any application except a very special one such as deep-space communication. All the same, it is certainly worth while to investigate the fundamental limitations of optical communication that are independent of the present state of technology. For the Gaussian fading dispersive radio channels discussed by Kennedy,[1] it has been shown that with proper signals and reception techniques the incoherence attributable to Doppler spread or time spread does not reduce the channel capacity. A very complicated receiver is required, though, to realize the full potential of the channel. Similar results can be shown to be true for optical channels.

This work finds the optimum receivers for log-normal fields in spatially and temporally white Gaussian background noise and evaluates their performance. Because we have tried to use a quite realistic model for the field, we present some features that are not commonly considered in papers on detection theory as it is known today. First, the problem deals with detection of a field in two spatial dimensions and time, instead of a stochastic process varying in time only. Second, signal fading is not Gaussian but log-normal. Third, the field has to be quantized in optical frequencies in order to get complete results. It turns out that it has not been possible to solve the problem completely. In some cases the optimum receiver seems complex to construct, and may be critical to detailed information of the field statistics. In any case, the work gives very valuable insight into the ways that optimum receivers combat background noise, quantum noise, and incoherence of the field. This is very helpful in furnishing guidelines for the design of suboptimum receivers. The performance estimates developed here serve as yardsticks that help evaluate whether and how much the performance of a given receiver

1

may still be improved.

1.2 REVIEW OF MODELS AND DETECTION OF FIELDS

Before optimum receivers can be considered a model for the optical channel is needed. The propagation of electromagnetic waves through a turbulent atmosphere has been analyzed by Tatarski[2] and his colleagues in the Institute of Atmospheric Physics of the Academy of Sciences of U.S.S.R. Their basic results use the similarity theory of turbulence created by Kolmogorov. The solution is found by using the Rytov approximation, which is also called the "method of smooth perturbations." The applicability of the perturbation technique has created a wide controversy. The theory has been extended to consider more terms of the perturbation expansion by Tatarski[3] and de Wolf.[4] There is a wealth of experimental evidence to support these results, but some results obtained by Gehrels,[5] and by Gurvich, Kallistratova, and Time[6] do not completely agree with the theory of Tatarski, even in its present form. Hence it seems that the theory is by no means complete, and a major part of the work may yet remain to be done. This report is based on the present theories (cf. Tatarski,[2] Chernov,[7] Hufnagel and Stanley,[8] Fried,[9] Beckmann,[10] Hoversten,[11] and Strohbehn[12]). The logarithm of the complex field excitation is found to be a locally homogeneous Gaussian field. The field changes rather slowly, its correlation time is more than 1 ms. The channel can be considered to be singly spread with flat fading. Because of the difficulties in working with this signal field model and because the noise is Gaussian, a normal (Gaussian) signal field model is also used in this work. These classical models have to be quantized to obtain a complete picture of the electromagnetic field with its particle and wave aspects. The quantum theory leans heavily on the results on coherence developed by Glauber,[13] and Mandel and Wolf.[14] It turns out that there is a very close correspondence between the classical and quantum pictures of stochastic fields. The solution of the classical problem in many cases is also correct quantum mechanically.

Figure 1 shows the general procedure for obtaining the optimum receiver for a field created by one of M possible signals. The likelihood functionals $l_1, \ldots, l_M$ are found from the probability density of the field. For this purpose, the field is usually represented by an infinite vector, whose joint probability density is then written. (Of course, the probability density has to exist. In general, the likelihood ratios and functionals are defined by an analogous procedure in terms of Radon-Nikodym derivatives.)

The most popular representations are the sampling expansion, the Fourier-series expansion, which in this case is called the "plane-wave representation," and the Karhunen-Loève expansion, which has uncorrelated coefficients. For a log-normal field the probability density can be written easily only for the sampling representation. The optimum receiver performance does not depend on the representation chosen, but the obvious interpretation of the optimum receiver structure is related to the representation. For example, samples of the field in the aperture can be found by using an array of
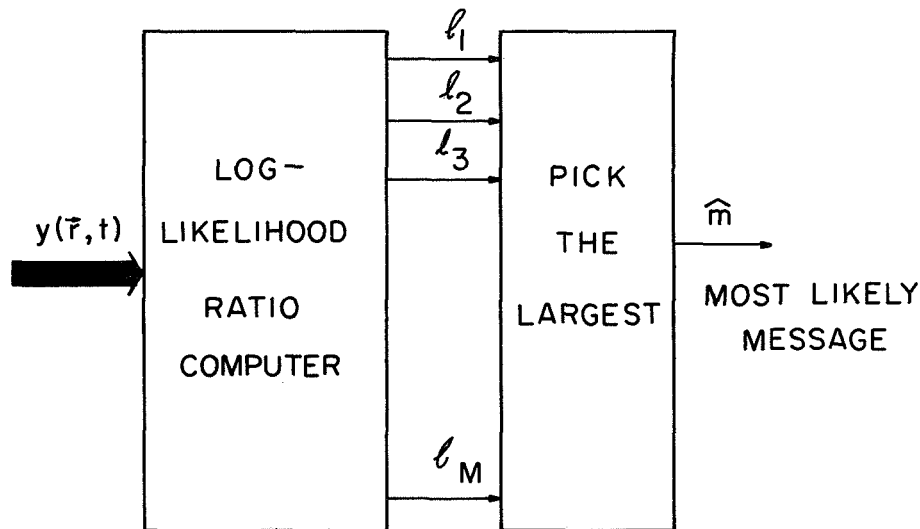
Fig. 1. The optimum receiver for field $y(\vec{r}, t)$, under the assumption of equally likely messages, computes the log-likelihood ratio for each message $m = 1, \ldots, M$, and then picks the largest of them.

sensors in the aperture plane, while the plane-wave coefficients can be found by using the same sensors in the focal plane. The appropriate scaling of sizes is assumed. Hence it would be desirable to know the field probability density for the plane-wave representation, too. In this representation, however, even the moments of the coefficients are difficult to evaluate, not to mention the complete joint probability density. Some results on the moments were evaluated by Chernov.[7]

For large apertures it was felt by Tatarski that the Central Limit theorem should hold, although no explicit statement was made. The Central Limit theorem for stochastic processes or dependent time series seems to be a fairly recent development. Rosenblatt[15] proved it by assuming the condition of strong mixing. After that more complete results have been published, for example, by Volkonski and Rozanov.[16a] These results should be extended in terms of the known properties of log-normal fields.

Little is known about the general properties of the Karhunen-Loève coefficients for log-normal fields. In fact, the usefulness of this expansion is greatly reduced because the eigenfunctions and eigenvalues are very difficult to solve for in general. Also, the coefficients may still be highly dependent although uncorrelated.

We are concerned with detecting a field in two dimensions, in particular when the field is log-normal and quantized. Some work that is related to these aspects of detection theory has been done. The optimum receiver for a classical Gaussian field is obtained in the same way as for Gaussian processes. The well-known results of Price[16b] and Kennedy[1] can be used. Many results have been obtained in connection with sonar and seismometric applications (Gaarder,[17] Schweppe,[18] Capon[19]) and with optical applications (Harger,[20] Kennedy[21]). The classical log-normal model is much harder to analyze. Assuming independent

samples and an orthogonal signal set (short signals) in white Gaussian background noise, Kennedy and Hoversten[22] have found the channel capacity and the zero-rate error exponent. The radar detection case with log-normal fading has been considered by Heidbreder and Mitchell,[23] and by Fried and Schmeltzer[24] in the case of one sensor and assuming a suboptimum receiver structure. The quantum detection theory was formulated by Helstrom[25] and extended by Jane W. S. Liu.[26] Among other things, Helstrom considers the threshold detection of Gaussian signals in Gaussian noise. Liu investigates optimum receivers and their performance for Gaussian signals in Gaussian noise in general, and in the optimal case when all eigenvalues are equal.

Much work has been done in constructing and evaluating the performance of various optical receivers based on direct detection, local heterodyning, or transmitted reference systems by such workers as Goldstein, Miles, and Chabot,[27] Miller and Tillotson,[28] Ross,[29] Cooper,[30] Kerr,[31] Brookner, Kolker, and Wilmotte,[32] and Denton and Kinsel.[33] Direct detection is a simple and convenient method, but requires a subcarrier or pulsing for modulation. Background noise can be limited only by using optical interference filters, which are usually sensitive to the angle of arrival of the wavefront. When local heterodyning is used, it does not pay to increase the aperture area beyond the coherence area of the incident radiation. The diameter of this area ranges from a fraction of a centimeter to a few centimeters. On the other hand, a large mixing gain and a wide selection of modulation methods are available and additional background filtering can be done in electronic circuits. In the transmitted reference systems much of the transmitted power is consumed by the reference, but the heterodyning area is unlimited.

1.3 OUTLINE OF THE REPORT

In Section II we begin with a discussion of available results on the statistical properties of a plane wave that has propagated in a turbulent atmosphere. The amplitude and phase distributions, the correlation properties and the limitations of the model are considered. The time dependence is modelled by postulating "frozen atmosphere" blown by crosswind. The Doppler spread and the time spread of the log-normal channel are discussed.

We start with classical electromagnetics, and then introduce the quantization procedure, mode decomposition, and density operators in either P-representation or number representation. The relationship between the representations and the correlation properties of the field are considered, and the background noise present in optical propagation in a turbulent atmosphere is introduced. The effects of particle scattering are not discussed in this work.

Section III is devoted to a discussion of the representations of the field. We introduce the sampling representation and the plane-wave representation, and general orthogonal representations of the field. The probability density of the log-normal field in sampling representation and its moments are discussed. The properties of the

plane-wave coefficients, and the coefficients of any orthogonal representation, are discussed, with special emphasis on either very large or very small apertures. For large apertures the Central Limit theorem is shown to hold for the plane-wave coefficients, except for some very special cases. The conditions for the Central Limit theorem to hold are also discussed.

To confirm the results that have been obtained and probe further the behavior of the plane-wave coefficients, simulations and measurements of the channel were undertaken. The simulations of sums of real and complex independent log-normal variables with random numbers are discussed. The resulting amplitude distributions are tested against the relevant distributions, log-normal, normal or Rayleigh. The phase distribution is also computed. The independence of uncorrelated plane-wave coefficients is also examined. The measurements of the intensity distribution of focal-plane samples are discussed.

Section IV is concerned with the structure and performance of an optimum receiver for reception in a turbulent atmosphere. The classical field detection problem for Gaussian fields is solved; this is a straightforward application of the procedures used for processes. The optimum receiver can be realized in several ways, for instance, by using a diversity structure. The spatial and temporal filtering required to combat background noise are discussed for signals that are very short or very long in comparison with field correlation time. The receiver performance is evaluated by using bounding techniques.

The detection of a log-normal field in background noise is analyzed. The general case is very difficult to carry through, but the extremes of very strong or very weak noise are considered in detail. The structure and the performance are again evaluated.

The quantum formulation of the detection problem is introduced. Both the Gaussian and log-normal fields are considered in quantum terms, optimum receivers and their performance are discussed in some cases, and the relationship to the classical limit is examined.

Section V summarizes the results of this research. The implications for receiver design are pointed out. Suggestions for further research are made.

5

II. MODELS FOR THE ELECTROMAGNETIC FIELD IN THE APERTURE

2.1 STATISTICAL PROPERTIES OF A PLANE WAVE PROPAGATING THROUGH A TURBULENT ATMOSPHERE

2.1.1 Amplitude and Phase Distributions

Using Kolmogorov's similarity theory of turbulence, Tatarski[2] has derived the statistical properties of a plane wave that has propagated through a turbulent atmosphere. Using Rytov's approximation, he shows that the perturbation of the logarithm of the normalized scalar complex excitation of the field has the following solution:

$$\gamma_1(\vec{r}) = \log u(\vec{r}) = \chi_1 + i\theta_1 = \frac{k^2}{2\pi u_o(\vec{r})} \iiint_V n_1(\vec{r}') u_o(\vec{r}') \frac{e^{ik\cdot|\vec{r}-\vec{r}'|}}{|\vec{r}-\vec{r}'|} d^3\vec{r}', \tag{1}$$

where $u_o(\vec{r})$ is the excitation of the field in the initial plane, V is the volume between the initial and final planes, $n(\vec{r}) = 1 + n_1(\vec{r})$ is the index of refraction of the air, and $k = 2\pi/\lambda$, the wave-number vector. Here $d^3\vec{r}'$ is the three-dimensional volume element, χ is the log-amplitude (the logarithm of the amplitude), and θ the phase of the field. The important feature of this solution is its linearity. In many cases the distance between the initial and final planes is large enough so that the integral comprises many statistically independent contributions of the same order of magnitude. In this case the Central Limit theorem applies, so that the real and imaginary parts of the log excitation γ_1 are asymptotically normal. Hence we are justified in assuming that the excitation $u(\vec{r}) = u_o(\vec{r}) \cdot \exp \gamma_1(\vec{r})$ is log-normal.

Log-normality can be demonstrated by use of the following simple model. Divide the volume between the initial and the final planes into small slices with planes that are parallel to the initial and final planes. On the path of propagation from plane n to plane $n+1$ the charge of excitation is obviously proportional to the current value of the field:

$$u = u_{n+1} - u_n = u_n a_n. \tag{2}$$

The increment a_n is postulated to be independent of u_n and of any other increments. The following approximate result follows (Cramér[34]) for any finite subdivision of the path of propagation:

$$a_1 + a_2 + \ldots + a_N = \int_1^N \frac{du}{u} = \ln u_N - \ln u_1. \tag{3}$$

But the distribution of this sum approaches the normal distribution by the Central Limit theorem. Hence u_N becomes log-normal.

The log-normality of the field in the receiving plane is partly an unresolved issue. The Rytov approximation breaks down for large propagation distances and/or strong turbulence. Measurements reported by Tatarski,[2] Gracheva,[35] and Fried, Mevers, and Keister[36] agree with the log-normal hypothesis. The measurements of Höhn,[37] Gurvich, Kallistratova, and Time,[6] and Gehrels[5] have shown agreement with the log-normal distribution in some cases, while for large turbulence the results differ somewhat from log-normal on both tails of the distribution. Gehrels pointed out apparent agreement with the Rayleigh distribution for the lower tail, presumably because of noise, while the upper tail is closer to the log-normal distribution. Gurvich, et al. deny agreement with Rayleigh distribution, but do not elaborate for partial agreement. By plotting Gurvich's and Gehrels' results in the same graph, it was found that their agreement is very good. Because the log-normal model is the best available, and very accurate in most cases, it is used through much of this work.

The general properties of the log-normal distribution have been thoroughly discussed in the real case by Aitchison and Brown.[38] Much less is known about the complex log-normal variable. Because of the normality of the logarithm of the field it is sufficient to characterize it by its mean and by its 2×2 covariance matrix.

The mean of the log-amplitude, together with its variance, determines the average intensity of the field. The excitation will be divided into a constant part and a variable part as follows:

$$u(\vec{r}) = Z z(\vec{r}). \tag{4}$$

The dimension of u and Z are taken to be $W^{1/2} m^{-1}$, while z is dimensionless. The field is assumed to be homogeneous within the aperture area. The probability density of z then has the following form for every point $\vec{r}$ of the aperture (in polar coordinates $z = |z| e^{i\theta}$)

$$p(z) = p(|z|, \theta) = \frac{1}{(2\pi)^{3/2} \sigma |z|} \exp\left[- \frac{(\ln |z| - \mu)^2}{2\sigma^2} \right]. \tag{5}$$

Here μ is the mean of $\log |z|$, while σ^2 is the variance of $\log |z|$. The average intensity of any aperture point becomes

$$I(\vec{r}) = \overline{|u(\vec{r})|^2} = Z^2 e^{2(\mu + \sigma^2)}. \tag{6}$$

This relationship makes it possible to normalize the randomly varying part of $u(\vec{r})$, $z(\vec{r})$, so that $\mu = -\sigma^2$. Hence $\overline{|z(\vec{r})|^2} = 1$. The virtue of this or any other normalization of the log-normal variable (such as $\mu = 0$) is to reduce the number of parameters in the part of the problem where difficult integrals often have to be evaluated and tabulated.

The variance of log-amplitude is clearly zero or very close to it for short path lengths L. Then following Tatarski,[39] we have

$$\sigma^2 = 0.31 \, C_n^2 k^{7/6} L^{11/6}, \qquad (\sqrt{\lambda L} \gg \ell_o), \tag{7}$$

where C_n^2 is the structure constant of the refraction index, typically of the order of 10^{-14}-10^{-15} m$^{-2/3}$, and ℓ_o is the inner scale of turbulence (cf. Tatarski[1]), where the viscous dissipation starts, typically of the order of 1-10 mm. The condition stated along (7) means physically that the beamwidth of the scattering cone contains many inhomogeneous blobs or eddies of turbulence in its cross section. This cone contains all of the space that contributes to the energy caught by the receiver aperture.

It has been found both theoretically (Tatarski,[13] de Wolf[4]) and experimentally (Gracheva,[35] Gurvich, Kallistratova, and Time[6]) that the Rytov approximation used to derive (7) breaks down for long paths. Actually the variance saturates at a value less than unity. In terms of standard deviations we have $0.5 < \sigma_{max} < 0.9$. The saturation begins gradually when the result calculated from (7) exceeds 0.5.

2.1.2 Spatial Coherence

Having propagated in the atmosphere, the field is no longer spatially coherent. The log-amplitude covariance function has also been determined by Tatarski[40]:

$$K_\chi(\rho) = 1.30 \, C_n^2 k^2 L \int_0^{\kappa_m} J_0(\kappa\rho) \left[1 - \frac{k}{\kappa^2 L} \sin \frac{\kappa^2 L}{k} \right] \kappa^{-8/3} \, d\kappa. \tag{8}$$

Here $\kappa_m = 5.92/\ell_o$ is the spatial frequency cutoff of the wave-number spectrum of the refraction index field, $k = 2\pi/\lambda$, and κ refers to the transversal component of the propagation vector $\vec{k}$. A good idea of this covariance function is obtained from Strohbehn.[41] The first zero of the covariance function occurs at $\rho = 0.72 \sqrt{\lambda L}$ for $\lambda = 0.6$ µm, $\ell_o = 1, \ldots, 10$ mm, $L = 100$ m $- 10$ km. The form of this covariance function seems to agree reasonably well with results reported by Gracheva,[35] Gurvich et al.,[6] and Deitz.[42]

The phase covariance function is given by Strohbehn[12]:

$$K_\theta(\rho) = 1.30 \, a C_n^2 k^2 L \int_0^\infty \left[1 + \frac{k}{\kappa^2 L} \sin \frac{\kappa^2 L}{k} \right] J_0(\kappa\rho) \frac{e^{-\kappa^2/\kappa_m^2}}{\left(1 + \kappa^2 L_o^2\right)^{11/6}} \, d\kappa, \tag{9}$$

where a is a constant that is about $L_o^{11/3}$, with some numerical factors close to unity neglected. This form keeps the phase variance finite. The correlation goes to zero at distances $\rho \gg L_o$, the outer scale of turbulence.

The wave-number power spectrum used by Tatarski leads to infinite phase variance. Because the phase variance is quite large compared with 1 in any actual measurements, the phase covariance function (9) is not necessarily the most interesting function describing correlation properties of the field. Instead the phase-structure function is commonly used:

$$D_\theta(\vec{\rho}) = \overline{|\theta(\vec{r}+\vec{\rho})-\theta(\vec{r})|^2} \cong 1.72\ C_n^2 l_o^{-1/3} k^2 L \rho^2, \qquad \rho \ll \ell_o$$

$$\approx 1.46\ k^2 L C_n^2 \rho^{5/3}, \qquad l_o \ll \rho \ll \sqrt{\lambda L} \tag{10}$$

$$\approx 2.91\ k^2 L C_n^2 \rho^{5/3}, \qquad \rho \gtrsim \sqrt{\lambda L}.$$

This result has been given by Tatarski.[43] The phase structure function is also a growing function of the path length L. According to Tatarski,[3] for large L or heavy turbulence the structure function of the phase saturates and ceases to grow as a function of L.

Very few measurements have been made on the phase structure function of the optical field. In this laboratory Moldon[44] measured phase-structure functions. He obtained results showing that the phase variance seems to be surprisingly low, of the order of 100 rad^2. The path length was 4.5 km.

The field can be said to be locally coherent up to a certain distance, if the phase (or amplitude) fluctuations are highly correlated within it. The measure of coherence used in this work is the coherence distance r_c or coherence radius, which is defined as the distance for which $D_\theta(r_c) = 1$. This coherence radius r_c is related to Fried's r_o through $r_o = 3.18\ r_c$ (Fried and Cloud[45]). As pointed out above, the amplitude is not coherent either. The correlation distance of log-amplitude is of the order of $\sqrt{\lambda L}$. Usually this is several times larger than the phase correlation distance.

The phase coherence distance was defined as an ensemble average. Next an example of a nonergodic field is considered, which gives a particularly simple form of phase-structure function. (This example will be referred to in section 3.4.) Assume an ensemble of pure plane waves with wave-number vectors $\vec{k} = \vec{e} + \vec{\kappa}$. Here $\vec{e}$ is the component of $\vec{k}$ perpendicular to the aperture plane while $\vec{\kappa}$ is the component parallel to this lane. Then the structure function for phase is readily evaluated.

$$D_\theta(\vec{r}_1-\vec{r}_2) = \overline{(\theta_1-\theta_2)^2} = \overline{(\vec{k}\cdot(\vec{r}_1-\vec{r}_2))^2} = \overline{|\vec{\kappa}|^2\ |\vec{r}_1-\vec{r}_2|^2\ \cos\phi_{12}}$$

$$= C_{12}|\vec{r}_1-\vec{r}_2|^2, \tag{11}$$

where ϕ_{12} is the angle between $\vec{\kappa}$ and $(\vec{r}_1-\vec{r}_2)$, and $C_{12} = \overline{|\vec{\kappa}|^2 \cos^2\phi_{12}}$. For an isotropic field C_{12} obviously does not depend on the orientation of $\vec{r}_1 - \vec{r}_2$. In this case the form of structure function agrees with that on the first line of (11). The spatial average of a plane wave obviously need not agree with (11). Hence the field is non-ergodic.

The log-amplitude and phase are not completely independent. The cross spectrum of the log-amplitude and the phase has been evaluated by Tatarski (cf. Strohbehn[46]). It is easy to get a bound for the crosscorrelation coefficient by using that expression

9

$$|\overline{\chi\theta}| < 0.23 \; C_n^2 k^{7/6} L^{11/6}, \qquad (\sqrt{\lambda L} \gg \ell_o). \tag{12}$$

By comparing this with (7) it becomes obvious that the dependencies between log-amplitude and phase may be quite significant.

2.1.3 Behavior of the Field in Time

The time behavior of the field, its fading, is obtained to first approximation by assuming that the "frozen atmosphere" is blown across the aperture (Tatarski[2]). The temporal and spatial covariances are connected through normal wind velocity as follows:

$$R(\tau) \approx K(v_n \tau). \tag{13}$$

The spectral behavior of intensity is also of interest. The spectral density has been evaluated by Tatarski.[2] These results have been extensively checked experimentally by measurements reported by Tatarski,[2] Gracheva,[35] Gurvich et al.,[6] Ehrenberg,[47] and Gehrels.[5] The results do not agree in detail with Tatarski's theory, but are still quite close. The spectral density has a maximum on or somewhat below the frequency $f_{max} = v_n/\sqrt{\lambda L}$, as predicted by the theory.

The theory of aperture field statistics outlined above for plane-wave propagation has also been extended to the case of spherical waves (Tatarski[2]) and beam propagation (Kon and Tatarski,[48] Fried and Seidman[49]). When the aperture size is much smaller than the beam size, the plane-wave model can be used with success. If the initial beamwidth is much smaller than the diffraction width $\lambda L/\ell_o$ caused by the turbulent blobs, most of the diffracted or rather scattered energy from the beam will not contribute to fluctuations in the point of observation. The phase structure function now depends logarithmically, not linearly, on L, the path length.

Another way of looking at the fading is to say that there is a random Doppler shift involved, which depends on the motion of the scattering inhomogeneities relative to the receiver. For small scattering angles, the Doppler shift is given by

$$\Delta f = \frac{f_o}{c} \vec{v}_n \cdot \frac{\vec{\kappa}}{k} = \frac{1}{2\pi} \vec{v}_n \cdot \vec{\kappa}, \tag{14}$$

where $\vec{v}_n$ is the normal component of the wind velocity with respect to the path, and $\vec{\kappa}$ is the component of the propagation vector on the aperture plane. Roughly speaking, $\sqrt{\overline{\phi^2}} = \lambda/(2\pi r_c) = 10 \; \mu\text{rad}$ for $\lambda = 0.63 \; \mu\text{m}$, $r_c = 1$ cm. Hence $\sqrt{\overline{\Delta f^2}} = 16$ Hz for $v_n = 1$ m/s. The atmosphere causes a Doppler shift, which is around the frequency for which the spectral density of the fluctuations has its maximum, f_{max}. The size of the Doppler spread ranges between 10 Hz and 1000 Hz. For higher spatial frequencies the Doppler spread is obviously higher.

The turbulent atmosphere causes also some multipath effect, in other words, time spread. The amount of time spread is closely related to phase fluctuations, as $\theta = \omega t$,

where the angular frequency ω is assumed to be constant. Hence the amount of time spread is

$$L = \text{time spread} = \sqrt{D_\theta(\rho_{max})/\omega_o} \tag{15}$$

for just one coherent radius, and $\lambda = 0.63$ m, $L = 0.3 \cdot 10^{-15}$ s. For large apertures the time spread can increase to almost a picosecond (Brookner[50]), which can be quite significant in future applications. This conjecture has not yet been tested experimentally. For most applications, though, the turbulent atmospheric channel can be considered as a singly spread channel, with flat fading.

2.2 QUANTUM DESCRIPTION OF A PARTIALLY COHERENT FIELD

We shall discuss the quantization procedure briefly. Random fields will be modelled by using mixtures of coherent fields, weighted in a proper manner. The density operators describing these fields will be introduced and several examples given, when there is only one mode involved. This will be generalized to the case of fields with an arbitrary number of modes. For these fields the connection between density operators and covariance functions or wave-number spectra is indicated.

2.2.1 Quantization of the Electromagnetic Field

In quantum theory the electromagnetic field is described by using Hamiltonian formulation and postulating commutation relations between the operators that describe physical observables (for example, Louisell[51]). It is convenient to use the artifice of enclosing the observed field within a large resonator of volume V, so that the signal can be expanded in terms of its modes. Because the signal duration is limited, the field as a function of time can be expressed as a Fourier series in time and space. Consequently the field can be pictured as an ensemble of harmonic oscillators excited by the signal transmitted. The quantization is effected on each of these oscillators.

The electromagnetic field (in Coulomb gauge) can be expressed by using the vector potential (Louisell[51]):

$$\vec{A}(\vec{r}, t) = \sum_{\underline{m}} \sqrt{\frac{\hbar}{2\omega_{\underline{m}} \epsilon_o V}} \; \vec{e}_{\underline{m}} \left(a_{\underline{m}} e^{i(\vec{k}_{\underline{m}} \cdot \vec{r} - \omega_{\underline{m}} t)} + a_{\underline{m}}^{+} e^{-i(\vec{k}_{\underline{m}} \cdot \vec{r} - \omega_{\underline{m}} t)} \right), \tag{16}$$

where $\hbar = h/2\pi$, h is Planck's constant, and $\vec{k}_{\underline{m}}$ is the propagation or wave-number vector corresponding to the vector index $\underline{m} = (m_1, m_2, m_3, \delta)$. The integers m_1, m_2, and m_3 refer to the orientation of the vector $\vec{k}_{\underline{m}} = (2\pi m_1/L_1, 2\pi m_2/L_2, 2\pi m_3/L_3)$. L_1, L_2, and L_3 are the sides of the rectangular cavity. The fourth index δ, being either 0 or 1, refers to the polarization of the particular mode. The coordinate system has been selected so that the z axis agrees with the general direction of propagation of the electromagnetic field. The unit vector $\vec{e}_{\underline{m}}$ is perpendicular to $\vec{k}_{\underline{m}}$, and its polarization

11

can be either 0 or 1. These two polarizations are taken to be orthogonal. The frequency of oscillation $\omega_{\underline{m}}$ is connected to the propagation vector $\vec{k}_{\underline{m}}$ by the relation $k_{\underline{m}} = \omega_{\underline{m}} c^{-1}$, where c is the velocity of light. ϵ_o is the dielectric constant of vacuum. $V = L_1 L_2 L_3$ is the volume of the cavity. If the signal duration is T, there is an integer n such that $\omega_{\underline{m}} = 2\pi n/T$. By taking $L_3 = cT$, the whole signal fits into the cavity, and obviously some of the natural frequencies of the cavity agree with discrete frequencies used to describe the signal. Finally, the coefficients $a_{\underline{m}}$ and $a_{\underline{m}}^+ = a_{\underline{m}}^*$ give the amplitude of the particular mode $\underline{m}$, which is a complex number in general.

The field is quantized by introducing the following commutation rules into the coefficients $a_{\underline{m}}$ and $a_{\underline{m}}^+$, now called "operators."

$$\left[a_{\underline{m}}, a_{\underline{m}'}^+ \right] = \delta_{\underline{mm}'}$$

$$\left[a_{\underline{m}}^+, a_{\underline{m}'}^+ \right] = [a_{\underline{m}}, a_{\underline{m}'}] = 0. \tag{17}$$

Here $\delta_{\underline{mm}'} = 1$, for $\underline{m} = \underline{m}'$, and 0 otherwise. The bracket symbolizes the commutator operation $[x, y] = xy - yx$, where x and y are operators. By using the quantization relations, the Hamiltonian of the electromagnetic field will be simplified as follows (Louisell[52]):

$$H = \frac{1}{2} \iiint\limits_V \left[\epsilon_o \left[\frac{\partial \vec{A}}{\partial t} \right]^2 + \frac{1}{\mu_o} (\vec{\nabla} \times \vec{A})^2 \right] d^3\vec{r}$$

$$= \sum_{\underline{m}} \left[a_{\underline{m}}^+ a_{\underline{m}} + \frac{1}{2} \right] \hbar \omega_{\underline{m}}. \tag{18}$$

For operators the symbol plus in a^+ means the adjoint operator of the operator a. The operators for which the adjoint operator is the same as the original operator are called Hermitian.

Physically, operators, particularly Hermitian operators, stand for measurements made on the quantum-mechanical system. The system is in some state, usually unknown. The measurement changes the state of the system to an eigenstate of the measurement operator, while the result of the measurement is the eigenvalue corresponding to that state. Left by itself the state of the system evolves according to the equations of motion of the system.

A very important example of an operator is the "number" operator $N_{\underline{m}} = a_{\underline{m}}^+ a_{\underline{m}}$. It corresponds to the measurement of the number of photons in the given mode. The state vectors of kets corresponding to an eigenstate are denoted $|n_{\underline{m}}\rangle$. The eigenvalues of $N_{\underline{m}}$ are integers denoted by $|n_{\underline{m}}\rangle$.

$$N_{\underline{m}} \left| n_{\underline{m}} \right\rangle = n_{\underline{m}} \left| n_{\underline{m}} \right\rangle. \tag{19}$$

The result of the measurement corresponding to the number operator when the system is in the state of $n_{\underline{m}}$ photons is just $n_{\underline{m}}$. The Hamiltonian operator (18) obviously represents the energy in the system. The operators $a_{\underline{m}}$ and $a_{\underline{m}}^+$ are called the annihilation and creation operators of the mth mode. The names become obvious by application of these operators on the number operator eigenstates:

$$a_{\underline{m}} \left| n_{\underline{m}} \right\rangle = \sqrt{n_{\underline{m}}} \left| n_{\underline{m}}-1 \right\rangle, \qquad a_m \left| 0 \right\rangle = 0$$

$$a_{\underline{m}}^+ \left| n_{\underline{m}} \right\rangle = \sqrt{n_{\underline{m}}+1} \left| n_{\underline{m}}+1 \right\rangle. \tag{20}$$

The operator $a_{\underline{m}}$ reduces the number of photons in the mode $\underline{m}$ by one, while $a_{\underline{m}}^+$ adds another photon. These operators are related to the complex classical envelope of the mode, and also to absorption and emission of photons. $\left| 0 \right\rangle$ is the "vacuum" state.

Another important operator is the electric field strength (Louisell[51])

$$\vec{E}(\vec{r}, t) = \vec{E}^{(+)}(\vec{r}, t) + \vec{E}^{(-)}(\vec{r}, t), \vec{E}^{(-)}(\vec{r}, t) = \left[\vec{E}^{(+)}(\vec{r}, t) \right]^+$$

$$\vec{E}^{(+)}(\vec{r}, t) = i \sum_{\underline{m}} \sqrt{\frac{\hbar \omega_{\underline{m}}}{2 \epsilon_o V}} \, a_{\underline{m}} \vec{e}_{\underline{m}} \, e^{i(\vec{k}_{\underline{m}} \cdot \vec{r} - \omega_{\underline{m}} t)}. \tag{21}$$

The operator $a_{\underline{m}}$ also has an eigenstate $\left| a_{\underline{m}} \right\rangle$

$$a_{\underline{m}} \left| a_{\underline{m}} \right\rangle = a_{\underline{m}} \left| a_{\underline{m}} \right\rangle. \tag{22}$$

It can be shown (Louisell[51]) that the field driven by a classical sinusoidal source (one that is not reacted upon by the field generated by it), originally in the vacuum state, will end up in the annihilator operator eigenstate $\left\{ \left| a_{\underline{m}} \right\rangle \right\}$, where the wave bracket denotes the direct product of all of the mode states $\left| a_{\underline{m}} \right\rangle$. This state $\left| a_{\underline{m}} \right\rangle$ is called a "coherent" state. The eigenvalue corresponding to the final coherent state is proportional to the amplitude of the driving source. The coherent states, together with the number operator eigenstates, will be used in the following work. The theory of coherent states and their representations has been developed by Glauber.[53]

2.2.2 Density Operators

When the radiation propagates through a slowly varying random medium, the field at the receiving aperture can be modelled by saying that it is driven by a classical source, which stays constant within the short interval of observation, but its amplitude and phase, as well as its optical coherence properties, are unknown in advance. Only its statistical properties are assumed to be known. This kind of situation is usually

described as a mixture of pure states, each of which occurs with a given probability. To represent this kind of mixture of states, density operators are commonly used. Two representations will be used for density operators. According to Glauber[53] most radiation fields that occur in optics can be represented as a mixture of coherent states. This is called the "P-representation":

$$\rho = \iint P(\beta) |\beta\rangle\langle\beta| \, d^2\beta, \tag{23}$$

where ρ is the density operator, $P(\rho)$ a function analogous to probability on the complex plane of values of β, and $d^2\beta$ is the area element in this complex plane. For the problems of interest here the function $P(\beta)$ is real-valued and positive definite in some sense. Also, its trace is unity. In general, it may have negative values. In certain cases the density operator will be diagonal in the number representation:

$$\rho = \sum_{n=0}^{\infty} r(n) |n\rangle\langle n|. \tag{24}$$

For a general density operator the representations will be much more complex than those of (23) or (24) (Glauber,[53] Landau, Lifshitz[54]).

Table 1 shows several important density operators in operator form, P-representation, and when applicable in diagonal number representation. For derivations we refer to Glauber,[53] Louisell,[51] and Lachs.[55]

The density operator of the field describes a mixture of the states of the field, which in turn are direct products of the states of the individual modes. The P-representation in this case would be

$$\rho = \iint \cdots \int P(\{\beta_{\underline{m}}\}) \prod_{\underline{m}} |\beta_{\underline{m}}\rangle\langle\beta_{\underline{m}}| \, d^2\beta_{\underline{m}}. \tag{25}$$

The weight function $P(\{\beta_{\underline{m}}\})$ factors out into a product of the individual mode weight functions if the modes are statistically independent. If the field is Gaussian with a correlation matrix $\underline{K}$, the elements of which are

$$k_{\underline{mm}'} = \text{Tr}\left(\rho a_m^+ a_{m'}\right), \tag{26}$$

where $\text{Tr}\,(\cdot)$ stands for the trace of the operator or matrix, then the weight function, following Helstrom,[25] is

$$P(\{\beta_{\underline{m}}\}) = \frac{1}{\pi^M |\det \underline{K}|} \exp(-\underline{\beta}^+ \underline{K}^{-1} \underline{\beta}), \tag{27}$$

where $\underline{\beta}^+ = (\{\beta_{\underline{m}}^*\})$. For fields other than Gaussian the density operator is obtained as

Table 1. Examples of single-mode density operators.

No.	Description	Operator Form	$P(\beta)$	$r(n)$
1	Coherent state	$\lvert a\rangle\langle a\rvert$	$\delta^2(\beta-a)$	not diagonal
2	Random phase		$\delta(\lvert\beta\rvert-\sqrt{N})/(2\pi\lvert\beta\rvert)$	$e^{-N}\,N^n/n!$
3	Rayleigh (normal)		$\dfrac{e^{-\lvert\beta\rvert^2/N}}{\pi N}$	$(1+N)^{-1}\,(N/(1+N))^n$
4	Log-normal signal		$\dfrac{e^{-(\sigma^2+\ln\lvert\beta\rvert)^2/2\sigma^2}}{2\pi\sqrt{2\pi}\,\sigma\lvert\beta\rvert}$	$\displaystyle\int_0^\infty \dfrac{N^n x^{2n-1}}{\sqrt{2\pi}\,\sigma n!}\,e^{-x^2 N-(\sigma^2+\ln x)^2/2\sigma^2}\,dx$
5	Thermal noise $N=(e^{\hbar\omega/kT}-1)^{-1}$		$\dfrac{e^{-\lvert\beta\rvert^2/N}}{\pi N}$	$(1+N)^{-1}\,(N/(N+1))^n$
6	Coherent signal with thermal noise $w=\hbar\omega/kT$ μ = signal amplitude	$(1-e^{-w})\,e^{-w(a^+-\mu)(a-\mu^*)}$	$\dfrac{e^{-\lvert\beta-\mu\rvert^2/N}}{\pi N}$	not diagonal
7	Random phase with thermal noise		$\dfrac{2}{N}e^{-\lvert\beta\rvert^2-\lvert\mu\rvert^2/N}\,I_0(2\lvert\beta\mu\rvert)$	$\dfrac{e^{-S/(N+1)}}{N+1}\left[\dfrac{N}{N+1}\right]^n L_n(-S/N(N+1))$
8	Normal signal in thermal noise		$\dfrac{e^{-\lvert\beta\rvert^2/(S+N)}}{(S+N)\pi}$	$\dfrac{1}{(N+S+1)}\left[\dfrac{N+S}{N+S+1}\right]^n$

S = average number of signal photons in the mode.
N = average number of noise photons in the mode.
δ, δ^2 = one-dimensional and two-dimensional delta functions.

15

in the Gaussian case. The coherent states are averaged over the classical joint probability density function of the complex mode amplitudes (cf. Glauber[53]).

2.2.3 Evaluation of the Covariance

With the density operator known, the field covariance functions can be evaluated. The field covariance functions were introduced by Glauber.[53] The field operator $\vec{E}^{(+)}(\vec{r}, t)$ defined in (21) satisfies the following eigenvalue equation when the eigenstates are the coherent states of the field:

$$\vec{E}^{(+)}(\vec{r}, t)|\{a_{\underline{m}}\}\rangle = \mathscr{E}^{(+)}(\vec{r}, t)|\{a_{\underline{m}}\}\rangle, \tag{28}$$

where

$$\mathscr{E}^{(+)}(\vec{r}, t) = i \sum_{\underline{m}} \sqrt{\frac{\hbar\omega_{\underline{m}}}{2\epsilon_o V}} \, a_{\underline{m}} e_{\underline{m}} \, e^{i(\vec{k}_{\underline{m}} \cdot \vec{r} - \omega_{\underline{m}} t)}. \tag{29}$$

The field covariance function will be defined in the following way:

$$K_{ij}(\vec{r}_1, t_1; \vec{r}_2, t_2) = Z_o^{-1} \, \text{Tr} \left\{ \rho E_i^{(+)}(\vec{r}_1, t_1) E_j^{(-)}(\vec{r}_2, t_2) \right\}, \tag{30}$$

where i and j refer to the ith and j^{th} components of the vector $\vec{E}$, while $Z_o = \sqrt{\mu_o/\epsilon_o}$ is the impedance of vacuum, which is needed to give the covariance function the dimension and magnitude of intensity. Using (28) and (21) in (25), we have

$$K_{ij}(\vec{r}_1, t_1; \vec{r}_2, t_2) = \int \ldots \int P(\{a_{\underline{\ell}}\}) \, \mathscr{E}_i^{(+)}(\vec{r}_1, t_1) \, \mathscr{E}_j^{(-)}(\vec{r}_2, t_2) \, \underset{\underline{\ell}}{\Pi} \, d^2 a_{\underline{\ell}}. \tag{31}$$

By expanding this according to (29), the covariance becomes

$$K_{ij}(\vec{r}_1, t_1; \vec{r}_2, t_2) = \int \ldots \int P(\{a_{\underline{\ell}}\}) \sum_{\underline{m}} \sum_{\underline{\ell}} \frac{\hbar\sqrt{\omega_{\underline{m}}\omega_{\underline{\ell}}} \, c}{2V} \, e_{\underline{m}i} e_{\underline{\ell}j} a_{\underline{m}} a_{\underline{\ell}}^*$$

$$\cdot \exp[i(\vec{k}_{\underline{m}} \cdot \vec{r}_1 - \vec{k}_{\underline{\ell}} \cdot \vec{r}_2)] \exp[-i(\omega_{\underline{m}} t_1 - \omega_{\underline{\ell}} t_2)] \, \underset{\underline{\ell}}{\Pi} \, d^2 a_{\underline{\ell}}$$

$$= \sum_{\underline{m}} \sum_{\underline{\ell}} \frac{\hbar c \sqrt{\omega_{\underline{m}}\omega_{\underline{\ell}}}}{2V} e_{\underline{m}i} e_{\underline{\ell}j} k_{\underline{m}\underline{\ell}} \, \exp[i(\vec{k}_{\underline{m}} \cdot \vec{r}_1 - \vec{k}_{\underline{\ell}} \cdot \vec{r}_2) - i(\omega_{\underline{m}} t_1 - \omega_{\underline{\ell}} t_2)], \tag{32}$$

where $e_{\underline{m}i}$ stands for the ith component of the vector $e_{\underline{m}}$, and $k_{\underline{m}\underline{\ell}}$ is the mode covariance as defined in (26). The case of stationary and homogeneous field has special interest in this work. Hence the covariance function will be evaluated in this case. Here $K_{ij}(\vec{r}_1, t_1; \vec{r}_2, t_2) = K_{ij}(\vec{r}_1 - \vec{r}_2, t_1 - t_2)$. The only way to obtain stationarity in (32) is

16

to require (Glauber[53]) that

$$\underline{k}_{\underline{m}\underline{\ell}} = \int \ldots \int P(\{a_{\underline{\ell}}\}) \, a_{\underline{m}} a_{\underline{\ell}} \prod_{\underline{\ell}} d^2 a_{\underline{\ell}} = n_{\underline{m}} \delta_{\underline{m}\underline{\ell}}. \tag{33}$$

Hence the modes of a stationary and homogeneous field are uncorrelated. (For finite apertures the field is no longer homogeneous, so the modes are correlated.) The number of photons in mode $\underline{m}$ is $n_{\underline{m}}$ on the average. The covariance function then becomes

$$K_{ij}(\vec{r}_1, t_1; \vec{r}_2, t_2) = \sum_{\underline{m}} \frac{\hbar c \omega_{\underline{m}}}{2V} e_{\underline{m}i} e_{\underline{m}j} n_{\underline{m}} \exp[i(\vec{k}_{\underline{m}} \cdot (\vec{r}_1 - \vec{r}_2) - \omega_{\underline{m}}(t_1 - t_2))]. \tag{34}$$

Now assume that $i = j$, and that the wavefront is very closely perpendicular to the z axis so that $e_{\underline{m}i}^2 \approx 1$. We have

$$K(\vec{r}_1 - \vec{r}_2, t_1 t_2) = \sum_{\underline{m}} \frac{\hbar c \omega_{\underline{m}}}{2V} n_{\underline{m}} \exp[i(\vec{k}_{\underline{m}} \cdot (\vec{r}_1 - \vec{r}_2) - \omega_{\underline{m}}(t_1 - t_2))]. \tag{35}$$

It is rather obvious from this formula that the wave-number spectrum of the field has a quite simple expression. A similar result for the energy spectrum is given by Glauber.[53] By taking the two-dimensional Fourier transform, the right side of (35), when $\vec{r}_1$ and $\vec{r}_2$ are taken on a plane perpendicular to the z axis so that $\vec{k}_{\underline{m}} \cdot \vec{r}_j = \vec{\kappa}_{\underline{m}} \cdot r_j$; $j = 1, 2$, and $t_1 = t_2$, becomes

$$S(\vec{\kappa}_{\underline{m}}) = \iint K(\vec{r}, 0) \, e^{-i\vec{\kappa}_{\underline{m}} \cdot \vec{r}} \, d^2 \vec{r} = \sum_{\underline{m}'} \iint \frac{\hbar c \omega_{\underline{m}}}{2V} n_{\underline{m}} \exp(-i(\vec{\kappa}_{\underline{m}} - \vec{\kappa}_{\underline{m}'}) \cdot \vec{r}) \, d^2 \vec{r}$$

$$= \frac{\hbar c \omega_{\underline{m}} n_{\underline{m}} L_1 L_2}{2 L_1 L_2 L_3} = \frac{\hbar c \omega_{\underline{m}} n_{\underline{m}}}{2cT} \tag{36}$$

$$= \frac{\hbar \omega_{\underline{m}} n_{\underline{m}}}{2T} = \frac{hc}{2\lambda T} n_{\underline{m}}.$$

In a similar way, it would be possible to obtain higher order covariance functions too. This goes beyond the scope of this work, however.

2.3 BACKGROUND NOISE

Background noise has important bearing on the spatial and temporal aspects of the detection problem. This noise is created by natural or artificial sources. It is usually distributed over a very wide frequency range, and also comes from all possible directions. It has been widely tabulated (Möller,[56] Ross[29]). It is of the order of

17

$N_r = 10^{-13}$ W/m^2 · str · Hz near the red wavelengths, and corresponds to 280°K black-body radiation for far infrared wavelengths. The quantity used in this work to describe background noise is N_o, $[N_o]$ = W/Hz. This is the spatial (two-dimensional) and temporal Fourier transform of the field autocovariance function. The connection between N_r and N_o is the following (small fields of view assumed):

$$N_o = \lambda^2 N_r.$$ (37)

III. STATISTICAL PROPERTIES OF FIELD REPRESENTATIONS

We shall consider the following classical model (Fig. 2) for the received signal complex envelope:

$$y(\vec{r}, t) = S_k(t) \, Zz(\vec{r}, t) + n(\vec{r}, t), \qquad \vec{r} \in \mathscr{A}_r, \quad t \in [0, T], \tag{38}$$

where $S_k(t)$ denotes the signal waveform with duration T and unit energy corresponding to a message k, $z(\vec{r}, t)$ denotes the varying part of the slow multiplicative fading because of the atmospheric turbulence, Z is the field strength, a constant in this model, $n(\vec{r}, t)$ stands for the spatially and temporally white Gaussian envelope noise with uniform spectral density N_o, and $\mathscr{A}_r$ refers to the receiving aperture, which has the area A_r. The justification for this model has already been discussed.
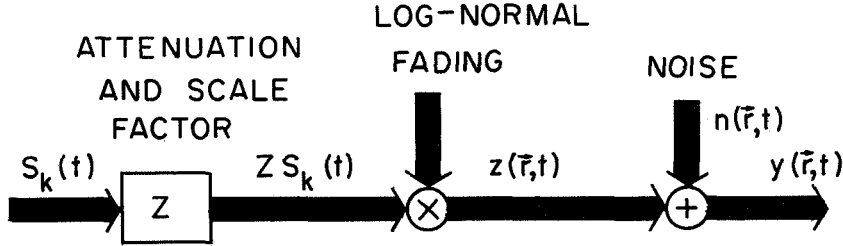
Fig. 2. Model of wave propagation in a turbulent atmosphere. The plane wave $S_k(t)$ suffers multiplicative fading $Zz(\vec{r}, t)$ and background noise $n(\vec{r}, t)$.

In order to express the probability densities needed in the likelihood functions (cf. Fig. 1), a convenient representation for the field has to be found. Usually, a manageable probability density can be found only for Gaussian-derived fields.

We shall discuss the extension of the usual Fourier-series, sampling, and Karhunen-Loève representations to two-dimensional fields. Then the joint probability density of an arbitrary number of samples of the log-normal field will be presented, and its moments evaluated. The probability density in other than sampling representation will then be investigated. Particularly, the coefficients of the plane-wave decomposition which represent focal plane properties are of interest.

For aperture sizes of the order of the coherent area the coefficients in question are connected with the log-normal distribution, although the moving diffraction pattern has to be considered. It sounds reasonable to apply the Central Limit theorem and argue that the joint density must eventually approach the normal or Gaussian density, if properly normalized. Both the small (see Appendix C) and large aperture cases will be examined in detail. For this a proof of the Central Limit theorem for fields will be presented. Under certain conditions that will be discussed the log-normal field satisfies

the Central Limit theorem.

The convergence toward Gaussian variables of sums of log-normal variables was further investigated by assuming a number of completely independent coherent areas in the aperture. In this case, because moments of all orders exist and the terms in the sum are independent, the Central Limit theorem holds, but convergence turns out to be slow.

In order to be on safer ground in theoretical arguments, we decided to measure the plane-wave component amplitude distribution in the focal plane of a lens. The results of this measurement will be discussed.

3.1 FIELD REPRESENTATION IN AN INFINITE APERTURE

Sampling theorems in two dimensions will now be discussed. The usual uncertainty principle is stated. These results are straightforward generalizations of the well-known one-dimensional results. The source books used in the theory of random fields with their wave-number and frequency spectra, correlation and structure functions are those of Yaglom,[57] Tatarski,[2] and Papoulis.[58]

Theorem 1. The wave-number spectrum of a homogeneous field is assumed to be square-integrable and to have a bandlimited (compact) support:

$$S(\vec{\kappa}) = 0, \quad |\kappa_x| \geq \kappa_1, \quad |\kappa_y| \geq \kappa_2. \tag{39}$$

Then the spatial correlation function of the field can be expressed in terms of its sampling expansion

$$K(\vec{r}) = \sum_{m=-\infty}^{\infty} \sum_{n=-\infty}^{\infty} K(\vec{r}_{mn}) \frac{\sin(\kappa_1 x - \pi m)}{\kappa_1 x - \pi m} \frac{\sin(\kappa_2 y - \pi n)}{\kappa_2 y - \pi n}, \tag{40}$$

where $\vec{r} = (x, y)$.

Proof: Obviously $S(\vec{\kappa})$ can be expressed in terms of a two-dimensional Fourier series.

$$S(\vec{\kappa}) = \sum_{m=-\infty}^{\infty} \sum_{n=-\infty}^{\infty} A_{mn} \exp -2\pi i \left[\frac{m\kappa_x}{2\kappa_1} + \frac{n\kappa_y}{2\kappa_2} \right], \quad |\kappa_x| < \kappa_1, \quad |\kappa_y| < \kappa_2, \tag{41}$$

where

$$A_{mn} = \frac{1}{4\kappa_1\kappa_2} \int_{-\kappa_2}^{\kappa_2} \int_{-\kappa_1}^{\kappa_1} d\kappa_x d\kappa_y \, S(\vec{\kappa}) \exp 2\pi i \left[\frac{m\kappa_x}{2\kappa_1} + \frac{n\kappa_y}{2\kappa_2} \right]. \tag{42}$$

But because

20

$$K(\vec{r}) = \frac{1}{(2\pi)^2} \int_{-\infty}^{\infty} \int d^2\vec{\kappa} \; S(\vec{\kappa}) \; e^{i\vec{\kappa}\cdot\vec{r}}, \tag{43}$$

$$A_{mn} = \frac{(2\pi)^2}{4\kappa_1\kappa_2} \; K\left[\frac{m\pi}{\kappa_1}, \frac{n\pi}{\kappa_2}\right]. \tag{44}$$

Here, and subsequently, the abbreviation $d^2\vec{\kappa} = d\kappa_x d\kappa_y$ is used, while $d^2\vec{r} = dxdy$. Now substitute (41) in (43), and use (44). Then

$$K(\vec{r}) = \sum_{m=-\infty}^{\infty} \sum_{n=-\infty}^{\infty} \frac{1}{4\kappa_1\kappa_2} \; K\left[\frac{m\pi}{\kappa_1}, \frac{n\pi}{\kappa_2}\right].$$

$$\cdot \int_{-\kappa_1}^{\kappa_1} \int_{-\kappa_2}^{\kappa_2} \exp i\kappa_x\left[x - \frac{m\pi}{\kappa_1}\right] + i\kappa_y\left[y - \frac{n\pi}{\kappa_2}\right] d\kappa_x d\kappa_y. \tag{45}$$

After the integrals are evaluated (40) follows.

Note: Expansion (40) can be put into the following forms (see Papoulis[58]):

$$K(\vec{r}-\vec{r}_0) = \sum_m \sum_n K(\vec{r}_{mn}-\vec{r}_0) \; \frac{\sin(\kappa_1 x - \pi m)}{\kappa_1 x - \pi m} \; \frac{\sin(\kappa_2 y - \pi n)}{\kappa_2 y - \pi n} \tag{46}$$

$$K(\vec{r}) = \sum_m \sum_n K(\vec{r}_{mn}-\vec{r}_0) \; \frac{\sin(\kappa_1(x+x_0)-\pi m)}{\kappa_1(x+x_0) - \pi m} \; \frac{\sin(\kappa_2(y+y_0)-\pi n)}{\kappa_2(y+y_0) - \pi n}, \tag{47}$$

where $\vec{r}_0 = (x_0, y_0)$. Equation 46 is obtained by going from $K(\vec{r})$ to $K(\vec{r}-\vec{r}_0)$, while (47) follows by setting $\vec{r} - \vec{r}_0 \to r$.

Theorem 2. (Sampling theorem). With the assumptions of Theorem 1, the field $y(r)$ itself can be expressed in terms of a sampling expansion

$$y(\vec{r}) = \lim_{M\to\infty} \sum_{m=-M}^{M} \sum_{n=-M}^{M} y\left[\frac{m\pi}{\kappa_1}, \frac{n\pi}{\kappa_2}\right] \frac{\sin(\kappa_1 x - \pi m)}{\kappa_1 x - \pi m} \; \frac{\sin(\kappa_2 y - \pi n)}{\kappa_2 y - \pi n}. \tag{48}$$

Proof: Denote the Mth partial sum of the series (48) by $\tilde{y}(r)$. Then consider the following average, and use (46).

$$e(\vec{r}) = \overline{(\tilde{y}(\vec{r})-y(\vec{r})) \; y^*(r_{mn})}$$

$$= \sum_{m'=-M}^{M} \sum_{n'=-M}^{M} K(\vec{r}_{m'n'}-\vec{r}_{mn}) \tag{49}$$

$$\cdot \frac{\sin(\kappa_1 x - \pi m')}{\kappa_1 x - \pi m'} \; \frac{\sin(\kappa_2 y - \pi n')}{\kappa_2 y - \pi n'} - K(\vec{r}-\vec{r}_{mn})$$

$$\to 0, \quad \text{as } M \to \infty.$$

21

Here, $\vec{r}_{mn} = (\pi m/\kappa_1, \pi n/\kappa_2)$. Hence $\tilde{y}(\vec{r}) - y(\vec{r})$ is orthogonal to every component of $y(\vec{r})$. It must follow that $\overline{(\tilde{y}(\vec{r})-y(\vec{r}))\; \tilde{y}^*(\vec{r})} = 0$. Also

$$\overline{(\tilde{y}(\vec{r})-y(\vec{r}))\; \tilde{y}^*(\vec{r})} = \sum_{m'=-M}^{M} \sum_{n'=-M}^{M} K(\vec{r}_{m'n'} - \vec{r})$$

$$\cdot \frac{\sin(\kappa_1 x - \pi m')}{\kappa_1 x - \pi m'}\; \frac{\sin(\kappa_2 y - \pi n')}{\kappa_2 y - \pi n'} \tag{50}$$

$$\to 0, \quad \text{as } M \to \infty$$

by (47) setting $\vec{r} = 0$, $\vec{r}_o = \vec{r}$. Now clearly

$$\lim_{M \to \infty} \overline{|\tilde{y}(\vec{r})-y(\vec{r})|^2} = 0. \tag{51}$$

The sampling theorem for two dimensions turns out to be analogous to the one-dimensional sampling theorem. The rectangular shape of the wave-number space support in (39) sounds strange and "uneconomical" for an isotropic field, the power spectrum of which is circularly symmetric. In this case the covariance function has an expansion of the kind in Theorem 1, but in terms of Bessel functions. No "circular" sampling expansion for the field $y(\vec{r})$ has been found (Papoulis[59]).

When the spatial correlation function has a rectangular support, it can obviously be expanded into a Fourier series similar to (41). Then the next theorem is obvious.

Theorem 3. Whenever a square-integrable correlation function $K(\vec{r})$ is nonzero on a finite support $\mathscr{A}_c$ only, such that

$$\underset{r \in \mathscr{A}_c}{\text{Max}} |\vec{r}| = r_o. \tag{52}$$

$K(\vec{r})$ has the following Fourier-series representation

$$K(\vec{r}) = \frac{1}{4\pi r_o^2} \sum_m \sum_n S(\vec{\kappa}_{mn}) e^{i\vec{\kappa}_{mn} \cdot \vec{r}}, \quad r \in \mathscr{A}_c$$

$$= 0, \quad \text{elsewhere}, \quad \vec{\kappa}_{mn} = \left[\frac{2\pi m}{r_o}, \frac{2\pi n}{r_o} \right]. \tag{53}$$

The usual uncertainty principle for Fourier transforms, as is known in quantum mechanics (for example, Louisell[51]), is valid. A Gaussian field pattern is maximally concentrated (in the mean-square sense) in both the aperture and wave-number domains (Papoulis[60]).

3.2 FIELD REPRESENTATION IN A FINITE APERTURE

3.2.1 Covariances and Wave-Number Power Spectra

The field itself can be represented by a Fourier series only within a finite (compact) aperture. The restriction of the field to the aperture area is no longer homogeneous because one cannot go beyond the edges. The field and the spatial covariance functions have to be modified by multiplying them with proper window functions (Blackman and Tukey[61]):

$$K_a(\vec{r}_1, \vec{r}_2) = K(\vec{r}_1 - \vec{r}_2) \, w(\vec{r}_1) \, w(\vec{r}_2), \tag{54}$$

$$w(\vec{r}) = 1, \quad \text{for } \vec{r} \in \mathscr{A}_r$$

$$= 0, \quad \text{elsewhere.} \tag{55}$$

The following wave-number spectra can now be defined:

$$S_{a1}(\vec{\kappa}_1; \vec{r}_2) = \iint K_a(\vec{r}_1, \vec{r}_2) \, e^{-i\vec{\kappa}_1 \cdot \vec{r}_1} \, d^2\vec{r}_1$$

$$= w(\vec{r}_2) \left[S(\vec{\kappa}_1) \, e^{-i\vec{\kappa}_1 \cdot \vec{r}_2} * W(\vec{\kappa}_1) \right] \tag{56}$$

$$S_{a2}(\vec{r}_1; \vec{\kappa}_2) = \iint K_a(\vec{r}_1, \vec{r}_2) \, e^{i\vec{\kappa}_2 \cdot \vec{r}_2} \, d^2\vec{r}_2$$

$$= w(\vec{r}_1) \left[S(\vec{\kappa}_2) \, e^{i\vec{\kappa}_2 \cdot \vec{r}_1} * W(\vec{\kappa}_2) \right] \tag{57}$$

$$S_{a12}(\vec{\kappa}_1, \vec{\kappa}_2) = \iiiint K_a(\vec{r}_1, \vec{r}_2) \, e^{-i(\vec{\kappa}_1 \cdot \vec{r}_1 - \vec{\kappa}_2 \cdot \vec{r}_2)} \, d^2\vec{r}_1 d^2\vec{r}_2$$

$$= W(\vec{\kappa}_1) * \left[W(\vec{\kappa}_1 - \vec{\kappa}_2) * S(\vec{\kappa}_1) \right], \tag{58}$$

where the star denotes the convolution operation in the wave-number domain. The Fourier transform of the window function $W(\vec{\kappa})$ is in fact the Fraunhofer diffraction image of the aperture, while $S(\vec{\kappa})$ describes the intensity distribution among the plane waves coming from different directions that compose the original field. In fact, it is easy to see that $S_{a12}(\vec{\kappa}_1, \vec{\kappa}_2)$ is nothing else but the covariance function in the focal plane (except for a constant and with Fresnel quadratic phase effects neglected). The wave-number vector $\vec{\kappa}$ and the focal plane coordinate vector $\vec{u}$ are related by $\vec{\kappa} = 2\pi\vec{u}/(\lambda F)$, where F is the focal length.

Strictly speaking, the tails of the window functions mean that the sampling Theorem 2 cannot be applied. As astronomers know full well, the wave-number window function $W(\vec{\kappa})$ (the diffraction image) for usual telescope apertures is considerably narrower than

the wave-number spectrum of a plane wave that has propagated through a turbulent atmosphere. By using a sufficiently fine grid the error arising from sampling representation can be made negligible.

3.2.2 Plane-Wave and Orthogonal Representations

The usual Fourier series expansion can be conveniently used to describe the field within the limited aperture. The coefficients can be measured in the focal plane, subject to errors from diffraction effects. Hence this expansion, also called "the plane-wave representation," is very important.

Often other than sampling or plane-wave representations are useful. Orthogonal representations are a very general, but still convenient, class of such representations. Any complete orthonormal (within the aperture) set of functions $\phi_i(\vec{r})$ can be used to represent the field. The sampling and Fourier series representations are a special case of such an orthogonal representation. The representation is

$$y(\vec{r}) = \sum_{i=0} Y_i \phi_i(\vec{r}), \qquad \vec{r} \in \mathscr{A}_r \tag{59}$$

$$Y_i = \int \int_{\mathscr{A}_r} y(\vec{r}) \, \phi_i^*(\vec{r}) \, d^2\vec{r}. \tag{60}$$

The orthonormality condition reads

$$\int \int_{\mathscr{A}_r} \phi_i(\vec{r}) \, \phi_j^*(\vec{r}) \, d^2\vec{r} = \delta_{ij}. \tag{61}$$

Here δ_{ij} is the Kronecker delta. The indices i can and are often taken to be integer vectors, in this case with two components.

A particularly simple example, as referred to above, is the set of plane waves, which is orthogonal in a rectangular aperture with sides a and b if the functions $\exp(i\vec{\kappa}_{mn} \cdot \vec{r})$ are chosen so that $\vec{\kappa}_{mn} = (4\pi m/a, 4\pi n/b)$.

The statistical properties of the coefficients of these orthogonal expansions are of great interest, and will be investigated in some detail. Now only second-order statistics of the coefficients will be discussed. The moments of the coefficients are derived from the moments of the field itself by linear transformations. The covariance matrix of the representation has the following entries:

$$k_{ij} = \overline{Y_i Y_j^*} = \iiiint_{\mathscr{A}_r} y(\vec{r}) \, y^*(\vec{r}') \, \phi_i^*(\vec{r}) \, \phi_j(\vec{r}') \, d^2\vec{r} d^2\vec{r}'$$

$$= \iiiint_{\mathscr{A}_r} K(\vec{r}-\vec{r}') \, \phi_i^*(\vec{r}) \, \phi_j(\vec{r}') \, d^2\vec{r} d^2\vec{r}'. \tag{62}$$

24

The covariance matrix is diagonal if and only if

$$\int\int_{\mathscr{A}_r} K(\vec{r}-\vec{r}') \; \phi_i(\vec{r}') \; d^2 r' = \lambda_i \phi_i(\vec{r}) \tag{63}$$

for some constant λ_i. This particular representation has been named after Karhunen and Loève. The covariance matrix entries then are $k_{ij} = \lambda_i \delta_{ij}$.

For the plane-wave decomposition it is easy to see the similarity between Eqs. 62 and 58. Hence

$$k_{ij} = A_r^{-1} S_{a12}(\vec{\kappa}_1, \vec{\kappa}_2), \tag{64}$$

where S_{a12} was defined in (58).

To obtain the diagonal, or Karhunen-Loève representation, the integral Eq. 63 has to be solved. Sometimes, for example, if the kernel is Gaussian, it may be separable:

$$K(\vec{r}) = K'(x) \; K''(y). \tag{65}$$

If, also, the aperture is rectangular, the integral equation factors into two one-dimensional integral equations. Even these are usually hard to solve.

For infinite apertures the plane waves are the solutions to the integral (63), since

$$\int_{-\infty}^{\infty} \int K(\vec{r}-\vec{r}') \; e^{-i\vec{\kappa}_j \cdot \vec{r}'} \; d^2\vec{r}' = S(\vec{\kappa}_j) \; e^{-i\vec{\kappa}_j \cdot \vec{r}}. \tag{66}$$

For practical purposes, only a finite number of coefficients can be used. The actual number depends on the purpose of the expansion. A measure to this number D, the number of "degrees of freedom" of the field can be obtained by taking the number of Fourier coefficients below wave-number "cutoff," viz.:

$$D = (\kappa_0 a/\pi + 1)^2 \sim (a/r_c)^2, \tag{67}$$

where a is the side of the rectangular aperture, and r_c the coherence radius of the field, somehow defined. This is analogous to the known number of degrees of freedom of an approximately time (T) and bandlimited (W) signal, (2WT + 1).

3.3 STATISTICAL PROPERTIES OF THE LOG-NORMAL FIELD IN SAMPLING REPRESENTATION

3.3.1 Probability Density

According to the material presented in Section II the plane wave sent through a turbulent atmosphere suffers a random multiplicative distortion (see Fig. 2), which is modelled as log-normal. If we set $\gamma(\vec{r}) = \log z(\vec{r})$, its probability density is Gaussian. The probability density of the samples of $\gamma(\vec{r})$ is

$$p_{\underline{Y}}(\underline{y}) = \lim_{N \to \infty} \frac{1}{(2\pi)^N \det \underline{K}_{\underline{Y}}^{1/2}} \exp\left(-\frac{1}{2}(\underline{y}-\bar{\underline{y}})^T \underline{K}_{\underline{Y}}(\underline{y}-\bar{\underline{y}})\right),$$

(68)

where $\underline{y}$ and $\underline{K}_{\underline{Y}}$ stand for following $1 \times 2N$ and $2N \times 2N$ matrices (the symbol T means transpose operation)

$$\underline{y}^T = [x_1, x_2, \ldots, x_N, \theta_1, \theta_2, \ldots, \theta_N]$$

(69)

$$\underline{K}_{\underline{Y}} = \overline{(\underline{y}-\bar{\underline{y}})(\underline{y}-\bar{\underline{y}})^T}.$$

(70)

In the sampling representation used here $\gamma_k = \gamma(\vec{r}_k) = \chi_k + i\theta_k$, $k = 1, \ldots N$. The sampling representation is the most natural, because of the following memoryless exponential transformation.

The probability density for the field $z(\vec{r})$ is obtained from (68) by the following transformation of variables:

$$z_k = z_k^r + i z_k^i, \quad z_k^r = e^{\chi_k} \cos \theta_k, \quad z_k^i = e^{\chi_k} \sin \theta_k$$

(71)

for $k = 1, \ldots, N$. The expression for the density of $\underline{z}$ becomes

$$p_{\underline{Z}}(\underline{Z}) = p_{\underline{Y}}(\underline{\gamma}(\underline{Z})) \left|\frac{\partial(\underline{z})}{\partial\underline{\gamma}}\right|^{-1} = p_{\underline{Y}}(\underline{\gamma}(\underline{Z})) \prod_{k=1}^{N} \left(z_k^{r^2} + z_k^{i^2}\right)^{-1},$$

(72)

where $\partial(\underline{z})/\partial\underline{\gamma}$ is the Jacobian of the transformation. There is no closed-form expression for the marginal distributions of the real or imaginary part of the field $z(\vec{r})$.

3.3.2 Sample Moments

The moments of the components of the $\underline{z}$-vector are easy to evaluate. Because the phase variance is very large the phase can be taken to be uniform. Then all of the odd-order moments of the components of $\underline{z}$ vanish. In fact, the same fate befalls all of the moments $\overline{z_{k1}^{n1} z_{k2}^{n2} \ldots z_{11}^{*m1} z_{12}^{*m2}} \ldots$, for which $n1 + n2 + \ldots \neq m1 + m2 + \ldots$ (see Theorem 5). Two theorems will now be presented, the first concerning the covariance function of $z(\vec{r})$, which is due to Fried,[62] the second generalizing this result to moments of an arbitrary order. In preparation the amplitude and phase-structure functions are defined as follows:

$$D_\chi(\vec{r}_1, \vec{r}_2) = \overline{|\chi(\vec{r}_1)-\chi(\vec{r}_2)|}^2$$

(73)

$$D_\theta(\vec{r}_1, \vec{r}_2) = \overline{|\theta(\vec{r}_1)-\theta(\vec{r}_2)|}^2.$$

(74)

As before, we shall assume that the amplitude is a homogeneous field and the phase is locally homogeneous only.

26

Theorem 4. The following assumptions will be made concerning the log-amplitude and phase of a log-normal field $z(\vec{r})$.

1. The log-amplitude $\chi(\vec{r})$ is homogeneous within the aperture, and normal with variance σ^2 and mean $-\sigma^2$, so that $\overline{|z|^2} = 1$.

2. The phase $\theta(\vec{r})$ is locally homogeneous with mean zero and a structure function that depends on the difference of the aperture points only. Then the covariance function of the field is a function of the amplitude and phase-structure functions:

$$K(\vec{r}_1, \vec{r}_2) = \exp[-(D_\chi(\vec{r}-\vec{r}_2)+D_\theta(\vec{r}_1-\vec{r}_2))]. \tag{75}$$

Proof: We denote $\chi(\vec{r}_1) = \chi_1$, $\theta(\vec{r}_2) = \theta_2$, etc. Using the matrices defined by (69) and (70) with $A^T = [1, 1, i, -i]$ we have

$$K(\vec{r}_1, \vec{r}_2) = \overline{z(\vec{r}_1)\, z^*(\vec{r}_2)} = \overline{e^{\chi_1+\chi_2+i\theta_1-i\theta_2}} = \overline{e^{\underline{A}^T \underline{r}}}$$

$$= \int \cdots \int \frac{\exp\left[\underline{A}^T \underline{\gamma} - \frac{1}{2}(\underline{\gamma}-\underline{\bar{\gamma}})^T \underline{K}_\gamma^{-1}(\underline{\gamma}-\underline{\bar{\gamma}})\right]}{(2\pi)^2 \left|\det \underline{K}_\gamma\right|^{1/2}} d^4\underline{r}$$

$$= \frac{\exp\left[\frac{1}{2}\underline{A}^T \underline{K}_\gamma \underline{A} + \underline{\gamma}^T \underline{A}\right]}{(2\pi)^2 \left|\det \underline{K}_\gamma\right|^{1/2}}$$

$$\cdot \int \cdots \int \exp\left[-\frac{1}{2}(\underline{\gamma}-\underline{K}_\gamma\underline{A}-\underline{\bar{\gamma}})^T \underline{K}_\gamma^{-1}(\underline{\gamma}-\underline{K}_\gamma\underline{A}-\underline{\bar{\gamma}})\right] d^4\underline{r}$$

$$= \exp\left[\frac{1}{2}\underline{A}^T \underline{K}_\gamma \underline{A} + \underline{\bar{\gamma}}^T \underline{A}\right]. \tag{76}$$

Using the definition of $\underline{K}_\gamma$ (in Eq. 70), we can see that

$$K(\vec{r}_1, \vec{r}_2) = \exp\left[\frac{1}{2}\overline{[(\underline{\gamma}-\underline{\bar{\gamma}})^T \underline{A}]^2} + \underline{\bar{\gamma}}^T \underline{A}\right]$$

$$= \exp\left[\frac{1}{2}\overline{(\chi_1+\chi_2-\bar{\chi}_1-\bar{\chi}_2+i(\theta_1-\theta_2))^2} + \bar{\gamma}_1 + \bar{\gamma}_2\right]$$

$$= \exp\left[\bar{\chi}_1 + \bar{\chi}_2 + \frac{1}{2}\overline{(\chi_1+\chi_2-\bar{\chi}_1-\bar{\chi}_2)^2}\right] \exp\left[-\frac{1}{2}\overline{(\theta_1-\theta_2)^2}\right]$$

$$\cdot \exp\left[2i\overline{(\theta_1-\theta_2)(\chi_1+\chi_2-\bar{\chi}_1-\bar{\chi}_2)}\right]. \tag{77}$$

Then we observe that

$$(\chi_1 + \chi_2)^2 = 2\left(\chi_1^2 + \chi_2^2\right) - (\chi_1 - \chi_2)^2$$

$$\overline{\chi}_1 + \overline{\chi}_2 + \frac{1}{2}\overline{(\chi_1 + \chi_2 - \overline{\chi}_1 - \overline{\chi}_2)^2} = \overline{\chi}_1 + \overline{\chi}_2 + \overline{\chi_1^2} + \overline{\chi_2^2} - \frac{1}{2}(\overline{\chi}_1 + \overline{\chi}_2)^2 - \frac{1}{2}\overline{(\chi_1 - \chi_2)^2}$$

$$\overline{(\theta_1 - \theta_1)(\chi_1 + \chi_1 - \overline{\chi}_1 - \overline{\chi}_1)} = \overline{(\theta_1\chi_1 - \theta_2\chi_2)} + \overline{(\theta_1\chi_2 - \theta_2\chi_1)}. \tag{78}$$

The cross terms between θ and χ vanish because these crosscorrelation functions depend only on distance for the homogeneous fields assumed: $\overline{\theta_i\chi_j} = K_{\theta\chi}(|\vec{r}_i - \vec{r}_j|)$ $i, j = 1, 2$. Now we use assumption 1 and notice that $\overline{\chi^2} = \sigma^2(1 + \sigma^2)$. Then Eq. 75 follows.

According to Section II and with Tatarski's[63] equations applied to (75), we have

$$K(\vec{r}_1, \vec{r}_2) = \exp{-\frac{1}{2}\left|\frac{\vec{r}_1 - \vec{r}_2}{r_{c12}}\right|^{a_{12}}}. \tag{79}$$

The subscripts 12 in a_{12} and r_{c12} help to keep in mind that they, too, depend on the difference between the two points $\vec{r}_1$ and $\vec{r}_2$. For distances much smaller than the inner scale of turbulence the exponent $a_{12} = 2$. For distances considerably beyond the inner scale of turbulence the exponent is 5/3. With practical aperture sizes the outer scale of turbulence will never be reached. The scaling constant r_{c12} is also different in these two regions.

Theorem 5. With the assumptions of Theorem 4 the moment of an arbitrary order of the field $z(\vec{r})$ is equal to

$$\overline{z_1^{n_1} z_2^{n_2} \ldots z_{m-1}^{n_{m-1}} z_m^{*n_m} \ldots z_N^{*n_N}} = \exp\left[\sum_{k=1}^{N} \overline{\chi}_k + \frac{1}{2}\overline{\left[\sum_{k=1}^{N} n_k(\chi_k - \overline{\chi}_k)\right]^2}\right]$$

$$\cdot \exp\left[-\frac{1}{2}\overline{\left[\sum_{k=1}^{m-1} n_k\theta_k - \sum_{k=m}^{N} n_k\theta_k\right]^2}\right]. \tag{80}$$

Proof: The proof is exactly like that in Theorem 4 up to Eq. 77. The cross terms consisting in crosscorrelation functions $\overline{\theta_i\chi_j}$ again vanish by homogeneity.

It is easy to see that those moments for which the number of added θ_k's is different from the number of θ_k's subtracted will always have a very large negative contribution from the phase in the exponent. Because of the inhomogeneous but locally homogeneous character of the phase, the squared average blows up in this case, so that the corresponding moment vanishes.

3.3.3 Even-Order Sample Moments in Terms of Amplitude and Phase-Structure Functions

An interesting case, which will be used eventually, arises when all n_k's are 1's and $N = 2n$. This moment will be called $K_{2n}(\vec{r}_1, \ldots \vec{r}_{2n})$, and will be evaluated as follows. First look at the expression containing the log-amplitudes. This expression will be worked out as in (78) in Theorem 6.

$$\sum_{k=1}^{2n} \overline{\chi_k} + \frac{1}{2}\overline{\left[\sum_{k=1}^{2n}(\chi_k - \overline{\chi_k})\right]^2} = -2n\sigma^2 + \frac{1}{2}\overline{\left[\sum_{k=1}^{2n}\chi_k\right]^2} - \frac{1}{2}\left[\sum_{k=1}^{2n}\overline{\chi_k}\right]^2$$

$$= -2n\sigma^2 + \frac{1}{2}\left[\sum_{k=1}^{2n}\overline{\chi_k^2} + 2\sum_{k=1}^{2n}\sum_{j=k+1}^{2N}\overline{\chi_k\chi_j}\right] - 2n^2\sigma^4$$

$$= -2n\sigma^2 - 2n^2\sigma^4 + \overline{n\chi^2} + \frac{1}{2}\left[\sum_{k=1}^{2n}\sum_{j=k+1}^{2n}\left[\overline{\chi_k^2} + \overline{\chi_j^2} - \overline{(\chi_k - \chi_j)^2}\right]\right]$$

$$= -2n\sigma^2 - 2n^2\sigma^4 + \overline{n\chi^2} + \frac{1}{2}(2n-1)\sum_{k=1}^{2n}\overline{\chi_k^2} - \frac{1}{2}\sum_{k=1}^{2n}\sum_{j=k+1}^{2n}\overline{(\chi_k - \chi_j)^2}$$

$$= -2n\sigma^2 - 2n^2\sigma^4 + 2n^2\sigma^2(1+\sigma^2) - \frac{1}{2}\sum_{k=1}^{2n}\sum_{j=k+1}^{2n}D_\chi(\vec{r}_k - \vec{r}_j)$$

$$= +2n(n-1)\,\sigma^2 - \frac{1}{2}\sum_{k=1}^{2n}\sum_{j=k+1}^{2n}D_\chi(\vec{r}_k - \vec{r}_j). \tag{81}$$

The evaluation of the expression containing the phases is complicated by the alternately positive and negative signs of its terms.

$$\overline{\left[\sum_{k=1}^{n}(\theta_k - \theta_{k+n})\right]^2} = \sum_{k=1}^{n}\overline{(\theta_k - \theta_{k+n})^2} + 2\sum_{k=1}^{2n}\sum_{j=k+1}^{2n}\overline{(\theta_k - \theta_{k+n})(\theta_j - \theta_{j+n})}. \tag{82}$$

But again as in (78) the cross terms are replaced by squares of the differences. In this case the squares cancel out.

$$(\theta_k - \theta_{k+n})(\theta_j - \theta_{j+n}) = \theta_k\theta_j - \theta_k\theta_{j+n} - \theta_j\theta_{k+n} + \theta_{k+n}\theta_{j+n}$$

$$= \frac{1}{2}\left[(\theta_k - \theta_{j+n})^2 + (\theta_j - \theta_{k+n})^2 - (\theta_k - \theta_j)^2 - (\theta_{k+n} - \theta_{j+n})^2\right]. \tag{83}$$

29

Therefore after one more step the phase-structure function can be introduced.

$$
\overline{\left[\sum_{k=1}^{n}(\theta_k-\theta_{k+n})\right]^2} = \sum_{k=1}^{n}\sum_{j=1}^{n}\overline{(\theta_k-\theta_{k+n})^2} - \sum_{k=1}^{n}\sum_{j=k+1}^{n}\left[\overline{(\theta_k-\theta_j)^2}+\overline{(\theta_{k+n}-\theta_{j+n})^2}\right]
$$

$$
= \sum_{k=1}^{n}\sum_{j=1}^{n}D_\theta(\vec{r}_k-\vec{r}_{k+n}) - \sum_{k=1}^{n}\sum_{j=k+1}^{n}(D_\theta(\vec{r}_k-\vec{r}_j)+D_\theta(\vec{r}_{k+n}-\vec{r}_{j+n})).
$$

$$(84)$$

Combining (81) and (84) in (80), we obtain the covariance function of order $2n$

$$
K_{2n}(\vec{r}_1,\ldots,\vec{r}_{2n}) = \overline{z_1 \cdots z_n z_{n+1}^* \cdots z_{2n}^*}
$$

$$
= e^{2n(n-1)\sigma^2}\exp\left\{-\frac{1}{2}\left[\sum_{k=1}^{2n}\sum_{j=k+1}^{2n}D_\chi(\vec{r}_k-\vec{r}_j)\right.\right.
$$

$$
\left.\left.+ \sum_{k=1}^{n}\sum_{j=1}^{n}D_\theta(\vec{r}_k-\vec{r}_{k+n}) - \sum_{k=1}^{n}\sum_{j=k+1}^{n}(D_\theta(\vec{r}_k-\vec{r}_j)+D_\theta(\vec{r}_{k+n}-\vec{r}_{j+n}))\right]\right\}.
$$

$$(85)$$

For later use, a special case of (85) will be considered. Assume that the phase-structure function is quadratic; for example, the exponent in (79) is equal to two. The covariance function (85) can be bounded between the case in which the amplitude is the same across the whole aperture and the case in which the amplitudes in any two points of the aperture are completely uncorrelated. In the former case all amplitude structure functions vanish, in the latter case they are equal to $2\sigma^2$. The phase-structure function

$$
D_\theta(\vec{r}_1-\vec{r}_2) = |\vec{r}_k-\vec{r}_2|^2/r_c^2 \tag{86}
$$

when substituted in (84), after using the development backwards in Eqs. 84, 83, and 82, yields

$$
e^{-n\sigma^2}\exp\left[-\frac{1}{2}\left|\sum_{k=1}^{n}(\vec{r}_k-\vec{r}_{k+n})\right|^2 \bigg/ r_c^2\right] \leqslant K_{2n}(\vec{r}_1,\ldots,\vec{r}_{2n})
$$

$$
\leqslant e^{2n(n-1)\sigma^2}\exp\left[-\left|\sum_{k=1}^{n}(\vec{r}_k-\vec{r}_{k+n})\right|^2 \bigg/ 2r_c^2\right]. \tag{87}
$$

30

3.4 STATISTICAL PROPERTIES OF THE LOG-NORMAL FIELD IN ORTHOGONAL REPRESENTATIONS

3.4.1 General Considerations

The sampling representation was a particularly simple form of an orthogonal representation. Here orthogonal representations will be considered in general, and the plane-wave decomposition in particular. The coefficients of an orthogonal representation are evaluated by using (61). Their probability density is very hard to evaluate, even (72) being hard enough. Certain asymptotic statements, however, can be made.

A coefficient of an orthogonal representation is a weighted sum (in fact, integral) of the field over the whole receiver aperture. For small apertures the motion of the diffraction pattern has to be considered in addition to the log-normal fading. This case will be analyzed in Appendix C. On the other hand, for very large apertures compared with the coherent area of the field it seems plausible that the Central Limit theorem would hold. The statistics should then be first-order Gaussian.

3.4.2 Central Limit Theorem for Fields

If the coefficients of an orthogonal representation are normally distributed, then by (60) the field itself as a weighted sum of Gaussian variables must also be Gaussian by a well-known theorem (Cramér[64]). For any finite number of Gaussian variables their joint distribution can be orthogonalized; that is, the variables can be expressed in terms of linear combinations of independent Gaussian variables. By the theorem referred to, this property carries over to the infinite case. Hence the sum of possibly dependent Gaussian variables must also be Gaussian. If the original stochastic process or field is not Gaussian, neither can the coefficients be exactly Gaussian.

Next, the Central Limit theorem for stochastic fields will be proved. I have not met any proofs of the Central Limit theorem for this case. The proof will be carried through by using moment method. We have demonstrated that moments of any order exist and are finite for the field $z(\vec{r})$ in the aperture. The moment method is not a very elegant means and places many probably unnecessarily severe limitations on the convergence. Proofs of the Central Limit theorem for time series and stochastic processes have been presented by Rosenblatt,[15] Volkonski and Rozanov,[16] and Ibragimov.[65] The additional condition required to validate the Central Limit theorem in these cases when the terms of the sum are dependent is that of strong mixing. If A is an event that happens at times $(-\infty, t)$ and B another event that happens at times $(t+\tau, \infty)$, the strong mixing condition requires that

$$\sup_{t} \; \sup_{A, B} \; \left| \Pr(A \cap B) - \Pr(A)\, \Pr(B) \right| = \alpha(\tau) \to 0 \tag{88}$$

as $\tau \to \infty$. It has been shown by Volkonski and Rozanov that this is equivalent to the condition

$$\sup_{t} \sup_{\eta, \zeta} \left| \overline{\eta \zeta} - \overline{\eta}\, \overline{\zeta} \right| = a'(\tau) \leqslant 16\, a(\tau) \to 0. \tag{89}$$

As $\tau \to \infty$, where η is a random variable measurable in the algebra of events at times $(-\infty, \tau)$, and ζ is a random variable measurable in the algebra of events at times $(t+\tau, \infty)$. Furthermore, $|\eta| < 1$, $|\zeta| < 1$ are required. Certain conditions have to be imposed as the speed $a(\tau)$ approaches zero depending on the other conditions of the Central Limit theorem, such as Lyapunov's or Lindeberg's conditions. These conditions obviously depend also on the dimension of the process parameter, time, so that the proof for one-dimensional time does not apply without modifications for fields with at least two dimensions. Instead of presenting a proof on the lines of Volkonski and Rozanov, the proof based on moment evaluations will be presented.

The strong mixing condition will be imposed in the following form:

$$\left| K_{2m}(\vec{r}_1, \vec{r}_2, \ldots, \vec{r}_{2m}) - \prod_{j=1}^{m} K\left(\vec{r}_{i_j}, \vec{r}_{k_j}\right) \right| \leqslant a_{2m}(R), \tag{90}$$

where $\{(i_j, k_j)\}$ is an arrangement of the indices $1, \ldots, 2m$ in pairs and the distance from one of these pairs to a member of any other pair is at least R. Another condition of the form

$$\left| K_{2m}(\vec{r}_1, \vec{r}_2, \ldots, \vec{r}_{2m}) \right| \leqslant \beta_{2m}(R) \tag{91}$$

for $\min \left| \vec{r}_j - \vec{r}_k \right| \geqslant R$, $j, k = 1, \ldots, 2m$. As $R \to \infty$, $a_{2m}(R) \to 0$ and $\beta_{2m}(R) \to 0$. Physically (90) means that the $(2m)^{\text{th}}$-order covariance factors into products of second-order covariance functions if the pairs of points are sufficiently distant from each other. Equation 90 indicates that the covariance functions vanish at a certain speed when the distance of some point to all the other points is large enough. Similar conditions have to be true for the odd-order covariance functions.

<u>Theorem 6</u>. (Central Limit theorem for fields). Consider the normalized integral of a real homogeneous field $z(\vec{r})$, whose moments of all orders exist and are finite; in particular, its mean is zero and variance unity.

$$\zeta_{\mathscr{A}_r} = \frac{1}{\sqrt{A_r A_c}} \int \int_{\mathscr{A}_r} z(\vec{r})\, d^2\vec{r}. \tag{92}$$

Then the distribution of $\zeta_{\mathscr{A}_r}$ converges toward the $(0, 1)$-normal distribution, since the diameter of the aperture area goes to infinity, if the separability conditions (93) and (94) hold for the covariances of the field. A_c is a normalization factor defined as follows

$$A_c = \frac{1}{A_r} \int \int_{\mathscr{A}_r} \int \int_{\mathscr{A}_r} K_2(\vec{r}_1, \vec{r}_2)\, d^2\vec{r}_1 d^2\vec{r}_2 \tag{93}$$

(With this condition $\overline{\zeta^2}_{\mathscr{A}_r} = 1$.)

32

<u>Proof</u>: The idea of the proof is to bound the integral of the difference of a moment of $(2m)^{th}$ order of $z(\vec{r})$ and the corresponding Gaussian moment (Eq. 94). The Gaussian moment is the sum of products of m covariance functions $K_2(\vec{r}_j, \vec{r}_k)$, where j and k go through all of the $(2m-1)!! = (2m-1) \cdot (2m-3) \ldots 3.1$ possibilities of taking the points $\vec{r}_1, \ldots, \vec{r}_{2m}$ in pairs. The integral of the difference is divided into three parts that are bounded separately. In the first part, I_1, the integration is carried over the domain $\mathscr{D}_1$ where the points $\vec{r}_1, \ldots, \vec{r}_{2m}$ are arranged in pairs so that the points in a pair are close together but each pair is far from any other pair. In this case the approximate factoring of (90) occurs and the integrand turns out to be small. In the second part, I_2, some of the pairs may be close to each other so that the factoring of (90) no longer works. The corresponding domain of integration $\mathscr{D}_2$ turns out to be infinitesimal compared with the total domain $\mathscr{D} = \mathscr{A}_r \times \ldots \mathscr{A}_r$ (2m times). Finally, in the domain $\mathscr{D} - \mathscr{D}_1 - \mathscr{D}_2$ some of the points are far away from every other point, so that the integrand again turns out to be small because of (91). In the course of bounding the three parts of the integral some sufficient conditions will be imposed on $\alpha_{2m}(R)$ and $\beta_{2m}(R)$. By using a different technique in the proof, these conditions can be made less restricting. The proof for moments of odd order goes analogously, except that $\mathscr{D}_1$ is picked so that one point is separated from all of the pairs. The integrand then is negligible. For $\mathscr{D}_2$ and $\mathscr{D} - \mathscr{D}_1 - \mathscr{D}_2$ the proof goes exactly as in the case of the even moments. In the case of log-normal fields the odd moments are zero initially.

We want to consider the difference

$$e = \overline{\frac{\zeta^{2m}}{\mathscr{A}_r}} - (2m-1)!!$$

$$= A_r^{-m} A_c^{-m} \int \ldots \int_{\mathscr{D} = \mathscr{A}_r \times \ldots \times \mathscr{A}_r} \left[K_{2m}(\vec{r}_1, \vec{r}_2, \ldots, \vec{r}_{2m}) - \sum_{k=1}^{(2m-1)!!} \prod_{\ell=1}^{m} K_2\left(\vec{r}_{i_\ell}, \vec{r}_{j_\ell}\right) \right] d^{4m}\underline{r},$$

(94)

where k stands for an integer labeling a particular arrangement of the set $\{1, 2, \ldots, 2m\}$ into pairs. The symbol $\times$ stands for the Cartesian product of sets. The differential $d^{4m}\underline{r}$ means $d^2\vec{r}_1 d^2\vec{r}_2 \ldots d^{2m}\vec{r}_{2m}$. The vector $\underline{r}$ stands for $\{\vec{r}_1, \vec{r}_2, \ldots, \vec{r}_{2m}\}$.

It is helpful to introduce the sets for given distance R:

$$\mathscr{D}_{jk} = \{\underline{r}: |\vec{r}_j - \vec{r}_k| \leqslant R\}$$

(95)

$$\mathscr{D}_{jk}^c = \mathscr{D} - \mathscr{D}_{jk} = \{\underline{r}: |\vec{r}_j - \vec{r}_k| > R\}.$$

Next, we define the domains $\mathscr{D}_1$, $\mathscr{D}_2$ and $\mathscr{D} - \mathscr{D}_1 - \mathscr{D}_2$ in terms of these sets $\mathscr{D}_{jk}$ and their complements $\mathscr{D}_{jk}^c$:

$$\mathcal{D}_1 = \bigcup_{k=1}^{(2m-1)!!} \mathcal{D}_{1k}$$

$$\mathcal{D}_{1k} = \bigcap_{i_k, j_k} \mathcal{D}_{i_k j_k} \bigcap_{\ell \neq k} \left(\mathcal{D}^c_{i_k i_\ell} \cap \mathcal{D}^c_{i_k j_\ell} \cap \mathcal{D}^c_{j_k j_\ell} \right)$$

$$\mathcal{D}_2 = \bigcup_{k=1}^{(2m-1)!!} \bigcap_{i_k, j_k} \mathcal{D}_{i_k j_k} \bigcup_{\ell \neq k} \left(\mathcal{D}^c_{i_k i_\ell} \cup \mathcal{D}^c_{i_k j_\ell} \cup \mathcal{D}^c_{j_k j_\ell} \right)$$

$$\mathcal{D}_3 = \mathcal{D} - \mathcal{D}_1 - \mathcal{D}_2 = \bigcap_k \bigcup_{i_k, j_k} \mathcal{D}^c_{i_k j_k}. \tag{96}$$

Here the first union or intersection with index k sums over all possible ways of partitioning the set $\{1, 2, \ldots, 2m\}$ into pairs. The second sum goes over the m pairs specified by the partition.

The integral (94) will be divided into three parts as follows.

$$I = I_1 + I_2 + I_3$$

$$I_j = A_r^{-m} A_c^{-m} \int \ldots \int_{\mathcal{D}_j} (\qquad) d^{4m}\underline{r}, \quad j = 1, 2, 3. \tag{97}$$

The integral I_1 is integrated over domains $\mathcal{D}_{1k}$ for $k = 1, \ldots, (2m-1)!!$. Within a domain $\mathcal{D}_{1k}$

$$\left| K_{2m}(\underline{r}) - \prod_{i_k, j_k} K_2(\vec{r}_{i_k}, \vec{r}_{j_k}) \right| \leq \alpha_{2m}(R), \tag{98}$$

$$\left| \sum_{k' \neq k} \prod_{i_{k'}, j_{k'}} K_2(\vec{r}_{i_{k'}}, \vec{r}_{j_{k'}}) \right| \leq [(2m-1)!! - 1] \beta_2^2(R). \tag{99}$$

These bounds follow from the strong mixing conditions (90) and (91). In (99) it has been assumed that $|K_2| \leq 1$. In each term on the left side of (99) at least two covariance functions have distances $|\vec{r}_{i_{k'}} - \vec{r}_{j_{k'}}| \geq R$, by Eq. 96. In each integral over $\mathcal{D}_{ik}$ we make the change of variables

$$\vec{u}_\ell = \vec{r}_{i_k}, \vec{v}_\ell = \vec{r}_{i_k} - \vec{r}_{j_k}, \quad \ell = 1, \ldots, m \tag{100}$$

over all $\vec{r}_{i_k}$. Clearly, $|\vec{v}_\ell| < R$. The areas for different ℓ will in general overlap. So the following bound is obtained

$$D_{1k} = \int \ldots \int_{\vec{u}_i \in \mathcal{A}_r} d^{2m}\underline{u} \int \ldots \int_{\vec{u}_c - \vec{v}_c \in \mathcal{A}_r} d^{2m}\underline{v}$$

$$\leq A_r^m (\pi R^2)^m. \tag{101}$$

Because the number of the sets $\mathscr{D}_{1k}$ is $(2m-1)!!$ the integral I_1 is absolutely bounded by the expression

$$|I_1| \leq (2m-1)!! \left[\frac{\pi R^2}{A_c}\right]^m \left(a_{2m}(R) + (2m-1)!! \, \beta_2^2(R)\right). \tag{102}$$

For each m, $|I_1|$ can be made negligible by taking R large enough, provided that

$$a_{2m}(R) = o(R^{-2m}) \tag{103}$$

$$\beta_2(R) = o(R^{-m}) \tag{104}$$

for every m, where $o(x)/x \to 0$ as $x \to 0$, and $\beta_2(R)$ go to zero faster than any power. Such functions, for example, are $\exp(-R^a)$, $a \geq 0$, $\exp(-|\ln R|^a)$, $a \geq 1$.

The integrand in integral I_2 in (97) is bounded by $M_{2m} + (2m-1)!!$, where $|K_{2m}(\vec{r})| \leq M_{2m}$. The volume of the set $\mathscr{D}_2$ is bounded similarly to the volume of $\mathscr{D}_1$. Here, however, the distance of at least two pairs of points is less than R. Then the four points in question are contained in a circle of radius 1.5 R. Hence after the transformation of variables analogous to (100) we have

$$D_2 < A_r^{m-1}(\pi R^2)^{m-1}\left[\frac{9\pi R^2}{4}\right]^2. \tag{105}$$

Therefore

$$|I_2| < \frac{9\pi^{m+1}}{4} R^{2(m+1)} A_r^{-1} A_c^{-m}(M_{2m} + (2m-1)!!) = o\left(A_r^{-1}\right). \tag{106}$$

Hence $|I_2|$ is made negligible by taking A_r large enough.

In $\mathscr{D}_3$ the diameter of the set of vectors $\vec{r}_1, \ldots, \vec{r}_{2m}$ is more than R. Then by simple geometric reasoning it becomes obvious that the maximum distance of any vector $\vec{r}_k$ from any other vector is greater than or equal to $R \sin(\pi/m)$. Then, by (90) and (91),

$$|K_{2m}(\vec{r})| \leq \beta_{2m}\left(R \sin \frac{\pi}{m}\right) \tag{107}$$

$$\Pi \left|K_2\left(r_{i_k}, r_{j_k}\right)\right| \leq \beta_2(R). \tag{108}$$

The latter bound depends on the functional form of $\beta_2(R)$. It is true, for example, for $B_2 = \exp(-R^{1/2})$, while for $\beta_2 = e^{-R}$ the bound would be $\beta_2^{2m}(R \sin \pi/m)$. In any case it goes to zero, roughly speaking, as $\beta_2(R)$. Let the volume of a set $\mathscr{D}'(R)$ with vectors of diameter R in $\mathscr{D}$ be called $V(R)$. Clearly,

$$V(R) = A_r\left[\frac{\pi R^2}{4}\right]^{2m-1}. \tag{109}$$

Now the set $\mathscr{D}_3 \subset \sup_{R'>R} \mathscr{D}'(R')$. As R' grows it is possible to adjust the bounds (107) and (108) correspondingly. Then if the diameter of $\mathscr{A}_r$ is $CA_r^{1/2}$ for some constant C (set $p = (2m-1)!!$),

$$A_r^m A_c^m |I_3| \leq \left[\beta_{2m}\left(R \sin\frac{\pi}{m}\right) + p\beta_2(R)\right] V(R)$$

$$+ \int_R^{CA_r^{1/2}} dV(R) \left[\beta_{2m}\left(R \sin\frac{\pi}{m}\right) + p\beta_2(R)\right]. \tag{110}$$

Now assume that $\beta_{2m}(R) \leq B_{2m} R^{-2m-2\delta_1}$, $\beta_2(R) \leq B_2 R^{-2m-2\delta_2}$ with $\delta_1, \delta_2 > 0$. Then, with $C \leq 1$,

$$|I_3| < \left[\beta_{2m}\left(R \sin\frac{\pi}{m}\right) + p\beta_2(R)\right] A_r^{-m+1} A_c^{-m} \left[\frac{\pi R^2}{4}\right]^{2m-1}$$

$$+ \frac{\pi}{4} C^{2(m-1-\max(\delta_1,\delta_2))} \frac{(2m-1)}{m-1}\left[B_{2m} A_r^{-\delta_1} + p\beta_2 A_r^{-\delta_2}\right]. \tag{111}$$

Again this can be made negligible by choosing R large enough, when

$$\beta_{2m}(R) = o(R^{-2m}) \tag{112}$$

for every m.

The bounds (102), (106), and (111) show that the absolute value of the difference (94) can be made negligible by choosing R large enough in the sets (95) and large enough A_r, given that the strong mixing conditions (90) and (91) with (103), (104) and (112) are valid.

The convergence of the moments is sufficient to ensure the convergence of the probability distribution toward the Gaussian distribution by the moment convergence theorem (Feller[66]).

3.4.3 Application to the Log-normal Field

Obviously, a similar theorem holds for complex fields. It is very interesting to apply Theorem 9 to the covariance function of the log-normal field (85), while using the amplitude and phase structure functions introduced in Section II. It turns out that the atmospheric covariance functions satisfy the strong-mixing condition.

Before considering the covariance function of the log-normal field in detail a few comments are in order.

1. The second condition (91) is satisfied for large R because the phase variance is very large in the expression (85) for the covariance function $K_{2m}(\underline{r})$.

2. The factoring property (90) is fulfilled for the amplitude-structure functions in (111) because the amplitude structure function saturates soon at a value of twice the

36

log-amplitude variance $2\sigma^2$ as the separation between pairs of points.

Hence the phase properties are the important ones in determining under what conditions the log-normal field satisfies the Central Limit theorem.

Equation 85 is rewritten here for convenience

$$K_{2n}(\vec{r}_1, \ldots, \vec{r}_{2n}) = e^{2n(n-1)\sigma^2} \exp - \frac{1}{2} \left[\sum_{k=1}^{2n} \sum_{j=k+1}^{2n} D_A(\vec{r}_k - \vec{r}_j) \right]$$

$$\cdot \exp - \frac{1}{2r_c^a} f(\vec{r}_1, \ldots, \vec{r}_{2n}), \tag{113}$$

where $f(\vec{r}_1, \ldots, \vec{r}_{2n})$ contains the phase-structure functions from Section II:

$$f(\vec{r}_1, \ldots, \vec{r}_{2n}) = \sum_{k=1}^{n} \sum_{j=1}^{n} |\vec{r}_k - \vec{r}_{k+n}|^a - \sum_{k=1}^{n} \sum_{j=k+1}^{n} \left[|\vec{r}_k - \vec{r}_j| + |\vec{r}_{k+n} - \vec{r}_{j+n}|^a \right]. \tag{114}$$

Here the exponent $a \approx 2$ for small distances compared with the inner scale of turbulence, while in the turbulence domain it is 5/3, according to the theory of Obukhov and Tatarski.

The total number of positive terms in (114) is n^2, while the number of negative terms is $n^2 - n$. The number of terms containing a single variable, for example, $\vec{r}_1$, is $2n-1$, among which n are positive and $n-1$ are negative. Clearly, as $|\vec{r}_1| \to \infty$, while other $\vec{r}_k$'s, $k = 2, \ldots, 2n$ stay constant, the sum $f(\vec{r}_1, \ldots, \vec{r}_{2n})$ tends to plus infinity for any $a > 0$. Hence the weak-mixing condition (91) is satisfied. Also, the covariance will approach zero exponentially. This asymptotic behavior for large distances is not physically correct because large scale inhomogeneities cause saturation of the phase-structure function.

To look at the validity of the weak-mixing condition (90), the case for $n = 2$ is presented. The same procedure holds for any $n > 2$. We consider the case for which $\vec{r}_1 - \vec{r}_3 = \vec{u}$ and $\vec{r}_2 - \vec{r}_4 = \vec{v}$ are "small," while $\vec{r}_1 - \vec{r}_2 = \vec{r}$ will tend to infinity. Take $\vec{r} = (R, 0)$, then in terms of $\vec{u} = (u_1, u_2)$, $\vec{v} = (v_1, v_2)$ we have

$$f(\vec{r}_1, \vec{r}_2, \vec{r}_3, \vec{r}_4) =$$

$$|\vec{u}|^a + |\vec{v}|^a + \left[(R+v_1)^2 + v_2^2\right]^{a/2} + \left[(R-u_1)^2 + u_2^2\right]^{a/2} - R^a - \left[(R+v_1-u_1)^2 + (v_2-u_2)^2\right]^{a/2}$$

$$= |\vec{u}|^a + |\vec{v}|^a + R^a \left[1 + 1 - 1 - 1 + \frac{a}{2R}\left[2v_1 + \frac{|v|^2}{R} - 2u_1 + \frac{|u|^2}{R} - 2(v_1 - u_1) \right. \right.$$

$$\left. - \frac{|v|^2 + |u|^2 - v_1 u_1 - v_2 u_2}{R} \right] + \frac{a(a-2)}{8R^2} \left[4v_1^2 + 4u_1^2 - 4(v_1 - u_1)^2 \right] + 0(R^{-3}) \right]$$

$$= |u|^a + |v|^a - R^{a-2} \left[(a-1)u_1 v_1 + u_2 v_2 + 0(R^{-1}) \right]. \tag{115}$$

This result shows that the weak-mixing condition (90) is valid; that is, $f(\vec{r}_1, \vec{r}_2, \vec{r}_3, \vec{r}_4) \rightarrow g(\vec{u}) + g(\vec{v})$ as $R \rightarrow \infty$, if and only if $a < 2$. For $a = 2$ there will be cross terms for any R. For $R > 2$, the cross terms will in fact dominate.

The singular case $a = 2$ is analyzed in detail in Appendix A. It is easy to see that physically the Central Limit theorem cannot be true in this case. We have shown that the ensemble of pure plane waves gives the quadratic phase-structure function. When the aperture size grows the diffraction image of the plane wave gets smaller and smaller. Clearly, there is no convergence towards anything normal.

If the phase-structure function saturates quite soon (as indicated by Moldon[44]), the mixing condition is automatically satisfied.

3.4.4 Application to Coefficients of Orthogonal Representations

The Central Limit theorem was proved for the integral of the field over the aperture. It cannot hold for any orthogonal representation, as is obvious in considering the example of the sampling representation. The coefficient ζ_k corresponding to a given orthonormal function is obtained by performing the integration

$$\zeta_k = \int\int_{\mathscr{A}_r} z(\vec{r})\, \phi_k^*(\vec{r})\, d^2\vec{r}. \tag{116}$$

The fourth-order moment of this (unnormalized) complex variable is equal to

$$\mu_4(k) = \overline{|\zeta_k|^4} = \int\int \overset{(8)}{\cdots}\int_{\mathscr{A}_r} K_4(\vec{r}_1, \vec{r}_2, \vec{r}_3, \vec{r}_4)\, \phi_k^*(\vec{r}_1)\, \phi_k^*(\vec{r}_2)\, \phi_k(\vec{r}_3)\, \phi_k(\vec{r}_4)\, d^8\underline{r}. \tag{117}$$

If we recall the proof of Theorem 6, it is obvious that the same proof will work if the weak-mixing conditions are valid for the following fourth-order (or similar kernel of any order) kernel:

$$\tilde{K}_4(\vec{r}_1, \vec{r}_2, \vec{r}_3, \vec{r}_4) = K_4(\vec{r}_1, \vec{r}_2, \vec{r}_3, \vec{r}_4)\, \phi_k^*(\vec{r}_1)\, \phi_k^*(\vec{r}_2)\, \phi_k(\vec{r}_3)\, \phi_k(\vec{r}_4). \tag{118}$$

This kernel is no longer homogeneous, but the proof actually requires only boundedness in addition to separability. The plane-wave decomposition is an example of orthogonal representation that preserves the separability property of the covariance function. In addition to the limiting cases of very large or very small apertures the moments of the representation coefficients should be evaluated. The fourth moment can be evaluated analytically only when the phase-structure function exponent is equal to two. For moments of higher than second order this model is highly unrealistic. At present, the only workable approach would be to find the actual distributions in some numerical or experimental method. If the plane-wave decomposition is used, Eq. 117 means evaluating an eightfold Fourier integral over the Cartesian product of the apertures. The result is analogous to (58); that is, the infinite Fourier transform of the fourth-order covariance function will be "smoothed" by the diffraction pattern in some complicated way.

The question of the distribution of a single coefficient of an orthogonal representation has been given some asymptotic answers. The next question is the joint distribution of two or more coefficients of an orthogonal representation. In principle, the joint density can be developed, given a set of moments of the distribution, by using a Gram-Charlier type of expansion. This method will not be pursued in this work.

3.4.5 Covariance of Representation Coefficients

It is of great interest to evaluate at least the covariance function of the representation coefficients. This means the evaluation of (63). The most interesting case is the plane-wave representation. This covariance is then proportional to the actual covariance in the focal plane, when Fresnel quadratic phase effects are ignored. The formula in this case becomes (64) where (58) is to be used. The intensity in the focal plane has been evaluated by Chernov.[7]

The covariance function will be evaluated directly as in (63). We have

$$
K_2(\vec{\kappa}_1, \vec{\kappa}_2) = \overline{\zeta_1 \zeta_2^*} = A_r^{-1} \int \dots \int w(\vec{r}_1)\, w(\vec{r}_2)\, K(\vec{r}_1, \vec{r}_2)\, e^{-i\vec{\kappa}_1 \cdot \vec{r}_1 + i\vec{\kappa}_2 \cdot \vec{r}_2}\, d^2\vec{r}_1 d^2\vec{r}_2. \tag{119}
$$

Here $w(\vec{r})$ stands for the aperture function as defined in (55). The variables are transformed so that $\vec{r}_1 = \vec{v} + \vec{u}/2$, $\vec{r}_2 = \vec{v} - \vec{u}/2$, $\vec{\kappa}_o = (\vec{\kappa}_1 + \vec{\kappa}_2)/2$, $\vec{\kappa}_\Delta = \vec{\kappa}_1 - \vec{\kappa}_2$. Assuming the field to be homogeneous so that $K(\vec{r}_1, \vec{r}_2) = K(\vec{r}_1 - \vec{r}_2)$, we have

$$
K_2(\vec{\kappa}_1, \vec{\kappa}_2) = A_r^{-1} \int \overset{\infty}{\underset{-\infty}{\dots}} \int w\left(\vec{v} + \frac{\vec{u}}{2}\right) w\left(\vec{v} - \frac{\vec{u}}{2}\right) K(\vec{u})\, e^{-i\vec{\kappa}_\Delta \cdot \vec{v} - i\vec{\kappa}_o \cdot \vec{u}}\, d^2\vec{u}\, d^2\vec{v}. \tag{120}
$$

Here the Fourier integral of the overlapping area of the shifted apertures has to be found. For a rectangular aperture we have the following expression for this integral, the diffraction image of the overlapping area of the shifted apertures:

$$
\text{diff}(a, \vec{\kappa}_\Delta, \vec{u}) = 4\, \frac{\sin(\kappa_{\Delta 1}(a - |u_1|)/2)}{\kappa_{\Delta 1}}\, \frac{\sin(\kappa_{\Delta 2}(a - |u_2|)/2)}{\kappa_{\Delta 2}}, \tag{121}
$$

where $\vec{\kappa}_\Delta = (\kappa_{\Delta 1}, \kappa_{\Delta 2})$, and a is the aperture size. For a circular aperture the result is qualitatively comparable, but has a very complicated form. Finally,

$$
K_2(\vec{\kappa}_1, \vec{\kappa}_2) = A_r^{-1} \int\int_{-\infty}^{\infty} \text{diff}(a, \vec{\kappa}_\Delta, \vec{u})\, K(\vec{u})\, e^{-i\vec{\kappa}_o \cdot \vec{u}}\, d^2\vec{u}. \tag{122}
$$

Now assuming that the aperture area is large compared with the coherent area, it can be seen in (122) that $\text{diff}(a, \vec{\kappa}_\Delta, \vec{u})$ changes slowly as a function of $\vec{u}$ (at least for $\vec{\kappa}_\Delta$ small enough). To obtain a simple result, the u-dependence is suppressed (this will give an upper bound to $K_2(\vec{\kappa}_1, \vec{\kappa}_2)$), so that

39

$$K_2(\vec{\kappa}_1,\vec{\kappa}_2) \cong \frac{\sin\,(\kappa_{\Delta x}a/2)}{\kappa_{\Delta x}a/2}\,\frac{\sin\,(\kappa_{\Delta y}a/2)}{\kappa_{\Delta y}a/2}\,S(\vec{\kappa}_o),$$ (123)

where $\vec{\kappa}_\Delta = \vec{\kappa}_1 - \vec{\kappa}_2$, and $\vec{\kappa}_o = (\vec{\kappa}_1 + \vec{\kappa}_2)/2$. For apertures large compared with the coherent area the second-order covariance function of the field in the focal plane is approximately a product of two functions, one of which is the diffraction image of the aperture, and changes rapidly as a function of the difference of the two points $\vec{\kappa}_1$ and $\vec{\kappa}_2$. The other function is the wave-number spectrum of the field. It is much broader than the diffraction image, because of the atmospheric turbulence. It is in fact the intensity distribution in the focal plane. It specifies the magnitude of the covariance (123), as $\vec{\kappa}_1 \rightarrow \vec{\kappa}_2$ (see Fig. 3).
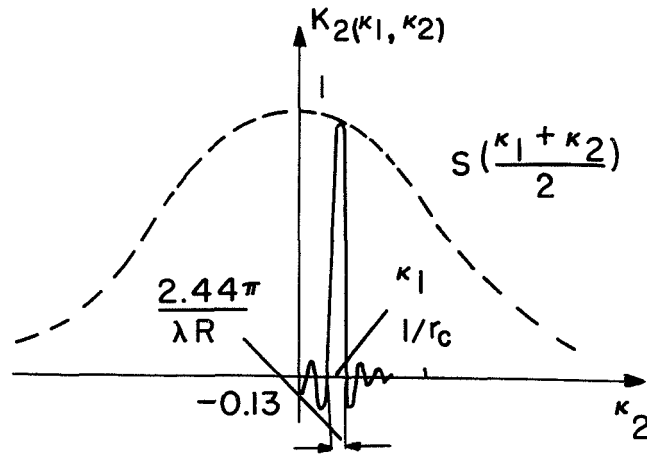
Fig. 3. Behavior of the covariance function of the
field in the focal plane.

3.5 SIMULATION RESULTS OF INDEPENDENT LOG-NORMAL
VARIABLES

3.5.1 General Considerations

Extensive simulations have been used because of the analytical difficulties in dealing with statistical questions concerning sums of log-normal variables. The variable whose statistical properties are being investigated by simulation is, for the most part, the Fourier coefficient of the field in the aperture. This variable relates physically to the field at a point on the focal plane. It was proved in Theorem 6 that the distribution of this coefficient converges eventually toward a normal distribution, as the aperture grows very large compared with the coherence area of the field. As the proof shows,

in the sense indicated by the strong-mixing condition (88)-(91) the plane-wave representation coefficient can be considered as a sum of independent log-normal variables. The simulation of the field with given correlation properties was not done because its creation from random numbers is difficult. It is very easy, on the other hand, to create a set of "independent" complex log-normal variables, or as they are called by statisticians, "complex log-normal deviates."

We shall now deal with sums of independent log-normal deviates. The basic variable generated is a complex log-normal deviate with given log-amplitude variance σ^2. The mean value of the log-amplitude was taken to be $-\sigma^2$ to give unit average "intensity," and the phase was either uniform or Gaussian with variable phase deviation from the average phase value zero. The generating method is discussed in Appendix B. The deviate thus created is denoted $z_k = z_k^r + i z_k^i$.

Two kinds of sums were generated, the sum of K complex log-normal deviates,

$$\zeta_K = \sum_{k=1}^{K} z_k , \tag{124}$$

and the sum of K absolute squared values of log-normal deviates

$$I_K = \sum_{k=1}^{K} |z_k|^2 . \tag{125}$$

The motivation for the last was the surprising results obtained experimentally by Fried, Mevers, and Keister,[36] and the desire to check the theoretical results of Mitchell[67] on the permanence of the log-normal distribution. The sum (125) obviously simulates the total energy collected by the aperture at a given moment. Clearly, the value of the simulations is somewhat restricted by the fact that the terms of the sums in (124) and (125) are not dependent in a way that would correspond to the locally homogeneous model introduced in Section II.

The problem of convergence of the distribution of the sum of independent log-normal variates has been analyzed by B. Levitt. His results agree with the simulations reported below.

3.5.2 Amplitude and Phase Distributions of Sums

The distribution function of ζ_K was computed from 1024 simulations that were grouped in 64 classes. This distribution function was plotted with the use of the computer on probability papers so that the amplitude statistics of ζ_K was compared with

41

Table 2. Hypothesis testing on the distributions of simulated sums of K complex log-normal variables having uniform phase and log-normal amplitude distributions, with the latter normalized so that the mean-square amplitude is unity. σ^2 represents the log-normal variance. The three hypotheses used were "Rayleigh distribution" or "log-normal distribution" for amplitude, and uniform distribution for phase.

σ / K	1.0	0.5	0.1
Rayleigh Amplitude			
1	‡	†	‡
4	‡	A	*
16	†	A	A
64	A	A	no test
Log-normal Amplitude			
1	A	A	A
4	A	†	‡
16	†	‡	‡
64	‡	‡	no test
Uniform Phase			
1	A	A	A
4	A	A	A
16	A	A	A
64	A	A	no test

Testing symbols: A = hypothesis acceptable, * = deviation from assumed hypothesis slightly significant (10% probability), † = deviation significant (1% probability), ‡ = deviation highly significant (0.1% probability). The probability levels (10%, 1%, .1%) indicate the probability of rejecting a given hypothesis when it is in fact correct.

42

log-normal and Rayleigh distribution, while the phase statistics were compared with the uniform distribution. The significance levels at which either the acceptance or the rejection of either the log-normal or the Rayleigh hypothesis was done were observed from the computer-generated plots. The results are shown in Table 2. The number of samples for each entry was 1024, except those that are marked with "no test."

The distributions of the initial log-normal variables for the values of σ that were selected change quite remarkably. The distribution for $\sigma = 1.0$ is peaked very close to the origin and highly spread. The distribution for $\sigma = 0.5$ peaks at some distance from the origin, showing a valley with gentle curves near the origin. Finally, the distribution for $\sigma = .1$ looks closely like a Rician distribution, forming a sharp ridge on the edge of the unit circle around the origin.

The convergence toward normal distribution, or rather Rayleigh distribution in amplitude and uniform distribution in phase, is fastest for $\sigma = .5$ for which it happens before K = 4. For the largest $\sigma = 1.0$ the convergence is "complete" at some point between K = 16 and K = 64. For this latter case the log-normal distribution can be used

Table 3. Hypothesis testing on the distributions of sums of K complex log-normal variables having the variance of log-amplitude $\sigma^2 = 1.0$, and Gaussian phase distribution with mean zero and phase deviation as indicated.

Phase Deviation / K	1.0	3.14	6.28	15.0
Rayleigh Amplitude				
4	‡	‡	‡	‡
16	‡	‡	‡	‡
64	‡	A	A	A
Log-normal Amplitude				
4	A	A	A	A
16	A	A	*	*
64	A	†	‡	‡
Uniform phase				
4	‡	A	A	A
16	‡	A	A	A
64	‡	A	A	A

Testing symbols: A = acceptable, deviation from test hypothesis is slightly significant (10%) for *, significant (1%) for †, and highly significant (0.1%) for ‡.

as a reasonable model up to some intermediate K between 4 and 16. The phase stays uniform over the entire range of σ and K.

Simulation results in Table 3 show a somewhat different behavior for sums of log-normal "intensities." Therefore we decided in the case of sums of complex log-normal variables to investigate what difference a range of phase deviations from 1 to 15 might make when compared with the results obtained with uniform phase distribution. The phase and the amplitude were made independent in the simulations of Tables 2 and 3. Table 3 gives the results of hypothesis testing for $\sigma = 1.0$, the sample size N = 1024, and for phase deviations of 1.0, 3.14, 6.28, and 15.0

These simulation results should be compared with the first column for $\sigma = 1.0$ in Table 2. The comparison shows that for phase deviations 6.28 and 15 the results are essentially the same as for the uniform phase in Table 2. For a phase deviation of 1 the log-normal distribution is a good fit to the actual amplitude distribution of the simulated sum over the whole range of K. The phase distribution is now very different from uniform. The case of phase deviation 3.14 is intermediate between the extremes of small

Table 4. Hypothesis testing on the distributions of sums of K real log-normal variables with mean = 1 and variance of logarithm $4\sigma^2$. (Sum of intensities.)

K \ σ	1.0	0.5	0.1
	Log-normal Amplitude		
1	A	A	A
4	A	no test	no test
16	*	A	A
64	*	A	A
256	A	no test	no test
	Normal Amplitude		
1	‡	‡	‡
4	‡	no test	no test
16	‡	†	A
64	‡	*	A
256	†	no test	no test

Testing symbols: A = acceptable, deviation from test hypothesis is slightly significant (10%) for *, significant (1%) for †, and highly significant (0.1%) for ‡.

44

and large phase deviations.

Simulation results on sums of log-normal intensities are given in Table 4. This table conveys the message that for sums of real log-normal variables the resulting distribution can be well fitted to a log-normal distribution for all K and σ. The fit seems to be better for small than for large σ. Eventually the sums will approach normal random variables when properly normalized. Hence Mitchell's argument agrees with these simulation results. Because the actual field in the aperture has amplitude correlations, however, the speed of convergence cannot be inferred very easily either from his results or from Table 4. The speed of convergence can be seen from Levitt's results.[68]

The other test hypothesis was chosen to be normal instead of χ^2-distribution because convergence was expected for rather high values of K, and the normal approximation is close to the χ^2-distribution for K > 30. In fact, for $\sigma = 0.1$, a χ^2-distribution having a broad shape would be a very poor approximation to the actual spiky distribution.

The simulation results show that for large apertures the field samples in the focal plane look to be first-order Gaussian. On the other hand, the experimental results of Fried, Mevers, and Keister[36] show that even for large apertures the total power collected by the aperture looks log-normal. Although this sounds strange, this seems to be the actual behavior. According to the results of Ohta and Koizumi,[69] the total power in the case of a Gaussian field is indeed closely log-normal.

The results established on amplitude and phase statistics by simulations of log-normal sums indicate that in many cases using either log-normal or normal distribution that is properly fitted gives satisfactory approximations to the actual statistics. The convergence toward the normal distribution seems to be very slow indeed for $\sigma = 1.0$, and no doubt even slower for larger log-normal variances.

3.5.3 Testing the Independence of Fourier Coefficients

The one-dimensional marginal distributions of the amplitude and phase do not even specify the actual distribution of the log-normal sum in a single point because something has to be specified about their dependency. The following simulations intend to clarify the question of independence of the amplitude and the phase in a single point, and the independence of amplitudes and phases in two points in the simulated focal plane, where the points are taken to be the closest two points with zero correlation. The arrangement of the simulation and the tests that were used are discussed in Appendix B.

Table 5 displays the results of 1024 simulations. Two contingency table sizes were tried. The χ^2 test of independence is most reliable, when each entry of the contingency table contains a large number, preferably more than 10. Unfortunately this was not the case in either size selected for the contingency tables. Small numbers tend to increase χ^2, so that the error will be more to the conservative side of rejecting the hypothesis of independence. The points of rejection on various probability levels were the following.

For 9 degrees of freedom

at probability level 10% χ^2 = 14.68

at probability level 1% χ^2 = 21.67

at probability level .1% χ^2 = 27.88.

For 81 degrees of freedom

at probability level 10% χ^2 = 101.8

at probability level 1% χ^2 = 117.5

at probability level .1% χ^2 = 125.8.

Table 5 shows clearly that there is a good reason to model the sum of at least 4 independent complex log-normal variables so that its amplitude and phase are independent.

Table 5. Test of independence of the amplitude and the phase of sums of K independent complex log-normal variables. The numbers in the table stand for χ^2_N, where N = 9 for the upper half and N = 81 for the lower half corresponding to the contingency tables used in the test.

K \ σ	1.0	0.5	0.1
	Contingency Table 4 × 4		
4	4.66	10.62	12.32
	A	A	A
16	3.28	11.13	4.18
	A	A	A
64	16.59	5.39	12.14
	*	A	A
	Contingency Table 10 × 10		
4	92.8	114.3	69.8
	A	*	A
16	94.4	78.0	57.0
	A	A	A
64	99.9	79.7	99.0
	A	A	A

σ^2 = variance of log-amplitude, A = independence hypothesis acceptable, * = independence hypothesis accepted at probability level 1% but rejected at probability level 10%; that is, deviation from the independence hypothesis is slightly significant. Sample size = 1024.

Table 6. Test of independence of amplitudes and phases in two close uncorrelated focal plane points. The numbers stand for χ^2 with 9 degrees of freedom.

σ \ K		1.0	0.5	0.1
2	Amplitude Phase ρ	1203 ‡ 86 ‡ .04	62 ‡ 24.3 † .03	1199 ‡ 448 ‡ .02
4	Amplitude Phase ρ	779 ‡ 8.7 A .09 †	34 ‡ 4.9 A .03	112 ‡ 8.0 A .02
8	Amplitude Phase ρ	1185 ‡ 12.5 A .05 *	5.7 A 5.8 A .01	22.6 † 5.9 A .02
16	Amplitude Phase ρ	786 ‡ 7.0 A .08 †	10.6 A 5.9 A .02	17.3 * 11.2 A .01
32	Amplitude Phase ρ	124 ‡ 3.0 A .02	8.1 A 5.7 A .02	8.5 A 17.8 * .05
64	Amplitude Phase ρ	78 ‡ 11.4 A .05	13.1 A 11.0 A .04	7.1 A 10.6 A .02
128	Amplitude Phase ρ	69 ‡ 13.0 A .03	no test	no test
256	Amplitude Phase ρ	12.5 A 8.8 A .02	no test	no test

σ^2 = log-amplitude variance, A = acceptable independence hypothesis, ρ = correlation coefficient of the two sums compared, and *, †, ‡ same as in Table 3.

47

The last set of simulations deals with the independence of amplitudes and phases in those two points in the simulated focal plane which are closest and have zero correlation. Table 6 lists 1024 simulations. The results of Table 6 show that if the number of terms in the sum K becomes larger, eventually the amplitudes and the phases in two uncorrelated points will become independent. The amplitude in point 1 and the phase in point 2 were not tested for independence, but a look at Table 5 shows that if the amplitude and the phase in the same point can be taken as independent for $K \geqslant 4$, then even more so must the amplitude in point 1 and phase in point 2 be. The convergence toward independence is fastest for $\sigma = 0.5$, while for $\sigma = 1.0$ it is very slow. The dependence between amplitudes is such that if the amplitude in point 1 is large, so probably is the amplitude in point 2. Similarly, if the amplitude is small in point 1. One could say that although the sums are uncorrelated, their amplitudes or absolute values may still be strongly correlated. The phases become independent after $K \geqslant 4$. The correlation coefficient was also monitored. Except for two cases the correlation was not significantly different from zero.

3.6 MEASUREMENTS OF PROBABILITY DENSITY ON THE FOCAL PLANE OF A LENS

3.6.1 Experimental Arrangement

The theoretical analysis carried out in section 3.4 applied to the limiting cases of either very large or very small apertures. The intermediate cases are very difficult to analyze. In addition to simulations we felt that a few measurements could add something to the picture of the statistics of plane-wave coefficients. Only the amplitude distribution was measured. The measurement of joint densities was originally contemplated, but this idea was later dropped.

Figure 4 presents the measurement arrangement at the receiving end of the link. A controlled portion of the incoming laser radiation was allowed to come in through a circular hole. The diffraction image was magnified by the eyepiece and imaged on the sampling aperture plate, which had holes of various sizes. The hole size was chosen to be somewhat less than the magnified Airy disc. The sampled focal-plane field was then focused on a photodiode. The low-level signal at the photodiode was chopped at approximately 2000 Hz by the chopper wheel indicated. Hence it could be amplified in an AC-coupled preamplifier. In the actual setup this narrow-band AC signal was recorded on a portable tape recorder. The tape was played back in the laboratory. The signal was then clamped, peaks were rectified and filtered to give a lowpass waveform standardized between -1 and +1 Volts. This signal which is proportional to the momentary intensity of the field in the focal plane was then sampled at ~1800 Hz and converted to digital form using 9 bits. This did not quite give a sufficient dynamic range for the measurements. By looking at both high and low levels separately, it was possible to get the complete picture.
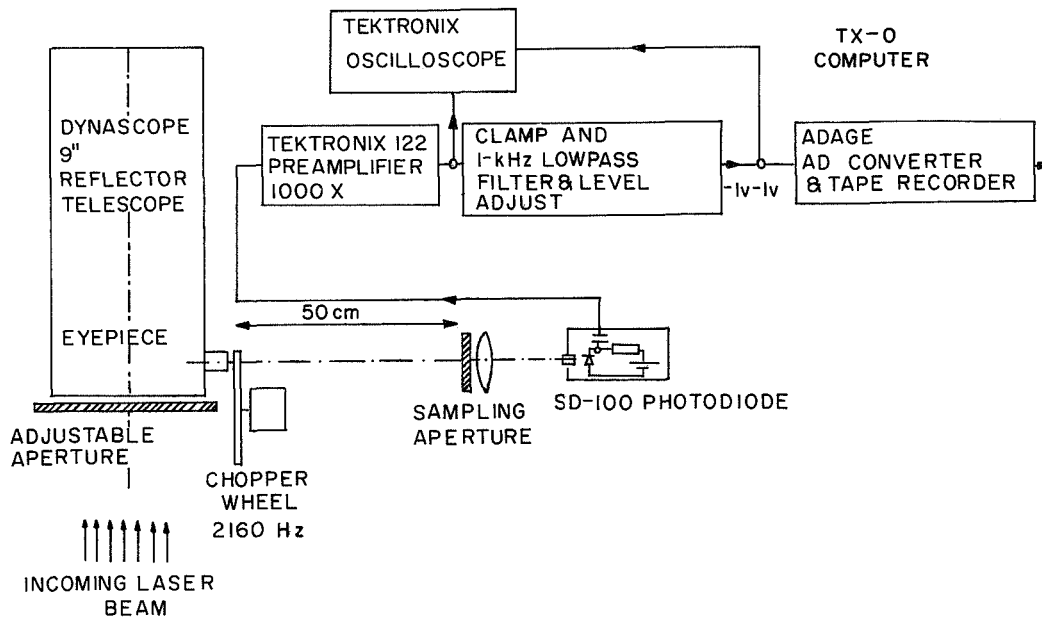
48

Fig. 4. Scheme for measuring intensity probability density
in the focal plane.

The measurements were done for four aperture sizes: 2.54 cm, 5.08 cm, 10.16 cm, and 20.32 cm. They were made on 30 May 1969, between 1 a.m. and 3 a.m. The weather data are the following.

Barometric Pressure	1001.8 mbar
Temperature	17.2 °C
Relative Humidity	84%
Wind Bearing	0° (N)
Wind Velocity	3.6 m/s
Velocity perpendicular to path	2.8 m/s

There is no easy quantitative way of measuring the coherence area. The coherent area was estimated subjectively as the largest aperture size that would still give a clean-looking Airy disc as its diffraction image. For somewhat larger apertures the pattern dissolves.

The measurements were carried out on a 3.8-km path between the top of the Green Building at M.I.T. in Cambridge and the roof of the Harvard Smithsonian Observatory on Garden Street, in Cambridge.

The transmitter was a Spectra-Physics Model 115 gas laser (He-Ne) working at 0.63-μm wavelength. The output power, ~1 mW, was collimated to form a beam with a 3-cm diameter. In this case, $\sqrt{\lambda L}$ = 4.8 cm, so that the collimated beam would be entering the far-field condition. This condition would be better satisfied by a smaller beam size. To make alignment less critical and to keep it more stable, it was necessary to defocus the beam a little so that the beam diameter at the receiver was approximately 3 m.
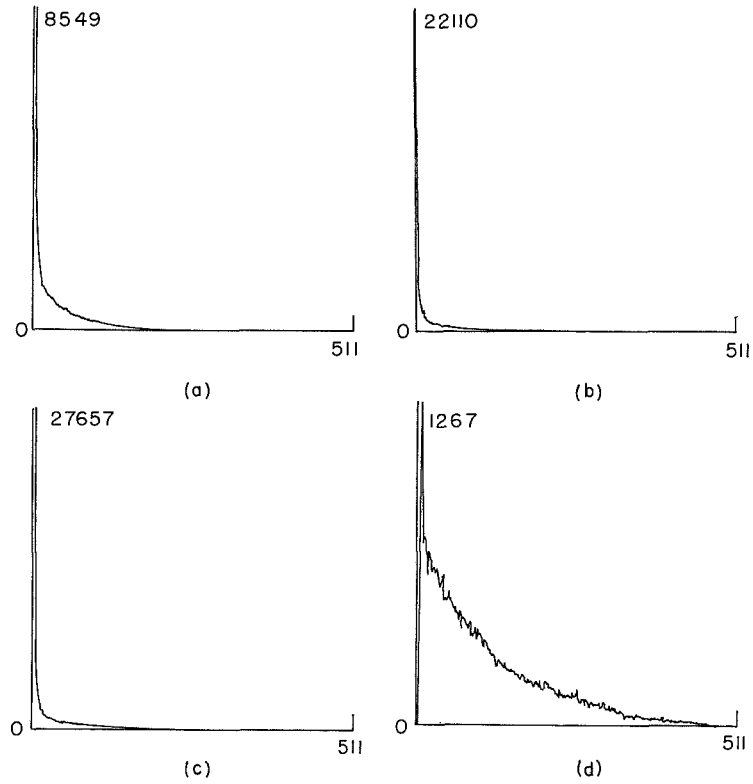
Fig. 5. Histogram of sampled focal plane intensity for aperture sizes:
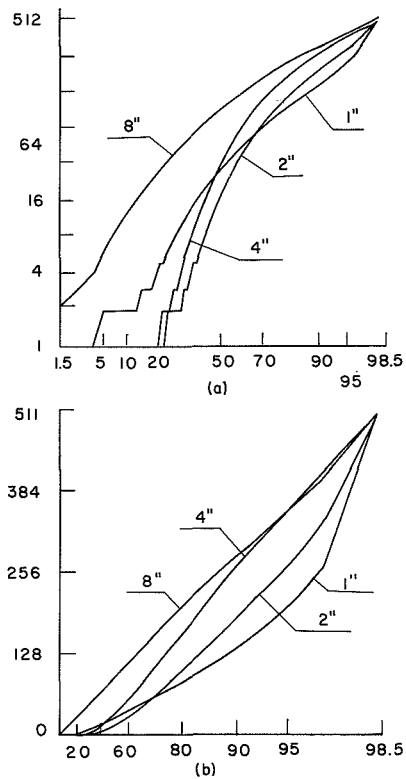(a) 2.54 cm; (b) 5.08 cm; (c) 10.16 cm; (d) 20.32 cm.

Fig. 6.

Focal plane sample distribution functions
plotted against (a) log-normal distribution
for 4 aperture sizes, (b) exponential dis-
tribution for 4 aperture sizes.

50

3.6.2 Results of Measurements

The results of the measurements are shown in the form of histograms in Fig. 5. The results for smaller aperture sizes show clearly the spiky nature of the probability distribution near zero intensity. This phenomenon will be explained in detail in Appendix C. To test the log-normal or exponential distribution hypothesis for the intensity, the distribution function was computed and properly transformed into a proper form so that the correct hypothesis would show in the display as a properly oriented straight line. The data were shown on a cathode-ray tube display and plotted by a Calcomp plotter. The data processing was initially done with the TX-0 computer, which had the proper interface with the Adage converter-recorder system. The histogram was then transmitted from the TX-0 computer to a PDP-1 computer using the link between these two computers of the Research Laboratory of Electronics. The PDP-1 computer had convenient floating point routines, CRT display, and graphic plotter.

Figure 6 shows the observed distribution functions plotted against the log-normal and exponential distributions. For the 1-in. aperture the tail of the distribution in Fig. 6a looks relatively linear up to the last plotting point, which is distorted by saturation. For larger apertures log-normality is less acceptable. Figure 6b indicates that the observed distribution approaches the exponential distribution as the aperture size grows. This observation agrees with the Central Limit theorem. For the largest part of the total probability the curves for the three smaller aperture sizes look parabolic. This fact is explained by the properties of the dancing Airy disc, as shown in Appendix C.

The effect of the moving Airy disc will become small for much smaller apertures than the smallest size (1 in.) that was used. In this case the result will be log-normal as shown in Appendix C. To avoid problems arising from low signal-to-noise ratio, very small apertures were not used. In all the cases observed the noise was negligible, that is, less than a quantization step.

The experimental results contribute to a very valuable understanding of the first-order statistics of the field in the focal plane. For small apertures the behavior is accounted for by the random motion of the diffraction pattern, because of fluctuating local wavefront tilt. Besides, the intensity suffers log-normal fading. This may cause very severe fading, as shown in the results discussed above. For apertures large compared with the coherence area the Central Limit theorem starts to work, and the intensity distribution becomes more and more exponential. It should be pointed out, however, that joint normality does not necessarily follow from the fact that the one-dimensional marginal distribution converges toward a normal distribution (and of course, its absolute square value converges toward an exponentially distributed value in distribution).

IV. OPTIMUM DETECTION OF LIGHT SIGNALS IN A
TURBULENT ATMOSPHERE

We have discussed the model of the field in detail. The field is modelled as a signal field (plane-wave) distorted by turbulence with an additive white-noise field. The turbulence causes log-normal amplitude fading and makes both amplitude and phase lose coherence at distances greater than the coherence radius of the field. The easiest representation turns out to be the sampling representation in which the samples are correlated. Orthogonal representations are also possible, although their statistical properties are hard to evaluate. The plane-wave representation coefficients approach Gaussian variables because of the Central Limit theorem. This has been shown to be true for the distribution of one coefficient distribution, but the behavior of the joint distributions is still unknown. For large apertures, however, the use of a Gaussian model of the field is of value in deducing the suboptimal receiver structures.

We shall start by discussing the detection of Gaussian signal fields in Gaussian noise

Table 7. Results of the detection of classical Gaussian fields in white Gaussian background noise.

Classical Gaussian Field	Smaller Apertures	Large Apertures $A_r \gg A_c$
Short Signals $T \ll \tau$	SP Figs. 10, 11 (149), (150) Spatial and temporal processors are separate	SP Figs. 13, 16, 17 (152), (153), (183), (184)
Intermediate Signals	SP General Case Figs. 7-9, 15 (142)-(146), (162)-(165)	
Long Signals $T \gg \tau$	Results of Price and Kennedy	SP Fig. 14 (159), (187) "Frozen atmosphere"

τ = field correlation time, A_r = receiver aperture area, A_c = field coherence area, S = receiver structure known (likelihood function ℓ_k evaluated), P = optimum performance known (error bound exponent E or error probability evaluated).

Table 8. Results of detection of classical log-normal fields in white Gaussian noise.

Classical Log-normal Field	Dependent Samples			Independent Samples
	Large Aperture $A_r \gg A_c$	Intermediate Aperture	Small Aperture $A_r \lesssim A_c$	
Strong Noise $\dfrac{Z^2 A_c}{N_o} = \alpha_p \ll 1$	SP (195) Gaussian model applicable (Sec. 4.1)	SP (195) Perturbation Expansion	SP Gaussian Model or One Sample	SP Results of Kennedy and Hoversten (209) (213) Figs. 20-22
Intermediate Noise	S	S Perturbation expansions either (195) or (204) One Sample	S	SP
Weak Noise $\dfrac{Z^2 A_c}{N_o} \gg 1$	S Fig. 19	S (204)	S One Sample	SP (214)

Short signals are assumed. S = structure known, P = performance known, $Z^2 A_c/N_o$ = energy-to-noise ratio on a coherence area. Open boundaries between blocks indicate that the respective blocks share some results.

53

fields. The analysis of the normal model is useful on two grounds. First, the representation coefficients of the field for large apertures are closely normal at least in their first-order statistic (cf. sec. 3.4). Second, the analysis, including the spatial aspects of the problem, can be easily carried out. The resulting receiver structure can be used as a suboptimum receiver, and is closely optimal for strong background noise.

The analysis of the detection of Gaussian fields in Gaussian noise parallels closely the analysis of the detection of Gaussian signals presented by Kennedy[1] and Van Trees.[70] The spatial aspect is involved in the interpretation of the results, and when eigenfunction solutions are required. The results are summarized in Table 7. The key equations and figures are indicated. When the signals are either very short or very long compared with the field correlation time and if, in particular, the receiver aperture is large compared with the coherence area of the field, more asymptotic results can be evaluated. Some numerical results are presented based on the assumed Gaussian field covariance function. The performance in this case is very closely optimal.

We shall use the log-normal model in a sampling representation. The structure and performance will be evaluated. Because this case is highly nonlinear and involved, simplifying assumptions have to be made about the independence of the samples to obtain detailed results. The results are summarized in Table 8. These results are related to the Gaussian results for the strong-noise case. The case of independent samples has

Table 9. Results of detection of quantized log-normal or Gaussian fields in or without white Gaussian (thermal) background noise.

Quantized Fields	General Case		Log-normal Field-Independent Samples
	Gaussian	Log-normal	
N ≫ 1 Classical Limit	Sec. 4.1. SP	Sec. 4.2.	Sec. 4.2. SP
Intermediate Case	SP (Liu) Figs. 23, 24 (225)-(228)	No	SP (234) (235)
N = 0 No Background	SP Figs. 23, 25 (230) Large Aperture (231)	Results	SP Fig. 26 (236) (237)

S = structure known, P = performance known.

been analyzed by Kennedy and Hoversten. An asymptotic result for small noise has been added.

Because of the prevalence of quantum noise in other than direct detection receivers without predetection bandpass filters, the quantum noise usually cannot be neglected. The detection problem is approached by using quantum models for the field. The results agree with the classical ones for high signal and noise fields. The key equations and figures are listed in Table 9. The Gaussian case, originally solved by Jane W. S. Liu, is discussed in some detail. The quantum log-normal case is solved only for independent samples. Some new results may be easily derived in the case of no background noise.

4.1 DETECTION OF GAUSSIAN SIGNAL FIELDS IN GAUSSIAN NOISE

4.1.1 Likelihood Functionals in the General Case

We shall consider the model of Fig. 2 with Gaussian fading instead of log-normal fading:

$$y(\vec{r}, t) = S_k(t) \, Zz(\vec{r}, t) + n(\vec{r}, t), \tag{126}$$

where $S_k(t)$ denotes the signal waveform with duration T and unit energy, corresponding to the message "k", Z denotes the scale factor, which accounts for the transmitter power level, path loss, and beam spread, $z(\vec{r}, t)$ denotes the normalized ($|z|^2 = 1$) slowly varying multiplicative fading (amplitude Rayleigh-distributed and phase uniformly distributed), $n(\vec{r}, t)$ denotes the spatially and temporally white Gaussian envelope noise with spectral density N_o (cf. sec. 2.3). This model is justified by previous discussions, except that the log-normality of z was changed to normality.

Denote $s_k(\vec{r}, t) = S_k(t) \, z(\vec{r}, t)$. This is a normal random variable with zero mean and the covariance

$$K_k(\vec{r}_1, t_1; \vec{r}_2, t_2) = s_k(\vec{r}_1, t_1) \, s_k^*(\vec{r}_2, t_2), \tag{127}$$

where the points $\vec{r}_1$ and $\vec{r}_2$ are assumed to be on the receiver aperture plane $\mathscr{A}_r$. The received signal can be represented in terms of a space-time orthogonal representation with uncorrelated coefficients, the Karhunen-Loève representation. The orthonormal functions $\phi_n^{(k)}(\vec{r}, t)$ satisfy the integral equation

$$\int_{\mathscr{A}_r} \int_T \int K_k(\vec{r}, t; \vec{r}', t') \, \phi_n^{(k)}(\vec{r}', t') \, d^2\vec{r}' dt' = \lambda_n^{(k)} \phi_n^{(k)}(\vec{r}, t) \tag{128}$$

with eigenvalues $\lambda_n^{(k)}$. Both the eigenfunctions and eigenvalues depend on the signal sent, k. The Gaussian signal field can now be developed in terms of these eigenfunctions:

$$s_k(\vec{r}, t) = \sum_{n=1}^{K} s_n^{(k)} \phi_n^{(k)}(\vec{r}, t), \tag{129}$$

where the signal field is expressed in terms of a signal vector $\underline{s}^{(k)}$ with uncorrelated Gaussian, hence independent, components. The number of eigenfunctions is assumed to be finite (degenerate case), but eventually $K \to \infty$ in the analysis. The noise field and the received field $y(\vec{r}, t)$ can also be expanded in terms of the functions $\phi_n^{(k)}(\vec{r}, t)$ with coefficient vectors $\underline{n}^{(k)}$ and $\underline{y}^{(k)}$. The vector components can be easily obtained because of the orthonormality of the functions $\phi_n^{(k)}(\vec{r}, t)$:

$$y_n^{(k)} = \int \int_{\mathscr{A}_r} \int_T y(\vec{r}, t) \, \phi_n^{(k)*}(\vec{r}, t) \, d^2\vec{r}\,dt \tag{130}$$

$$s_n^{(k)} = \int \int_{\mathscr{A}_r} \int_T s_k(\vec{r}, t) \, \phi_n^{(k)*}(\vec{r}, t) \, d^2\vec{r}\,dt \tag{131}$$

$$n_n^{(k)} = \int \int_{\mathscr{A}_r} \int_T n(\vec{r}, t) \, \phi_n^{(k)*}(\vec{r}, t) \, d^2\vec{r}\,dt. \tag{132}$$

The mean value and the variance of the signal and noise coefficients are

$$\overline{s_n^{(k)}} = 0, \quad \overline{\left| s_n^{(k)} \right|^2} = \lambda_n^{(k)} Z^2 \tag{133}$$

$$\overline{n_n^{(k)}} = 0, \quad \overline{\left| n_n^{(k)} \right|^2} = N_o. \tag{134}$$

Assume that the number of messages sent is M so that $k = 1, \ldots, M$. The field then is characterized by the vector y obtained by stacking the vectors $\underline{y}^{(k)}$ one above the other: $\underline{y}^T = (\underline{y}^{(1)T} : \underline{y}^{(2)T} : \ldots : \underline{y}^{(M)T})$, where T denotes matrix transposition, and : matrix partition.

To find the total probability density of the field, it is necessary to first define two densities $p_o^{(k)}$ and $p_1^{(k)}$. The density $p_o^{(k)}(\underline{y}^{(k)})$ assumes that the message sent, m, is different from k. Then the signal vector vanishes because of the assumed orthogonality of the signal set with respect to the channel.

$$p_o^{(k)}(\underline{y}^{(k)}) = \prod_{j=1}^{K} (\pi N_o)^{-1} \exp - \frac{\left| Y_j^{(k)} \right|^2}{N_o}. \tag{135}$$

The density $p_1^{(k)}(\underline{y}^{(k)})$ assumes that $k = m$. Then

$$p_1^{(k)}(\underline{Y}^{(k)}) = \prod_{j=1}^{K} \left(\pi \left(N_o + \lambda_j^{(k)} z^2 \right) \right)^{-1} \exp - \frac{\left| Y_j^{(k)} \right|^2}{N_o + \lambda_j^{(k)} z^2}. \tag{136}$$

The total probability density of the field, given that message m was sent, now becomes

$$p_{\underline{y}}(\underline{Y} \mid m) = p_1^{(m)}(\underline{Y}^{(m)}) \prod_{k \neq m} p_o^{(k)}(\underline{Y}^{(k)}). \tag{137}$$

Under the assumption that each of the signals m is equally likely, $m = 1, \ldots, M$, the minimum probability of error will be achieved by picking up that message which gives the largest probability density $p_{\underline{y}}(\underline{Y} \mid m)$. Instead of working with $p_{\underline{y}}(\underline{Y} \mid m)$ it is customary to divide it by $p_{\underline{y}}(\underline{Y} \mid 0)$, the probability density when none of the signals was sent. This ratio is called the likelihood ratio L_m corresponding to the signal m:

$$L_m = \frac{p_{\underline{y}}(\underline{Y} \mid m)}{p_{\underline{y}}(\underline{Y} \mid 0)} = \frac{p_1^{(m)}(\underline{Y}^{(m)})}{p_o^{(m)}(\underline{Y}^{(m)})}$$

$$= \prod_{j=1}^{K} \left(1 + z^2 \lambda_j^{(m)} \right)^{-1} \exp \frac{z^2 \lambda_j^{(m)} \left| Y_j^{(m)} \right|^2}{N_o \left(N_o + \lambda_j^{(m)} z^2 \right)}. \tag{138}$$

In addition to the likelihood ratio its logarithm, the likelihood function, is also useful

$$\ell_m = \ln L_m = \sum_{j=1}^{K} \left[\frac{z^2 \lambda_j^{(m)} \left| Y_j^{(m)} \right|^2}{N_o \left(N_o + \lambda_j^{(m)} z^2 \right)} - \ln \left(1 + \lambda_j^{(m)} z^2 \right) \right]. \tag{139}$$

The equivalent decision rule would be to compute ℓ_k for each k, and pick up that k as m, the message sent, for which ℓ_k is largest (see Fig. 1).

4.1.2 Optimum Receiver Structures

Figure 7 shows the structure of the optimum receiver, which mechanizes the operations in (139). It is assumed that the eigenvalues $\lambda_j^{(m)}$ do not depend on m. This receiver is called the "diversity form" of the optimum receiver structure. The receiver first computes the numbers $Y_j^{(m)}$ either by correlating the field against the eigenfunctions $\phi_j^{(m)}(\vec{r}, t)$ or by passing it through an array of corresponding space-time filters. The quantities $Y_j^{(m)}$ will then be passed through squarers and added in a diversity combiner network with weights c_j having the values
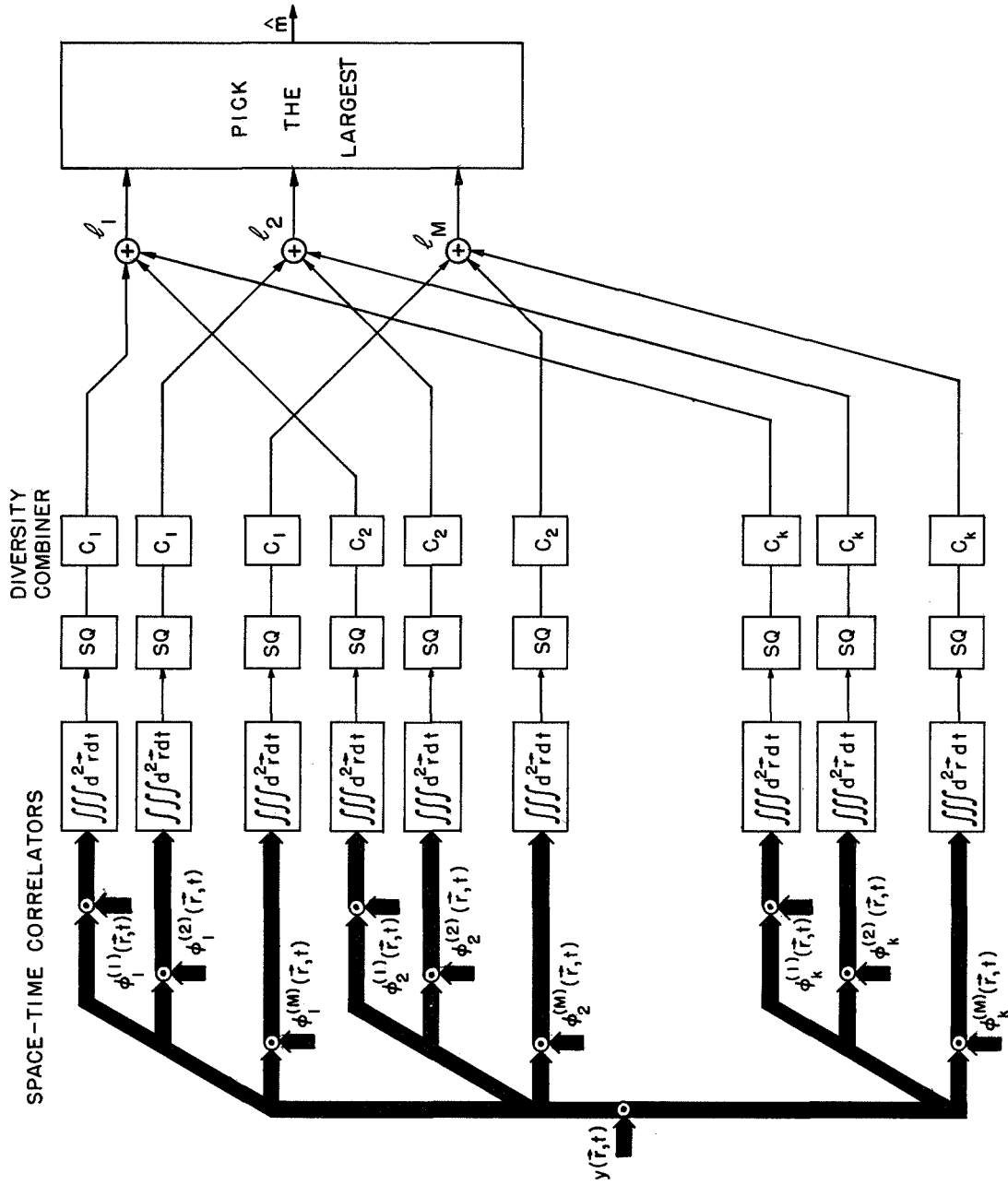
Fig. 7. Diversity form of the structure of an optimum receiver for a Gaussian field with additive white Gaussian noise. SQ = square law device, weights c_j from Eq. 140.

58

$$c_j = \frac{\lambda_j Z^2}{N_o\left(N_o + \lambda_j Z^2\right)} . \tag{140}$$

In addition to the diversity form of receiver structure there are, in analogy with the one-dimensional case (cf. Van Trees[70]), two other interesting realizations of the receiver structure. By recalling the definition of the vector component $Y_j^{(k)}$ in (130), it is obvious that the dependent part of the likelihood function ℓ_k' can be expressed in the following integral form:

$$\ell_k' = \frac{1}{N_o} \iiint_{\mathscr{A}_r T} y(\vec{r}, t)\, h_1^{(k)}(\vec{r}, t; \vec{r}', t)\, y^*(\vec{r}', t')\, d^2\vec{r}\, d^2\vec{r}'\, dt\, dt', \tag{141}$$

where the filter function $h_1^{(k)}$ is defined by the following expansion:

$$h_1^{(k)}(\vec{r}, t; \vec{r}', t') = \sum_{j=1}^{K} \frac{\lambda_j^{(k)} Z^2}{N_o + \lambda_j^{(k)} Z^2}\, \phi_j^{(k)}(\vec{r}, t)\, \phi_j^{(k)*}(\vec{r}', t'). \tag{142}$$

$h_1^{(k)}$ also satisfies the following integral equation, which is obtained by noticing that the coefficient in the eigenfunction expansion (142) satisfies the equation $h_j^{(k)}\left(N_o + \lambda_j^{(k)} Z^2\right) = \lambda_j^{(k)} Z^2$, and by replacing the vector coefficients in this equation by their definitions and by using the eigenfunction expansion for $K_k(\vec{r}, t; \vec{r}', t')$:

$$N_o h_1^{(k)}(\vec{r}, t; \vec{r}', t') + Z^2 \int_T \int \int_{\mathscr{A}_r} h_1^{(k)}(\vec{r}, t; \vec{r}'', t'')\, K_k(\vec{r}'', t''; \vec{r}', t')\, d^2\vec{r}''\, dt''$$

$$= Z^2 K_k(\vec{r}, t; \vec{r}', t'). \tag{143}$$

The operations of (141) lead to Fig. 8. This form of receiver structure is called an
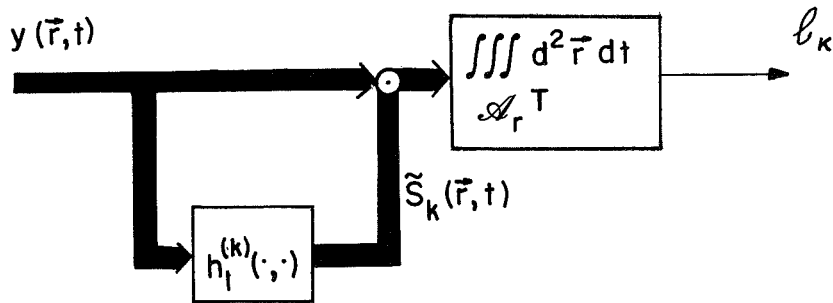

Fig. 8. Estimator-correlator receiver for Gaussian fields in white Gaussian noise.

59

estimator-correlator, because it forms an estimate of signal field, given that signal k was sent, and then correlates it against the actual field. No conjugation is present in Fig. 8, because in the block diagram the optical carrier is present, and the conjugation occurs automatically.

Because the filter function (142) is a positive operator when applied to the field, its square-root operator exists by the well-known results of functional analysis. The coefficients of the eigenfunction expansion of this square root are the square roots of the coefficients $h_j^{(k)}$. So denoting this new filter function by $h_f^{(k)}(\vec{r}, t; \vec{r}', t')$, we have

$$h_1^{(k)}(r, t; r', t') = \int_T \int_{\mathscr{A}} \int_r h_f^{(k)}(r, t; r'', t'') \, H_f^{(k)}(r'', t''; r', t') \, d^2r'' dt'' \tag{144}$$

$$h_f^{(k)}(\vec{r}, t; \vec{r}', t') = \sum_{j=1}^{K} \frac{Z\lambda_j^{(k)}}{N_o + Z^2\lambda_j^{(k)}} \, \phi_j^{(k)}(\vec{r}, t) \, \phi_j^{(k)^*}(\vec{r}', t'). \tag{145}$$

The likelihood function ℓ_k' can be expressed in terms of the filter function as follows

$$\ell_k' = \frac{1}{N_o} \iiint_{\mathscr{A}_r T} d^2r' \left| \iiint_{\mathscr{A}_r T} y(\vec{r}, t) \, h_f^{(k)}(\vec{r}', t'; \vec{r}, t) \, d^2\vec{r} dt \right|^2. \tag{146}$$

The receiver structure based on (146) is called a filter-squarer receiver. As shown in Fig. 9 it contains an array of filters, one for each signal, which filter the most relevant part of the incoming field with respect to that particular signal, then square and integrate over the receiver aperture and the signal duration.
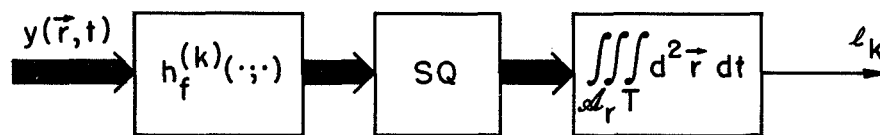

Fig. 9. Filter-squarer receiver for Gaussian fields in white Gaussian noise.

In order to interpret the receiver structures in Figs. 7-9 in terms of physical operations with hardware, the integral equations (128) or (143) ought to be solved. At the moment, progress can be made only in the case of very large apertures and either very short or very long signals compared with the correlation time of the field. We shall call the case of large apertures and very short signals the "short-signal" case, while the one with a large aperture and very long signals will be called the "long-signal" case. The field will be assumed to be homogeneous and stationary. The covariance function

K_k will still be nonstationary, and the filter function h_1 will be nonhomogeneous and non-stationary for any finite aperture and time interval. At the asymptotic case for large apertures and perhaps large time intervals Fourier transforms can be used to solve (128). Then the eigenfunctions become plane waves.

4.1.3 Receiver Structure for Short Signals

For short signals (for example, $T < 1$ ms) the fading can be assumed to be constant within the receiving interval. So we can set $z(\vec{r}, t) = z(\vec{r})$, and rewrite (127) as

$$K_k(\vec{r}_1, t_1; \vec{r}_2, t_2) = S_k(t_1) \, S_k^*(t_2) \, K_s(\vec{r}_1 - \vec{r}_2), \tag{147}$$

where $K_s(\cdot)$ is the field covariance function shown in (75), and (79). The eigenfunctions of the integral equation (128) factor into a product of the signal and a spatial eigenfunction

$$\phi_n^{(k)}(\vec{r}, t) = \psi_n(\vec{r}) \, S_k(t). \tag{148}$$

The likelihood function ℓ_k will now have the form

$$\ell_k = \sum_{j=1}^{K} \left[\frac{Z^2 \lambda_j \left| Y_j^{(k)} \right|^2}{N_o \left(N_o + \lambda_j Z^2 \right)} - \ln \left(1 + \lambda_j Z^2 \right) \right]. \tag{149}$$

The bias term is now independent of the signal, and hence has no influence on the decision. The simplification occurred because the eigenvalues no longer depend on the signal "k".

The integral form (141) now becomes

$$\ell_k' = \frac{1}{N_o} \iiint_{\mathscr{A}_r T} y(\vec{r}, t) \, S_k^*(t) \, h_1(\vec{r} - \vec{r}') \, S_k(t') \, y^*(\vec{r}', t') \, d^2\vec{r} \, d^2\vec{r}' dt dt'. \tag{150}$$

The estimator filter h_1 satisfies the following integral equation

$$N_o h_1(\vec{r}) + Z^2 \iint_{-\mathscr{A}_r} h_1(\vec{r}') \, K_s(\vec{r} - \vec{r}') \, d^2\vec{r}' = Z^2 K_s(\vec{r}) \tag{151}$$

where $-\mathscr{A}_r = \{\vec{r} : -\vec{r} \in \mathscr{A}_r\}$. It is known that the solution to the integral equation (151) exists and is unique, because its kernel is positive. The estimator-correlator and filter squarer realizations of the optimum receiver are shown in Figs. 10 and 11. In Fig. 10 the field is first correlated against the signal. Then the signal wavefront is estimated by using the optimum spatial estimator $h_1(\cdot)$. In Fig. 11 the signal wavefront is filtered by the optimum spatial filter $h_f(\cdot)$ and squared. Finally, the field is integrated over the whole aperture in both cases. It is obvious that in

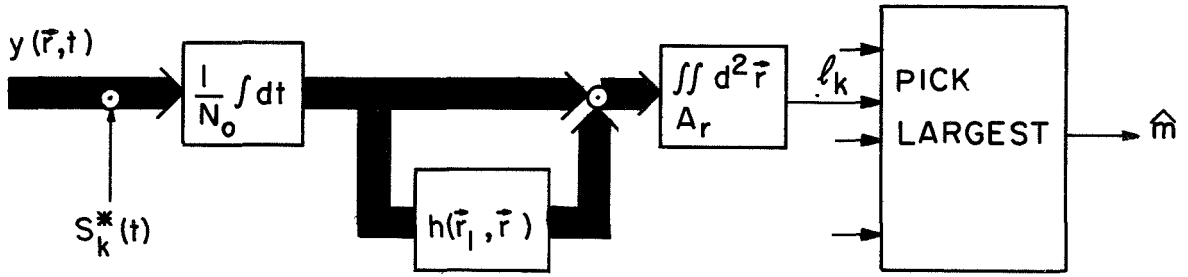Fig. 11 the spatial and the temporal filtering are commutative.

Fig. 10. One-shot estimator-correlator receiver for short signals. Field quantities are represented by thick lines.
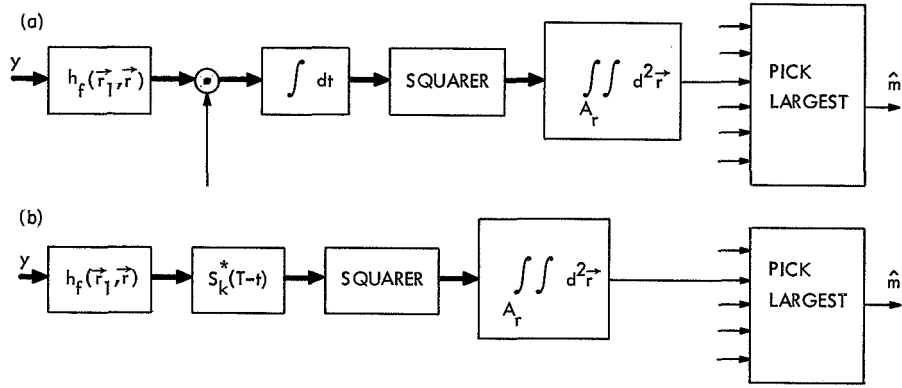

Fig. 11. One-shot filter-squarer receiver for short signals. Fading is assumed to be Gaussian. Alternatives are a) time correlator, and b) matched filter.

4.1.4 Case of Short Signals and Very Large Aperture

Equation 151 is easily solved for an infinite aperture by applying a two-dimensional Fourier transform. The transformed spatial estimator function $H_1(\vec{\kappa})$ then becomes

$$H_1(\vec{\kappa}) = \frac{Z^2 S_s(\vec{\kappa})}{N_o + Z^2 S_s(\vec{\kappa})}, \tag{152}$$

where $S_s(\vec{\kappa})$ is the wave-number spectrum of the field in the aperture. The transformed filter function $H_f(\vec{\kappa})$ is the square root of (152):

$$H_f(\vec{\kappa}) = \frac{Z^2 S_s(\vec{\kappa})}{N_o + Z^2 S_s(\vec{\kappa})}. \tag{153}$$
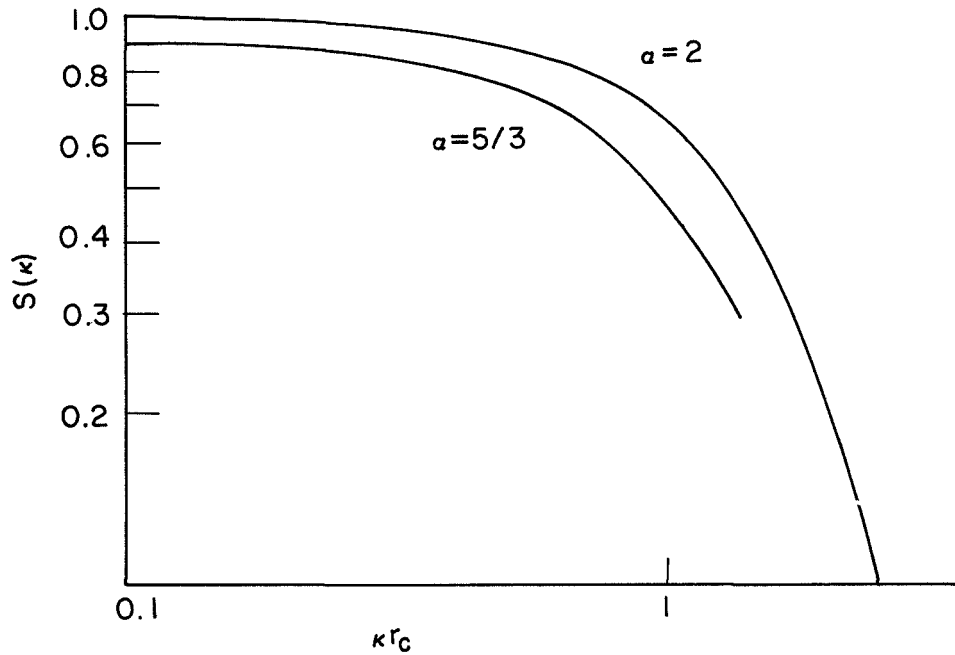
Fig. 12. Wave-number spectra corresponding to the covariance
function $K(\vec{r}) = \exp -\frac{1}{2}(r/r_c)^a$ for $a = 2$ and $a = 5/3$.

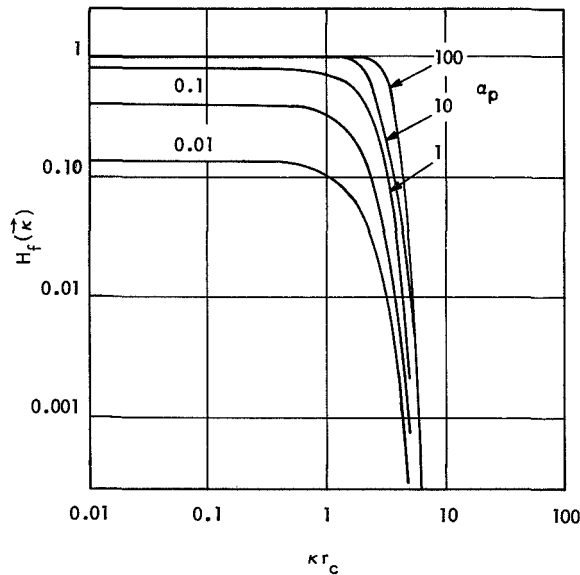
Fig. 13. Wave-number response of the optimum spatial filter
for Gaussian signal field with spatial covariance $K(\vec{r}) = \exp -\frac{1}{2}(r/r_c)^2$ in white Gaussian noise. $\left(a_p = Z^2 \pi r_c^2/N_o\right)$.

Figure 12 shows the wave-number spectra corresponding to the covariance function (79) for the values of $a = 2$ (Gaussian) and $a = 5/3$. It can be seen that the behavior of the wave-number spectra is roughly similar, so that the use of the Gaussian covariance function for the field is probably reasonable in this case.

The optimum spatial filter characteristics for different signal-to-noise ratios are shown in Fig. 13, the Gaussian covariance function being assumed. The wave number describes the direction of the incoming plane wave. The spatial filter limits the field of view so that most of the elementary signal wave components are passed through, while as much as possible of the uniform background radiation is excluded. The temporal filter (or correlation against the signal) similarly limits the frequencies accepted so that the signal is picked up, while the out-of-band noise is rejected. These operations of the optimum receiver are very natural and sensible, and should be remembered in designing any optical receivers to combat background noise. Obviously the function of the optimum spatial estimation or filtering functions $h_1(\cdot)$ and $h_f(\cdot)$ are the same for any size of aperture.

4.1.5 Receiver Structure for Long Signals and Large Aperture

For long signals ($T > 1$ s) and large apertures an asymptotic solution can be obtained to the integral equation (143) by using spatial and temporal Fourier transforms.

At this point we recall the concept of a "frozen atmosphere" introduced in section 2.1. The bulk of the temporal fluctuations are due to the wind blowing the turbulent blob pattern across the beam or wavefront. The following form of field covariance function will be assumed:

$$K(\vec{r}_1, t_1; \vec{r}_2, t_2) = \overline{z(\vec{r}_1, t_1)\, z^*(\vec{r}_2, t_2)}$$

$$= K_s(\vec{r}_1 - \vec{r}_2 + \vec{v}_n(t_1 - t_2)) \cdot K_t(t_1 - t_2), \tag{154}$$

where $K_s(\cdot)$ stands for the spatial covariance function (for $t_1 = t_2$), and $K_t(t_1 - t_2)$ describes the slow processes in the evolution of turbulence. This form of covariance obviously agrees with Eq. 13. It has to be considered as a first approximation only, and its usefulness is based on its simplicity. There is no theory nor are there any measurements that would prove or disprove the correctness of (154) beyond the fact that it agrees with the known and proved hypothesis of "frozen atmosphere."

To keep the analysis simple the signals are assumed to be sinusoidal.

$$S_k(t) = e^{i\omega_k t}/\sqrt{T}. \tag{155}$$

Then the covariance K_k turns out to be stationary.

$$K_k(\vec{r}_1, t_1; \vec{r}_2, t_2) = \frac{e^{i\omega_k(t_1 - t_2)}}{T} K_s(\vec{r}_1 - \vec{r}_2 + \vec{v}_n(t_1 - t_2)) K_t(t_1 - t_2). \tag{156}$$

Eventually the wave-number frequency spectrum of K_k will be needed:

$$S_k(\vec{\kappa}, \omega) = \frac{1}{T} \iiint e^{-i\vec{\kappa} \cdot \vec{\rho} - i\omega\tau} \, e^{i\omega_k\tau} \, K_s(\vec{\rho} + \vec{v}_n\tau) \, K_t(\tau) \, d^2\vec{\rho} \, d\tau$$

$$= \frac{1}{T} \int e^{i\vec{\kappa} \cdot \vec{v}_n} \, e^{-i(\omega - \omega_k)} \, K_t(\tau) \, d\tau \cdot S_s(\vec{\kappa})$$

$$= \frac{1}{T} \, S_s(\vec{\kappa}) \, S_t(\omega - \omega_k - \vec{\kappa} \cdot \vec{v}_n), \tag{157}$$

where $S_t(\omega)$ is the spectrum corresponding to the covariance $K_t(\tau)$. For an atmosphere that is really deeply "frozen" the spectrum $S_t(\omega)$ would be an impulse, for actual atmospheres may be less than 10 Hz wide. It probably also depends to some extent on the mixing properties of the cross wind $\vec{v}_n$. We shall assume that the wind blows completely horizontally or in the x direction. Its magnitude and direction may or may not be known. As is well-known the speed and direction of wind may vary significantly along the propagation path. In this analysis the wind is assumed to be uniform in the path with Gaussian distribution having mean zero and standard deviation v_o.

Application of Fourier transforms in the plane and time in (143) yields the following solution for the optimal estimating filter. Van Trees[70] has shown that this filter in fact gives the minimum mean-square (nonrealizable) estimate of distorted signal field.

$$H_1(i\vec{\kappa}, i\omega) = \frac{Z^2 S_k(\vec{\kappa}, \omega)}{N_o + Z^2 S_k(\vec{\kappa}, \omega)} \,. \tag{158}$$

Substituting (157), we have the following result for $H_1(i\vec{\kappa}, i\omega)$, the Fourier transform of the estimating filter:

$$H_1(i\vec{\kappa}, i\omega) = \frac{(Z^2/T) \, S_s(\vec{\kappa}) \, S_t(\omega - \omega_k - \vec{\kappa} \cdot \vec{v}_n)}{N_o + (Z^2/T) \, S_s(\vec{\kappa}) \, S_t(\omega - \omega_k - \vec{\kappa} \cdot \vec{v}_n)} \,. \tag{159}$$

The transform of the filter function $H_f(i\vec{\kappa}, i\omega)$ is the square root of this transform H_1.

Figure 14 shows a feedback realization of this estimating filter, although we realize
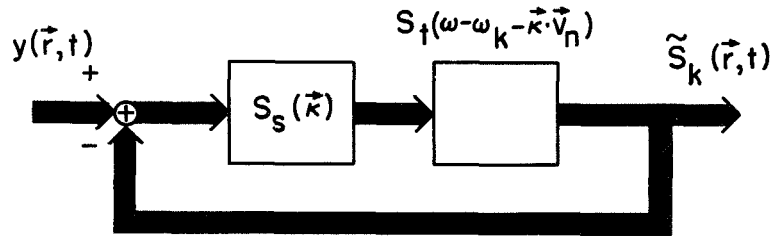

Fig. 14. Feedback realization of the optimum estimating filter for long signals. The signal angular frequency is ω_k, the cross-wind velocity is $\vec{v}_n$, and $\tilde{s}_k$ is the estimated signal field.

65

that there is little chance of building an optical feedback filter. It can be seen from Fig. 14 (or from Eq. 159) that the first section of the filter $S_s(\vec{\kappa})$ limits the field of view as in the small-signal case. The spatial frequencies can also be thought of as periodic spatial patterns. The vertical stripe pattern corresponding to the spatial frequency component κ_x is blown horizontally across the beam, thereby creating a Doppler shift in the plane-wave component diffracted into direction κ_x by that pattern. Obviously, the narrow-band filter S_t has to be shifted accordingly in frequency to avoid frequency cutoff of the signal. Unfortunately, this scheme requires knowledge of the exact or at least approximate value of the wind horizontal component.

It is worth noticing that the situation is anisotropic because the wind cannot be isotropic; it always blows in some favored direction. Again the operations of the optimum filter make a great deal of sense, although it must be admitted that it is probably very difficult to implement a receiver that treats the field according to (159).

4.1.6 Error Bounds and Reliability Functions

The performance of the optimum receiver for Gaussian fields in Gaussian white noise can be evaluated with a trivial modification of the methods developed before (cf. Price,[16b] Kennedy[1] or Van Trees[70]). The error probability is expressed in terms of the eigenvalues λ_j, which do not depend on the dimension or form of the corresponding eigenfunctions. The following general bounds are due to Kennedy.[1] Exact evaluation of error probabilities is hopelessly complicated.

The probability of error of the optimum receiver can be bounded above and below as

$$K_1 2^{-TCE} \leqslant P(\epsilon) \leqslant K_2 2^{-TCE}. \tag{160}$$

Here the quantity T is the signal length, C the channel capacity, E the error exponent, and K_1, K_2 slowly changing functions as compared with the exponential part of the expressions. The channel capacity is equal to the well-known infinite-bandwidth Gaussian channel capacity that is due to Shannon:

$$C = A_r Z^2 / (N_0 \ln 2), \qquad [C] = bits/s$$

$$= 1.44 \, aA_r/T, \qquad (1.44 \, aA_r/T), \tag{161}$$

where $a = Z^2 T / N_0$ is the energy-to-noise ratio on the average per transmission and receiver area. The error exponent is a function of the information rate $R = \log_2 M/T$, where $[R] = bits/s$. The relationship can be expressed in parametric form:

$$E = s\gamma'(s) - \gamma(s), \qquad -\frac{1}{2} \leqslant s \leqslant 0$$

$$\frac{R}{C} = (1+s) \, \gamma'(s) - \gamma(s), \tag{162}$$

where

$$\gamma(s) = -\frac{1}{A_r^a} \sum_{j=1}^{K} (\ln(1-sa\lambda_j) + s\ln(1+a\lambda_j)). \qquad (163)$$

The coefficients K_1 and K_2 are slowly varying, as is obvious from the relationships

$$K_1 = \frac{1}{64} e^{-A_r a/|s|}; \qquad K_2 = 2. \qquad (164)$$

Figure 15 shows the function $E = E(R)$, the "reliability" function of the channel for the optimum receiver. The top curve shows the reliability of a constant channel with white Gaussian noise, while the lower curve shows the optimum reliability for the Gaussian field in Gaussian noise (Kennedy[71]). The reliability curves start linearly with slope -1 at $R/C = 0$, so that the initial exponent $E(0) = -2\gamma(-.5)$. The linear part has $s = -.5$. The curved part starts at $R_{crit} = C(\gamma'(-.5)/2 - \gamma(-.5))$. The curved part ends at $s = 0$, where $\gamma(s) = 0$, $E = 0$, and $R = C\gamma'(0)$. It is easy to see that $\gamma'(0) \to 1$ for $a \to \infty$. It has been shown by Pierce[72] and by Kennedy that asymptotically the best performance is obtained for an equal strength diversity system, which has K equal eigenvalues $\lambda_j = 1/K$. The energy-to-noise ratio in a diversity path per transmission a_p has an optimum value for any rate a_p^o, for which the error exponent is largest. For very small rates the value $a_p^o = 3.07$, and the optimum diversity $D = K = A_r a/a_p^o$. The resulting error exponent for zero rate in this case is $E^o(0) = 0.149$. In the majority of cases it is not
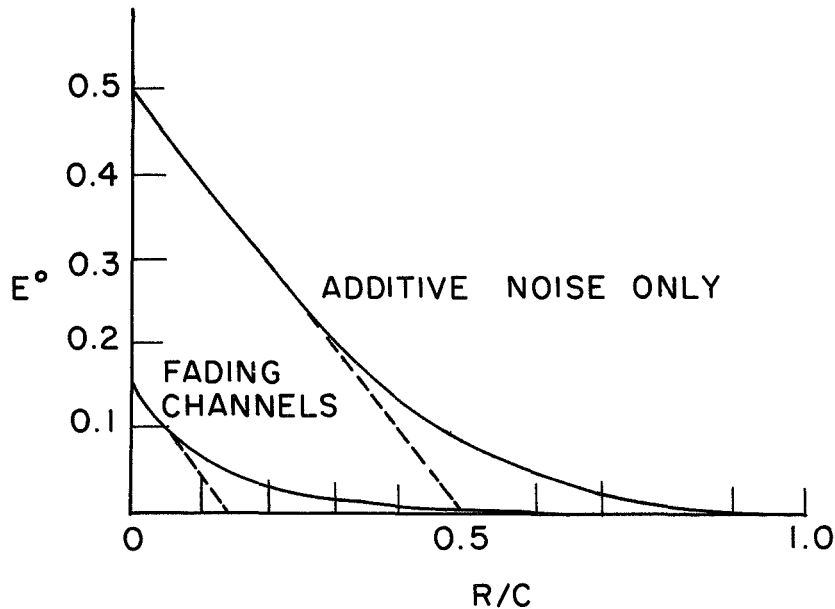

Fig. 15. Optimum error exponent $E^o(R)$ for constant and fading Gaussian channels (after Kennedy[71]) as a function of relative information rate R/C compared with the channel capacity.

possible, however, to control the eigenvalues sufficiently (by signal design, for example) to make them equal. Examples have been found (Kennedy[73]) that show very closely optimum performance even for simple signals in systems having unequal eigenvalues.

There are other ways of expressing the error bounds such as in terms of β, the average energy-to-noise ratio per information bit. The number of information bits per transmission is $\nu = \log_2 M$; hence,

$$\beta = A_r a / \nu. \tag{165}$$

Then the error bounds (160) have the equivalent form

$$K_1 2^{-\nu E_b} \le P(\epsilon) \le K_2 2^{-\nu E_b}, \tag{166}$$

where

$$E_b = \frac{C}{R} E = \frac{\beta E}{\ln 2}. \tag{167}$$

The error exponent can be obtained in an equivalent, but slightly different, format by using methods similar to those for obtaining random-coding bounds (Gallager[74]). The error exponent E then has the form

$$E = \max_{0 \le \rho \le 1} (E(\rho) - \rho R / C), \tag{168}$$

where

$$E(\rho) = -\frac{(1+\rho)}{A_r a} \ln \left[\int p_1^{1/(1+\rho)}(\underline{Y}) \, p_o^{\rho/(1+\rho)}(\underline{Y}) \prod_{j=1}^{K} d^2 Y_j \right], \tag{169}$$

where $d^2 Y_j = d(\text{Re}\{Y_j\}) \, d(\text{Im}\{Y_j\})$. It can be shown by using the densities $p_0(\underline{Y})$ and $p_1(\underline{Y})$ defined in (135) and (136) that

$$E(\rho) = \frac{1}{A_r a} \sum_{j=1}^{K} \left[(1+\rho) \ln \left[1 + \frac{\rho a \lambda_j}{(1+\rho)} \right] - \rho \ln (1 + a \lambda_j) \right]. \tag{170}$$

This expression agrees with (162) together with (163) when the substitution $s = \rho/(1+\rho)$ is made. The bit error exponent in terms of $E(\rho)$ becomes

$$E_b = \max_{0 \le \rho \le 1} \left[\frac{\beta E(\rho)}{\ln 2} - \rho \right]. \tag{171}$$

4.1.7 Reliability Function for Short Signals and Large Aperture

The error bounds (160) and (166) are the most important tools available for judging the performance of Gaussian channels when the information rate, signal characteristics,

and channel characteristics are given. Next, error bounds will be evaluated for the optimum receiver when $K(\vec{r}) = \exp -\frac{1}{2}(r/r_c)^2$. This is, in fact, too difficult to do for any aperture size. Only the asymptotic result for very large apertures will be discussed here. It turns out that the performance of the optimum receiver agrees very closely with the best possible performance, $E^o(0) = 0.15$.

The first task ahead is to find a way of evaluating an asymptotic expression of a, the logarithm of the Fredholm determinant

$$\ln D_{\mathscr{F}}(z) = \sum_{j=1}^{K} \ln(1+z\lambda_j). \tag{172}$$

For large apertures the eigenvalues are very close to the values of the wave-number spectrum. In fact, for small enough z

$$\ln(1+z\lambda_j) = \sum_{k=1}^{\infty} (-z)^k \frac{\lambda_j^k}{k}. \tag{173}$$

Because of the orthonormality of the spatial eigenfunctions $\psi_n(\vec{r})$ (cf. Eq. 148) the sum of the powers of eigenvalues can be expressed as follows:

$$\sum_{j=1}^{K} \lambda_j^k = \sum_{j=1}^{K} \int\int \dots \int_{\mathscr{A}_r} \lambda_j \psi_j(\vec{r}_1) \psi_j^*(\vec{r}_1) \dots \dots \lambda_j \psi_j(\vec{r}_k) \psi_j^*(\vec{r}_k) d^2\vec{r}_1 \dots d^2\vec{r}_k$$

$$= \int\int \dots \int_{\mathscr{A}_r} K(\vec{r}_1,\vec{r}_k) \dots K(\vec{r}_3,\vec{r}_2) K(\vec{r}_2,\vec{r}_1) d^2\vec{r}_1, \dots, d^2\vec{r}_k$$

$$= \int \int_{\mathscr{A}_r} K_k(\vec{r},\vec{r}) d^2\vec{r}, \tag{174}$$

where the eigenfunction expansion of the covariance function is used to give the result in terms of K_k, the k times iterated kernel. This familiar result from the theory of integral equations can be expressed in terms of the wave-number spectrum, as shown by Kennedy.[1] For apertures that are large compared with the coherence distance $K_k(\vec{r},\vec{r}) \approx K_k(0,0)$, except close to the edges. On the other hand, $K_k(\vec{r}_1,\vec{r}_2) \approx K_k(\vec{r}_1-\vec{r}_2)$ in the center area of the aperture, so that the wave-number spectrum $S_k(\vec{\kappa})$ exists. Then

$$\sum_{j=1}^{K} \lambda_j^k \cong A_r K_k(0) = A_r(2\pi)^{-2} \int\int_{-\infty}^{\infty} S_k(\vec{\kappa}) d^2\vec{\kappa} = A_r(2\pi)^{-2} \int\int S^k(\vec{\kappa}) d^2\vec{\kappa}. \tag{175}$$

The series (173) has convergence radius λ_j^{-1}. Assuming that λ_1 is the largest

eigenvalue, we have for $|z| < \lambda_j^{-1}$

$$\ln D_{\mathscr{F}}(z) \to \sum_{k=1}^{\infty} \frac{(-z)^k}{k} A_r \iint S^k(\vec{\kappa}) \frac{d^2\vec{\kappa}}{(2\pi)^2}$$

$$= A_r \iint_{-\infty}^{\infty} \ln (1+zS(\vec{\kappa})) \frac{d^2\vec{\kappa}}{(2\pi)^2}. \tag{176}$$

By analytic continuation this relationship is true for all z. The convergence as $A_r \to \infty$ can be easily proved in a rigorous way (cf. Gallager[75]).

The wave-number spectrum $S(\vec{\kappa})$ in this case is

$$S(\vec{\kappa}) = \iint_{-\infty}^{\infty} \exp -\frac{1}{2}(r/r_c)^2 \, d^2\vec{r} = 2\pi r_c^2 \exp -(\kappa r_c)^2/2. \tag{177}$$

Call $\pi r_c^2 = A_c$ the coherent area. Then for large A_r asymptotically

$$A_r^{-1} = \ln D_{\mathscr{F}}(z) = \iint_{-\infty}^{\infty} \ln \left[1 + 2zA_c \exp -\frac{1}{2}(\kappa r_c)^2 \right] \frac{d^2\vec{\kappa}}{(2\pi)^2}. \tag{178}$$

Next transform into polar coordinates and set $2zA_c \exp -\frac{1}{2}(\kappa r_c)^2 = t$. Then

$$A_r^{-1} \ln D_{\mathscr{F}}(z) = \frac{1}{2A_c} \int_0^{2zA_c} \frac{\ln (1+t)}{t} \, dt$$

$$= \frac{-1}{2A_c} \mathrm{Li}_2(-2zA_c), \tag{179}$$

where $\mathrm{Li}_2(\cdot)$ stands for the function dilogarithm

$$\mathrm{Li}_2(z) = -\int_0^z \frac{\ln (1-t)}{t} \, dt. \tag{180}$$

Tables of this function are given by Lewin[76] and by Abramowitz and Stegun.[77]

By using the logarithm of the Fredholm determinant the error exponent $E(\rho)$ defined in (170) can be readily evaluated.

$$E(\rho) = \frac{\rho}{2\alpha_p} \mathrm{Li}_2(-2\alpha_p) - \frac{(1+\rho)}{2\alpha_p} \mathrm{Li}_2\left(-\frac{2\rho\alpha_p}{1+\rho}\right), \tag{181}$$

where $D_i = A_r/A_c$ is the inherent diversity of the field (67), while $\alpha_p = \alpha/D_i$ is the energy-to-noise ratio per inherent diversity path. The zero-rate error exponent is obtained by setting $\rho = 1$. Then
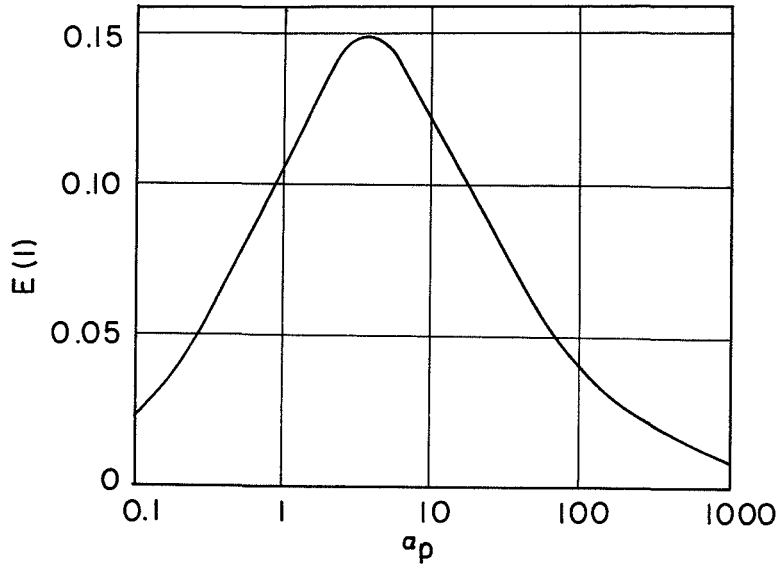
70

Fig. 16. Zero-rate error exponent E(1) from (182) as a function of a_p, the energy-to-noise ratio per diversity path, for Gaussian fields with Gaussian covariance function and short signals.
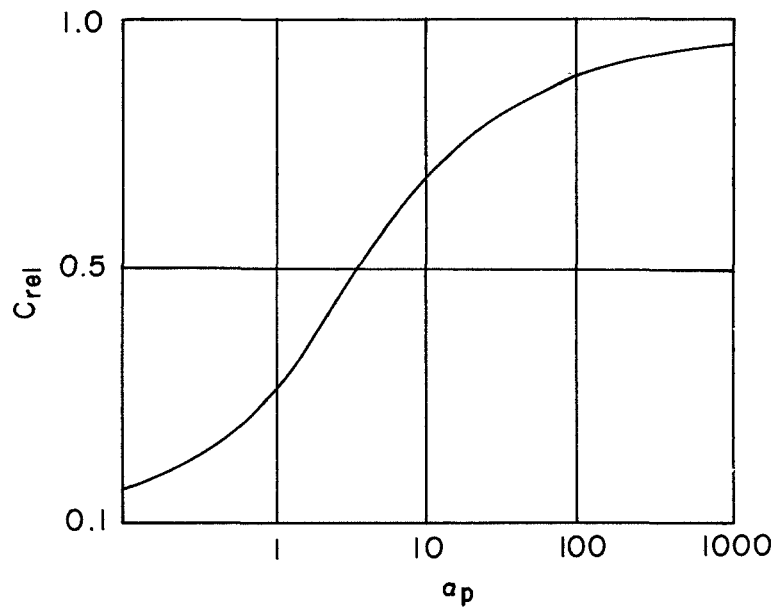

Fig. 17. Relative channel capacity for Gaussian fields with Gaussian covariance function and short signals (Eq. 184).

$$E(1) = \frac{1}{2a_p} \left[Li_2(-2a_p) - 2Li_2(-a_p) \right].$$ (182)

This exponent is shown in Fig. 16 as a function of a_p. It is seen to peak at $a_p \approx 4.0$ and the maximum value turns out to be 0.15, the theoretical optimum. In the same way Kennedy[73] has shown that for each ρ there is an optimum a_p. For rates close to capacity the error exponent has the following asymptotic form:

$$E(R) \to \frac{1}{a_p} \left[1 - \frac{R}{C} + \frac{Li_2(-2a_p)}{2a_p} \right]^2.$$ (183)

The channel capacity compared with the ideal value C equals

$$C_{rel} = 1 - \frac{(-Li_2(-2a_p))}{2a_p}.$$ (184)

This function is displayed in Fig. 17 as a function of a_p. For large signal-to-noise ratios in a diversity path it tends toward one. This behavior was thoroughly demonstrated by Kennedy.[78] Because the behavior of the wave-number spectrum for the covariance function $K(\vec{r}) = \exp -\frac{1}{2} (r/r_c)^{5/3}$ is very similar to the Gaussian spectrum, the behavior of error exponents also has to be very similar.

4.1.8 Reliability Function for Long Signals and Large Aperture

Somewhat similar results are available in the case of long signals. The logarithm of the Fredholm determinant will be different in this case. By using (147) and (158) in (157) and by using the obvious generalization of (179) this logarithm is brought to the following form:

$$\ln D_{\mathscr{F}}(z) = A_r T \int\!\!\int\!\!\int_{-\infty}^{\infty} \ln \left(1 + \frac{z}{T} S_s(\vec{\kappa}) S_t(\omega - \omega_k - \vec{\kappa} \cdot \vec{v}_n) \right) \frac{d^2\vec{\kappa}\, d\omega}{(2\pi)^3}.$$ (185)

Now introduce new variables $x_1 = \kappa_x r_c$, $x_2 = \kappa_y r_c$, $x_3 = (\omega - \omega_k - \kappa_x v_n)\tau_o$. Then, because of the symmetry of the integrand, another transformation into spherical coordinates can be made.

$$\ln D_{\mathscr{F}}(z) = \frac{A_r T}{\tau_o r_c^2} \int\!\!\int\!\!\int_{-\infty}^{\infty} \ln \left[1 + \frac{z(2\pi)^{1.5} r_c^2 \tau_o}{T} \exp\left(-\frac{x_1^2 + x_2^2 + x_3^2}{2} \right) \right] \frac{dx_1 dx_2 dx_3}{(2\pi)^3}$$

$$= \frac{A_r T}{(2\pi)^3 \tau_o r_c^2} 4\pi \int_0^{\infty} x^2 \ln \left[1 + z'2^{-\frac{1}{2}x^2} \right] dx,$$ (186)

72

where $z' = z(2\pi)^{1.5} r_c^2 \tau_o/T$. By expanding the integrand into a series that converges uniformly for $|z'| < 1$, after integration we have

$$\ln D_{\mathscr{G}}(z) = \frac{A_r T}{(2\pi)^{1.5} \tau_o r_c^2} \sum_{k=1} (-1)^{k-1} \frac{z'^k}{k^{2.5}}$$

$$= \frac{A_r T}{(2\pi)^{1.5} \tau_o r_c^2} (-\text{Li}_{2.5}(-z')) \tag{187}$$

because the series above defines the polylogarithm for $|z'| < 1$. By analytic continuation, the relationship (187) holds for all z', or z. The polylogarithm $\text{Li}_n(\cdot)$ is usually defined only for integers n, such as "dilogarithm" for $n = 2$ and "trilogarithm" for $n = 3$. In this case $n = 5/2$. A closely related function has been tabulated by McDougall and Stoner.[79] A rough idea of the behavior of $\text{Li}_{2.5}(\cdot)$ can be obtained by looking up Lewin's Tables for Li_2 and Li_3, and by interpolating. The error exponent now becomes

$$E(\rho) = \frac{1}{2a_p} \left[\rho \text{Li}_{2.5}(-2a_p) - (1+\rho) \text{Li}_{2.5}\left(-\frac{2\rho a_p}{1+\rho}\right) \right], \tag{188}$$

where the inherent diversity is taken to be $D_i = A_r T/\sqrt{2\pi} A_c \tau_o$, and $a_p = aA_r/D_i$. The bounds (160) and (166) are to be used with this reliability function $E(\rho)$. For example, the zero-rate error exponent is shown in Fig. 18. The behavior of this function is very similar to that in (181), but the exact numbers are different.
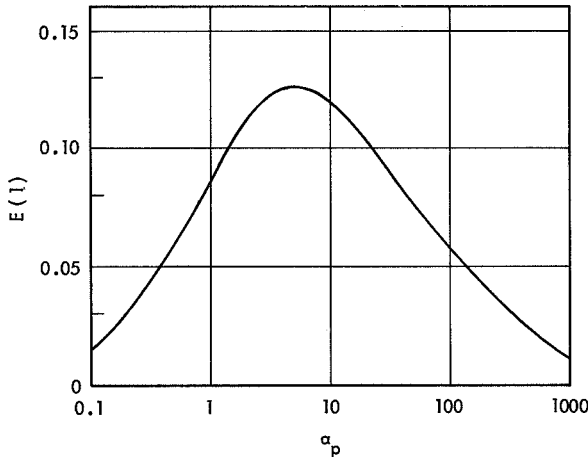
Fig. 18.
Zero-rate error exponent $E(1)$ from Eq. 188 as a function of a_p, the energy-to-noise ratio per diversity path, for Gaussian fields with Gaussian covariance function and long signals.

The performance of the optimum receiver for long T and short T has been found to be asymptotically very similar to that of the optimum case discussed by Kennedy,[1] under the assumption of equal eigenvalues. This performance can be achieved by using a complicated receiver, which processes the field in space and time in a manner that in most cases is not realizable with present technology.

4.2 DETECTION OF LOG-NORMAL FIELDS IN GAUSSIAN NOISE

4.2.1 Statement of the Problem

The log-normal statistics of a signal field when combined with a Gaussian white-noise field lead to a difficult nonlinear detection problem. Complete solution of this problem is, at present, out of sight. The general problem of finding the likelihood function will now be outlined, and then this function will be evaluated for the three special cases of strong noise, very weak noise, and independent samples. Sampling representation will be used throughout. Optimum receiver structures will be discussed in these three cases, then error performance will be evaluated whenever possible. Case 3 has been previously discussed by Kennedy and Hoversten.[22]

The likelihood ratio is obtained as in (127) by dividing $p_1^{(m)}(\underline{Y}^{(m)})$ by $p_0^{(m)}(\underline{Y}^{(m)})$. The density p_0 when the signal is absent is the same as before (see Eq. 124). The probability density p_1, however, is difficult to evaluate. We shall give some results on the form of p_1 in cases 1-3.

Short signals will be assumed. The field is modelled as follows:

$$y(\vec{r},t) = Zz(\vec{r})\,S_k(t) + n(\vec{r},t), \tag{189}$$

given that the signal k was sent. The vector coefficient in time is obtained by correlating (189) against $S_k(t)$. In spatial sampling representation we have

$$y_k(\vec{r}_j) = Zz(\vec{r}_j) + n_k(\vec{r}_j), \tag{190}$$

where $j = 1, \ldots, K$, and $k = 1, \ldots, M$. Here it is assumed that the spatial spectrum of the noise is somehow sharply limited to wave numbers $|\kappa_x| < \kappa_o$, $|\kappa_y| < \kappa_o$. The difference between adjacent sampling points is horizontally $\Delta x = \pi/\kappa_o$, and vertically $\Delta y = \pi/\kappa_o$. The variance of the samples $n_k(\vec{r}_j)$ is obviously

$$\left|n_k(\vec{r}_j)\right|^2 = N_o \kappa_o^2/\pi^2 = N_o/\Delta^2 \vec{x}, \tag{191}$$

where $\Delta^2 \vec{x} = \Delta x \Delta y = \pi^2/\kappa_o^2$. This notation helps us to notice when some expressions can be replaced by integrals. The density of $Y = \ln z$ is given by (68). Because the background noise is independent of the fading, the probability density of the vector $\underline{Y}^{(k)} = \{y_k(\vec{r}_j)\}$ is obtained by forming the convolution of the densities of z and n_k. In other words,

$$p_1(\underline{Y}^{(k)}) = \left(\frac{\Delta^2 \vec{x}}{N_o}\right)^K \prod_{j=1}^{N} \exp\left[-\frac{\Delta^2 \vec{x}}{N_o}\left|y_k(\vec{r}_j) - Zz(\vec{r}_j)\right|^2\right], \tag{192}$$

where the average is to be taken over $z(\vec{r}_j)$. It should be remembered at this point that the samples $z(\vec{r}_j)$ are in general dependent on each other. The dummy hypothesis p_o comes from (124), which is obtained from (192) simply by setting $Z = 0$. It does not depend on z. Hence, by dividing p_1 by p_o, we have

$$L_k = \prod_{j=1}^{K} \overline{\exp \frac{\Delta^2 \vec{x}}{N_o} \left(Z\left(y_k(\vec{r}_j) z^*(\vec{r}_j) + y_k^*(\vec{r}_j) z(\vec{r}_j) \right) - Z^2 |z(\vec{r}_j)|^2 \right)} \tag{193}$$

4.2.2 Strong-Noise Case

The first method used to evaluate the average in (193) is to develop the exponential in terms of a series and then use the results (80) and (85) of the moments of z and z^*. This approach works best for the case when noise is large so that the expansion would converge rapidly. The expansion is carried up to the fourth power of N_o^{-1}. In averaging, only terms that are of the same degree in terms of both z and z^* survive, which helps to simplify the result

$$L_k = 1 - \frac{Z^2 \Delta^2 \vec{r}}{N_o} \overline{\underline{z}^T \underline{z}^*} + \frac{Z^2 (\Delta^2 \vec{r})^2}{2! N_o^2} \left(2\underline{y}^T \overline{\underline{z}^* \underline{z}^T} \underline{y}^* + Z^2 \overline{(\underline{z}^T \underline{z}^*)^2} \right)$$

$$- \frac{Z^4 (\Delta^2 \vec{r})^3}{3! N_o^3} \left(6\underline{y}^T \overline{(\underline{z}^* \underline{z}^T)^2} \underline{y}^* + Z^2 \overline{(\underline{z}^T \underline{z}^*)^3} \right) + \frac{Z^4 (\Delta^2 \vec{r})^4}{4! N_o^4} \left(6\overline{(\underline{y}^T \underline{z}^*)^2 (\underline{z}^T \underline{y}^*)^2} \right.$$

$$\left. + 12 Z^2 \underline{y}^T \overline{(\underline{z}^* \underline{z}^T)^3} \underline{y}^* + Z^4 \overline{(\underline{z}^T \underline{z}^*)^4} \right) + 0\left(N_o^{-5} \right), \tag{194}$$

where the matrix notation $\underline{z}^T = (z(\vec{r}_1), \ldots, z(\vec{r}_K))$, $\underline{y}^T = (y(\vec{r}_1), \ldots, y(r_K))$ is used.

It is useful to introduce the matrix $\underline{Z} = \underline{z}^* \underline{z}^T$, and the sum of squares over the aperture $e_s = \underline{z}^T \underline{z}^* \Delta^2 \vec{r}$. The latter is obviously related to the instantaneous energy flowing through the aperture during time T. Also, it is easy to show by direct matrix multiplication that $\underline{Z}^2 = \underline{Z} e_s$. The average value of $\underline{Z}$ is obviously the correlation matrix of the field $\overline{\underline{Z}} = \underline{K}$. By using the notation that has been introduced, the likelihood function can be expressed as

$$\ell_k = \sum_{j=1}^{4} \frac{c_j (-Z^2)^j}{j! N_o^j} + \frac{Z^2 (\Delta^2 \vec{r})^2}{N_o^2} \underline{y}^T \left[\underline{K} - \frac{Z^2}{N_o} (\overline{\underline{Z} e_s} - \underline{K}(\overline{e}_s)) \right.$$

$$\left. + \frac{Z^4}{2N_o^2} \left(\overline{\underline{Z} e_s^2} - \underline{K}(\overline{e}_s)^2 - 2\overline{\underline{Z} e_s}(\overline{e}_s) \right) \right] \underline{y}^*$$

$$+ \frac{Z^4 (\Delta^2 \vec{r})^4}{4N_o^4} \sum_{j,k,l,m=1}^{K} (K_{jklm} - K_{jl} K_{km} - K_{jm} K_{kl}) y_j y_k y_l^* y_m^* + 0\left(N_o^{-5} \right), \tag{195}$$

75

where K_{jm} is the $(jm)^{th}$ entry of the covariance matrix K, and where $K_{jklm} = \overline{z_j^* z_k z_l^* z_m}$, the fourth-order covariance function of the field $z(\vec{r})$. All four sums run from 1 to K. Furthermore, c_j, $j = 1, \ldots, 4$ are the first four cumulants (semi-invariants) of e_s.

The first term in (196) is a constant bias term, which does not affect the receiver structure. The second term is of the form const $\cdot \underline{y}^T \underline{K}' \underline{y}^*$ and stands for a linear filtering operation. In fact, if $z(\vec{r})$ is Gaussian, it is easy to see by evaluating the averages involved, that $\underline{K}' = \left(\underline{1} + 2Z^2 \Delta^2 \vec{r} \underline{K}/N_o\right)^{-1} 2Z^2 \Delta^2 \vec{r} \underline{K}/N_o$ is the optimum linear estimator kernel. In the Gaussian case the fourth-order kernel vanishes identically, since, by using the well-known rule of pairing the variables in all possible ways, we obtain

$$K_{jklm} = \overline{z_j^* z_k z_l^* z_m} = \overline{z_j^* z_k}\ \overline{z_l^* z_m} + \overline{z_j^* z_l}\ \overline{z_k z_m} + \overline{z_j^* z_m}\ \overline{z_k z_l}$$

$$= K_{jl} K_{km} + K_{jm} K_{kl}. \tag{196}$$

In (196) the first term of the three vanishes, because of the wild fluctuations of the phase of the field. Hence it is seen that for a general non-Gaussian field the expansion of the likelihood function l_k in terms of powers of N_o^{-1} contains a bias term, a linear estimator-correlator term where the estimating kernel differs from the usual linear estimator kernel, and a succession of higher order correction kernels. Together the linear and the nonlinear kernels form nonlinear "estimates" of the field, then correlate the results with the actual field. In view of Kailath's results,[80] it is probable that these kernels form a minimum mean-square-error nonlinear estimate of the field. This topic will not be considered here. Hence the receiver structure of Fig. 10 is still valid if the optimum linear filter is replaced by the optimum nonlinear "estimating" filter. It would be interesting to know whether filter-squarer realizations also exist. The actual filters could be computed from the expansion (195) by using (85) to evaluate the moments. Unfortunately the interesting part of the expansion which differs from the Gaussian case can only be evaluated numerically.

In (195) the likelihood function contains sums of weakly dependent random variables for which the Central Limit theorem of Section 3.4 is applicable. Hence for large apertures the function ℓ_k converges toward a normal random variable in distribution. Also it can be shown, as in the proof of the Central Limit theorem, that the contribution of higher order kernels such as in (195) is essentially zero because the domain in which $K_{jklm} \approx K_{jl} K_{km} + K_{jm} K_{kl}$ covers almost all of the domain of summation. Hence the likelihood function ℓ_k in (195) tends toward the likelihood function of the equivalent Gaussian channel. The second-order kernel tends toward the Neumann-series expansion of the optimum linear filter. The fourth-order term behaves as $Z^4 A_c^3 A_r N_o^{-4}$, which is small compared with the second-order term if $\left(Z^2 A_c/N_o\right)^2 \ll 1$. Clearly, $Z^2 A_c/N_o$ is the energy-to-noise ratio on a coherent area.

4.2.3 Weak-Noise Case

The next case that can be analyzed is that of weak background noise. The density p_0 is taken as before, from (192) with $Z = 0$. The density p_1 will be computed in a different way, by averaging over noise instead of fading.

$$p_1(\underline{Y}^{(k)}) = p_{\underline{Y}}\left[\left\{\ln\frac{y_{jk} - n_{jk}}{Z}\right\}\right]\exp\left[-2\sum_{j=1}^{K}\text{Re}\left\{\ln\frac{y_{jk} - n_{jk}}{Z}\right\}\right]Z^{-2k}, \tag{197}$$

where $p_{\underline{Y}}$ is defined in (163). In the sequel a few vectors and matrices will be defined. Their dimension is 2K. They are all real. The large-signal assumption suggests the approximation

$$\gamma_{ik} = \ln\left(\frac{y_{ik} - n_{ik}}{Z}\right) = \ln y_{ij} - \frac{n_{ik}}{y_{ik}} - \ln Z + 0\left(\left|\frac{n_{ik}}{y_{ik}}\right|^2\right). \tag{198}$$

Hence we define the following vectors (in transposed form):

$$\widetilde{\underline{\gamma}}^T = [\ln|y_{ik}|\ldots\ln|y_{Kk}|:\arg\{y_{1k}\}\ldots\arg\{y_{Kk}\}]$$

$$\underline{\gamma}'^T = (-\sigma^2 + \ln Z)\underline{R}^T \tag{199}$$

$$\underline{R}^T = [1\ldots1:0\ldots0]$$

$$\underline{n}^T = \left[n_{1k}^r\ldots n_{Kk}^r:n_{1k}^i\ldots n_{Kk}^i\right].$$

Then (198) can be expressed in matrix form as

$$\underline{\gamma} = \widetilde{\underline{\gamma}} - \underline{Y}^{-1}\underline{n}, \tag{200}$$

where $\underline{Y}^{-1}$ is a matrix of four diagonal blocks, the elements of which are the real and the imaginary parts of n_{ik}/y_{ik}. Only $\underline{Y}^T\underline{Y}$ will be needed later, and is given in (198). Hence we have

$$p_1(\underline{\gamma}) = \frac{Z^{-2K}}{(2\pi)^K|\det\underline{K}_{\underline{\gamma}}|^{\frac{1}{2}}}\exp\left[-\frac{1}{2}(\underline{\gamma}-\underline{\gamma}')^T\underline{K}_{\underline{\gamma}}^{-1}(\underline{\gamma}-\underline{\gamma}') - 2\underline{R}^T\underline{\gamma}\right]$$

$$= \frac{(\Delta^2\vec{r})^K Z^{-2K}}{(\pi N_0)^K|\det\underline{K}_{\underline{\gamma}}\underline{Q}|^{\frac{1}{2}}}\exp\left[-(\widetilde{\underline{\gamma}}-\underline{\gamma}'')^T\left[I + \frac{2\Delta^2\vec{r}}{N_0}\underline{Y}^T\underline{Y}\underline{K}_{\underline{\gamma}}\right]^{-1}\right.$$

$$\left.\cdot\frac{\Delta^2\vec{r}}{N_0}\underline{Y}^T\underline{Y}(\widetilde{\underline{\gamma}}-\underline{\gamma}'') + 2\underline{R}^T\underline{K}_{\underline{\gamma}}\underline{R} - K\sigma^2\right], \tag{201}$$

77

where

$$\underline{Q} = \frac{\Delta^2 \vec{r}}{N_o} \underline{I} + \frac{1}{2} (\underline{Y}^{-1})^T \underline{K}_{\underline{Y}}^{-1} \underline{Y}^{-1}$$

$$= \frac{1}{2} (\underline{Y}^{-1})^T \left[\underline{I} + \frac{2\Delta^2 \vec{r}}{N_o} \underline{Y}^T \underline{Y} \underline{K}_{\underline{Y}} \right] \underline{K}_{\underline{Y}}^{-1} \underline{Y}^{-1}, \qquad (202)$$

$$\underline{Y}'' = \underline{Y}' - 2\underline{K}_{\underline{Y}} \underline{R},$$

and $\underline{K}_{\underline{Y}}$ is the covariance matrix of the logarithm of $z(\vec{r})$ defined in (70). The determinant can be put into the form

$$\det \underline{K}_r \underline{Q} = 2^{-2K} \det (\underline{Y}^T \underline{Y})^{-1} \det \left[\underline{I} + \frac{2\Delta^2 \vec{r}}{N_o} \underline{Y}^T \underline{Y} \underline{K}_r \right]. \qquad (203)$$

In the usual detection case where the time is the only variable the logarithms of the determinants in the Gaussian case are known to give an asymptotic expression similar to Shannon's famous formula for Gaussian channel capacity. A somewhat analogous formula might exist in this case, too (cf. Van Trees[81]).

The likelihood function is now obtained by dividing (201) by p_o and taking the logarithm.

$$l_k = \frac{\underline{y}^T \underline{y}}{N_o} \Delta^2 \vec{r} - (\widetilde{\underline{y}} - \underline{y}'')^T \left[\underline{I} + \frac{2\Delta^2 \vec{r}}{N_o} \underline{Y}^T \underline{Y} \underline{K}_{\underline{Y}} \right]^{-1} \frac{\Delta^2 \vec{r}}{N_o} \underline{Y}^T \underline{Y} (\widetilde{\underline{y}} - \underline{y}'')$$

$$+ \sum_{j=1}^{K} \ln \left| \frac{y_j}{Z} \right| - \frac{1}{2} \ln \left| \det \left[\frac{1}{2} \underline{I} + \frac{\Delta^2 \vec{r}}{N_o} \underline{Y}^T \underline{Y} \underline{K}_{\underline{Y}} \right] \right| + 2\underline{R}^T \underline{K}_{\underline{Y}} \underline{R} - K\sigma^2. \qquad (204)$$

Here the matrix $\underline{Y}^T \underline{Y}$ is found to have the following diagonal form

$$\underline{Y}^T \underline{Y} = \begin{bmatrix} |y_{1k}|^2 & & & & & 0 \\ & \ddots & & & & \\ & & |y_{Kk}|^2 & & & \\ \vdots & & & |y_{1k}|^2 & & \vdots \\ & & & & \ddots & \\ 0 & & \cdots & & & |y_{Kk}|^2 \end{bmatrix} \qquad (205)$$

The function ℓ_k consists of three parts (see Fig. 19). The first part in fact simply evaluates the total energy received during the signal duration T through the receiving aperture. The second part is a linear estimation-correlation for the logarithm of the

78

field. For large signals the estimation filter is essentially $\underline{K}_\gamma^{-1}$. Hence this term is close to the log-normal probability density exponent. It is close to zero for highly probable values of fields, but becomes a large negative quantity for fields deviating from the usual values, either too large or too small. This matrix filter depends on the input y in terms of the matrix $\underline{Y}^T\underline{Y}$. Hence it is a nonlinear filter. Its function is to de-emphasize those samples whose amplitude is particularly small, because these samples do not help much in making the decision if there are strong sample components present. It also tends to de-emphasize those spatial frequencies of the field logarithm, which are not well represented in the spectrum of $y(\vec{r}) = \ln z(\vec{r})$.

The third term in Eq. 206 is equivalent to the bias terms in (178) and (187). Here it is signal-dependent, however. For small y_j the sum of the logarithms becomes a large negative quantity, while the log of the determinant becomes close to zero. Hence small-sample values tend to make 1_k small. The logarithmic terms are obviously small compared with the quadratic term for small noise. Hence the optimum receiver just squares the samples straight if the signal is strong compared with the average sample noise. If the signal is not strong enough, the receiver will apply nonlinear filtering to those samples. Figure 19 shows the structure of the optimum receiver. The most important
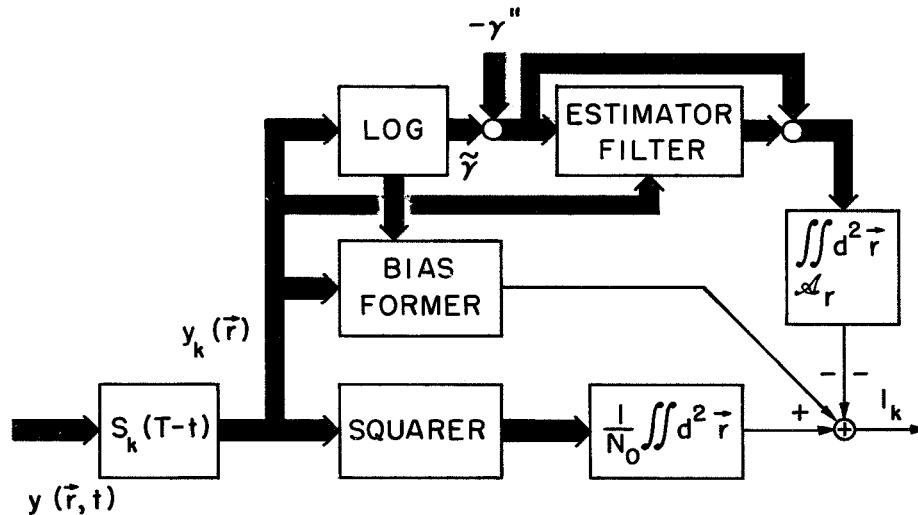

Fig. 19. Optimum receiver for large log-normal fields in white Gaussian noise.

operations in it are squaring and summing, which are due to the fact that the noise is Gaussian in nature.

4.2.4 Independent Samples

If the samples are assumed to be completely independent, much more can be said about the probability density p_1. In this case p_1 factors into K independent densities.

Let $\Delta^2\vec{r} = A_c$ denote the coherent area. Then

$$p_1(\underline{Y}^{(k)}) = \left(\frac{A_c}{N_o}\right)^K \prod_{j=1}^{K} \exp\left[-\frac{|y_{jk}|^2}{N_o} A_c\right] \overline{\exp\frac{A_c}{N_o}\left[2\,\mathrm{Re}\left\{y_{jk}^* z\right\}Z - Z^2|z|^2\right]}, \qquad (206)$$

where the average is evaluated for log-normal z with density function from Eq. 5 (uniform phase). Hence we have

$$\overline{\exp\frac{A_c}{N_o}\left(2Z\,\mathrm{Re}\left\{y_{jk}^* z\right\} - Z^2|z|^2\right)} = I_o\left[2|z|\,\frac{A_c Z|y_{jk}|}{N_o}\right]\exp\left[-\frac{A_c Z^2|z|^2}{N_o}\right]$$

$$= \overline{I_o\left[2|z|\alpha_p\,\frac{|y_{jk}|}{Z}\right]e^{-\alpha_p|z|^2}} = \mathrm{Fr}\left(\alpha_p,\,\frac{|y_{jk}|}{Z}\sqrt{\alpha_p}\,;\sigma\right), \qquad (207)$$

where $\alpha_p = A_c Z^2/N_o$ is the energy-to-noise ratio per coherent area or independent sample. The "frustration" function $\mathrm{Fr}\,(.\,,.\,;.)$ is defined as follows

$$\mathrm{Fr}\,(\alpha,\beta;\sigma) = \int_0^\infty I_o(2\beta u\sqrt{\alpha})\,e^{-\alpha u^2}\,\frac{e^{-(\ln u + \sigma^2)^2/2\sigma^2}}{\sqrt{2\pi}\,\sigma}\,du. \qquad (208)$$

The behavior of this function has been discussed by Halme, Levitt, and Orr[82] and by Halme.[83] By dividing (206) by p_o, using (207), and taking the logarithm, the likelihood functional is obtained

$$\ell_k = \sum_{j=1}^{K} \ln \mathrm{Fr}\left(\frac{A_c Z^2}{N_o},\,\frac{|y_{jk}|}{\sqrt{A_c^{-1}N_o}}\,;\sigma\right). \qquad (209)$$

The behavior of the function $\ln \mathrm{Fr}\,(.\,,.\,;.)$ is displayed in Fig. 20. It has been shown by Halme[84] that ℓ_k as a function of $|y_{jk}|$ always starts with a square-law portion, as was indicated before in connection with Eq. 196. For signals that are large compared with noise it is possible to use the generalization of the moment expansion of the convolution integral (for example, Papoulis[85]). If we look at (192), it seems obvious that the density $p_1(\underline{Y}^{(k)}|\underline{z})$ is highly peaked at $\underline{Y}^{(k)} = Z\underline{z}$, if the noise is small. Hence the moment expansion leads to the following approximation, which is correct up to the second-order correction, because of the symmetry of the noise density.

$$p_1(\underline{Y}^{(k)}) = \prod_{j=1}^{K} \frac{e^{-(\ln|y_{jk}/Z|+\sigma^2)^2/2\sigma^2}}{(2\pi)^{3/2}|y_{jk}|^2}. \qquad (210)$$
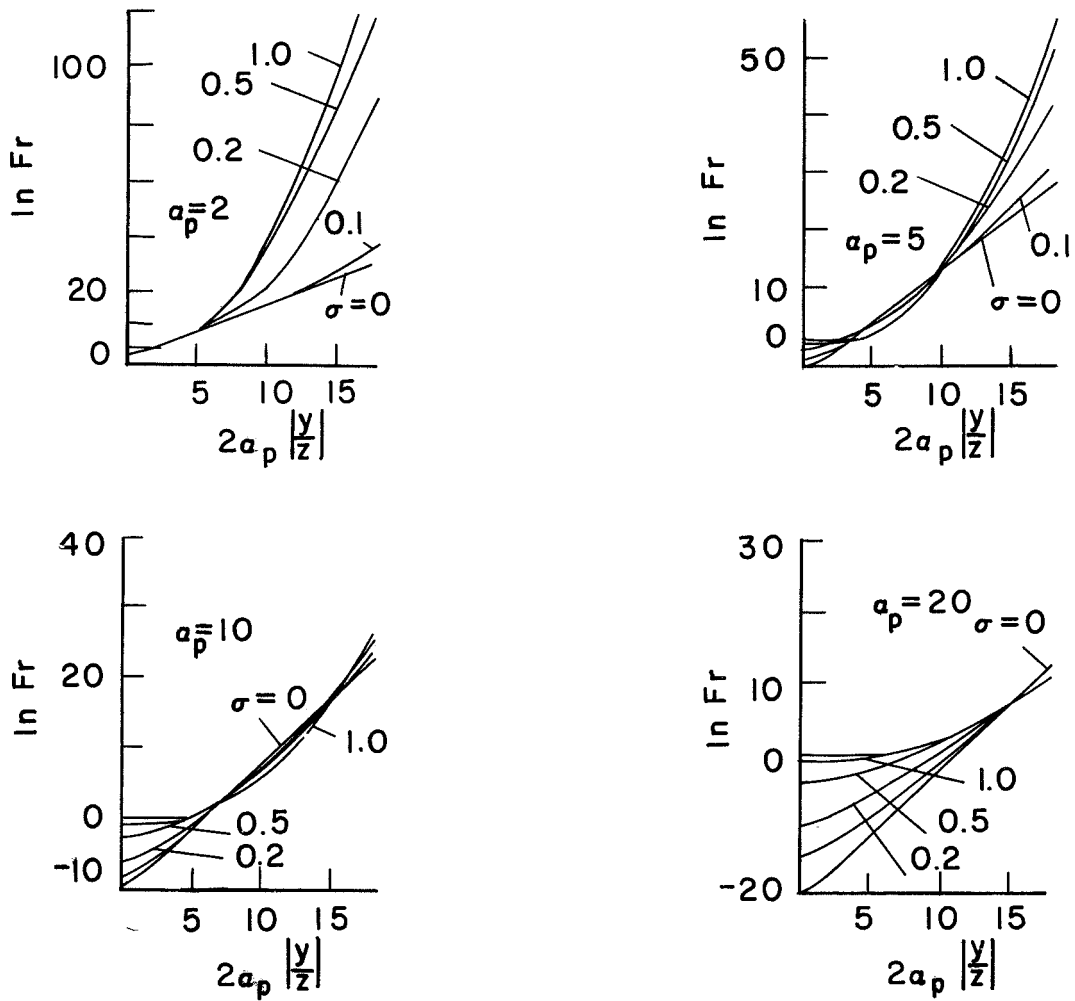
Fig. 20. Curves of the function in ln Fr $(a_p, \sqrt{a_p}\,y/Z; \sigma)$ (Eq. 209).

The likelihood functional then becomes to first approximation

$$\ell_k = \sum_{j=1}^{K} \left[\frac{A_c |y_{jk}|^2}{N_o} - \frac{1}{2\sigma^2} \left[\ln \left| \frac{y_{jk}}{Z} \right| + 3\sigma^2 \right]^2 + 4\sigma^2 + \ln \frac{N_o}{\sqrt{8\pi} \, A_c Z^2} \right].$$

(211)

This result agrees with the asymptotic formula (204).

The structure of the optimum receiver to implement Eq. 209 is shown in Fig. 21. The receiver is very similar to the optimum receiver for independent Gaussian samples.
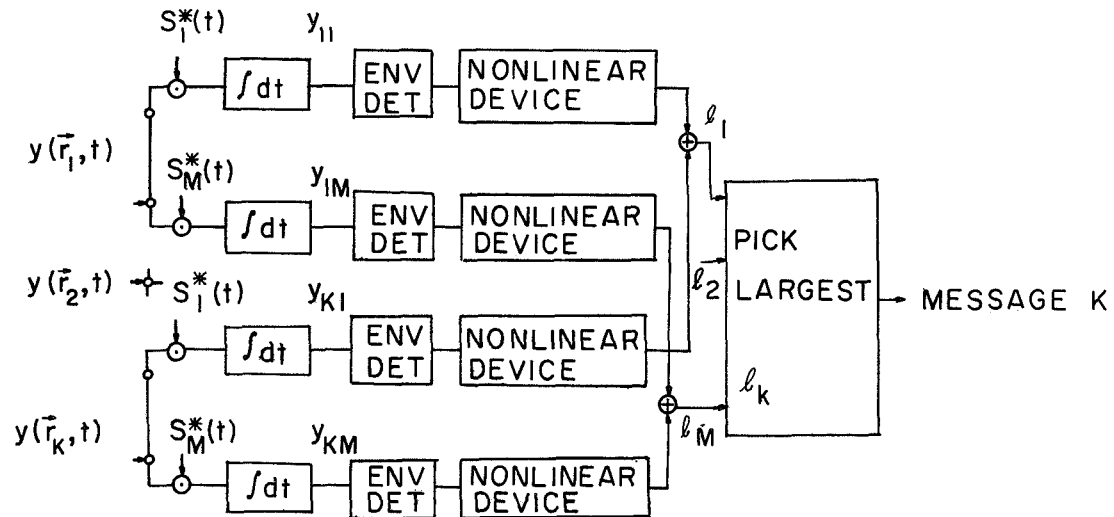

Fig. 21. Optimum receiver for independent samples of a log-normal field.

In the Gaussian case the nonlinear memoryless device, which implements $\mathrm{Fr}(.,\beta;.)$ would be a squarer.

The discussion on optimum receivers for log-normal classical fields with white Gaussian background noise shows that the receiver structures actually required are remarkably similar to the optimum receivers in the case of Gaussian fields discussed in section 4.1. This similarity depends basically on the Gaussian nature of the background noise. This agrees with the recent results obtained by Kailath[80] for optimum detection of stochastic (not necessarily Gaussian) signals in white Gaussian noise.

The evaluation of the performance for the optimum receivers for log-normal fields in white Gaussian noise is very difficult in general. Some partial results are available, however, in the cases of large noise, small noise, and of independent samples.

The error probability will again be bounded in the same way as in (191) or (197). The error exponent is to be evaluated by using (200). The probabilities p_o and p_1 have been evaluated previously. In particular, if the likelihood functional is available,

$$p_1 = p_o \exp \ell_k.$$

4.2.5 Reliability Function for Strong and Weak Noise Cases

In the case of large noise the likelihood functional is given by (196). This functional is of the form $\ell_k = c + Z^2(\Delta^2\vec{r})^2\underline{y}^T\underline{K}'\underline{y}^*/N_0 +$ higher order terms. Here c is the cumulant-generating function of e_s with parameter $\left(-Z^2/N_0\right)$, K' is the expansion of the linear part of the optimum estimator kernel, like the Neumann series of the estimator kernel in the linear (Gaussian) case. The error exponent then becomes

$$E(\rho) = \frac{(1+\rho)}{2A_r^a} \ln \left| \det\left[\underline{I} + Z^2\underline{K}'\Delta^2\vec{r}/(1+\rho)N_0\right] \right| - c/A_r^a. \tag{212}$$

This form may be convenient for numerical evaluation, but it does not display the fact that (212) and (201) are asymptotically the same. By starting from the second-order representation, however, and going over to Karhunen-Loève representation it is clear that the performance approaches that of the corresponding Gaussian receiver, when either the energy-to-noise ratio in the aperture is very small so that only the terms of the order of N_0^{-1} need be taken into consideration, or the aperture is so large that the contribution of the nonlinear terms becomes negligible while the energy-to-noise ratio per coherent area is small. Criteria for the required aperture size can be obtained by evaluating numerically some of the higher order covariance functions of the field. In these cases the channel capacity and the zero-rate error exponent can be obtained by using the results derived for the equivalent Gaussian channel, which has the same second-order properties as the actual log-normal channel.

4.2.6 Reliability Function for the Case of Independent Samples

In the case of large signals the error exponent can be readily written in an integral form by using (204). The integral is of the form of a generalized frustration function that is complicated to evaluate. For simplicity, we shall confine our discussion to the case of independent samples.

For the case of independent samples the error exponent has been evaluated by Kennedy and Hoversten.[22] The error exponent has the following form with (209) used:

$$E(\rho) = -\frac{(1+\rho)}{a_p}\ln\left[\frac{A_c}{\pi N_0}\iint \exp-\frac{A_c|y|^2}{N_0} Fr^{1/(1+\rho)}\left[\frac{A_c Z^2}{N_0}, \frac{|y|}{\sqrt{A_c^{-1}N_0}};\sigma\right] d^2y\right]$$

$$= -\frac{(1+\rho)}{a_p}\ln\left[\int_0^\infty du\, e^{-u} Fr^{1/(1+\rho)}(a_p,\sqrt{u};\sigma)\right]. \tag{213}$$

Here $a_p = Z^2 A_c/N_0$. Figure 22 shows the behavior of the zero-rate error exponent as evaluated by Kennedy and Hoversten.[22] These curves show typical diversity behavior: the error exponent has a maximum at a particular value of a_p, the energy-to-noise ratio
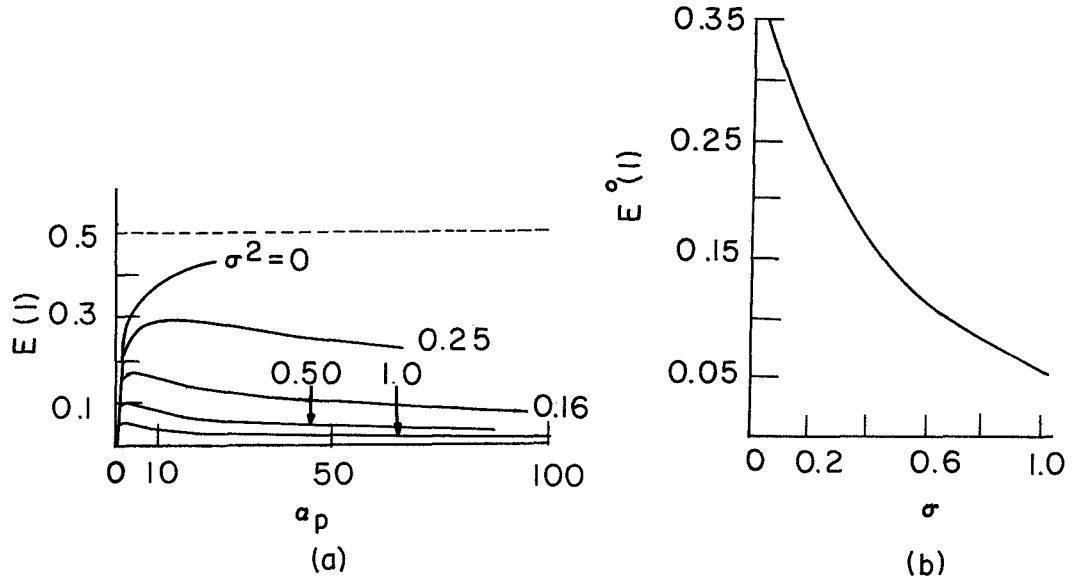
Fig. 22. (a) Zero-rate error exponent $E(1)$ and (b) its optimum value $E^o(1)$ for the independent sample receiver for log-normal fields.

per diversity path, in this case, per independent sample.

It is possible to obtain a less difficult expression than (213) for the error exponent by using the large-amplitude approximation (210) for p_1. By direct substitution we get

$$E(\rho) = -\frac{1}{a_p}\left(\ln a_p - \sigma^2(1+7\rho-4\rho^2) + \rho \ln \sigma + \frac{1+\rho}{2} \ln (1+\rho) - \frac{(1-3\rho)}{2} \ln 2 \right.$$

$$\left. -\frac{1-\rho}{2} \ln \pi + (1+\rho) \ln \mathrm{Fr}\left[\frac{a_p^\rho}{1+\rho} e^{\sigma^2(2+8\rho)}, \ 0; \ \sigma\sqrt{1+\rho} \right] \right) \tag{214}$$

The function $\mathrm{Fr}(a, 0;\sigma)$ is easy quite easy to calculate (cf. Halme,[83] Halme, Levitt, and Orr[82]). The exact behavior of $E(\rho)$ has to be evaluated numerically. Roughly speaking, by using the results of Halme, Levitt, and Orr,[82] $-\ln \mathrm{Fr}$ grows like $\ln^2 a_p$, so that $E(0)$ must have a maximum as a function of a_p.

From the curves of Kennedy and Hoversten it becomes clear that the optimum error exponent is .15 for $\sigma = .45$, is larger for smaller values of log-normal standard deviation, while for larger values of σ it goes rapidly toward zero. For $\sigma = 1.0$, the zero rate error exponent is about .05, requiring three times more power to obtain the same performance than the optimum Gaussian channel. For small $a_p < 1$, the performance is essentially similar to that of a Gaussian channel. Obviously the error exponent is then much less than .15, because there is too much diversity, or equivalently, the power level is too low.

84

4.3 QUANTUM TREATMENT OF THE FIELD-DETECTION PROBLEM

4.3.1 Quantum Formulation of the Detection Problem

In many cases of practical importance the quantum noise is the most important type of noise rather than the background noise just referred to. The quantum formulation of the detection problems allows the consideration of both the quantum and the background noise, together with the spatial and temporal coherence properties of the fields.

The formulation of the detection problem in quantum-mechanical terms was originally done by Helstrom.[25] This section is based on and uses many of the results of Liu.[26] We shall start with a short discussion of the optimum decision rule in quantum terms, then solve the Gaussian field-detection problem, and end with the log-normal field detection problem. The receiver structures and their performance will again be discussed emphasizing the weak or absent background noise case.

The maximum-likelihood decision rule will be formulated here as by Liu.[26] The received field is assumed to be in a statistical mixture of coherent states, which is described by a set of density operators ρ_k, $k = 1, \ldots, M$, one for each of the M signals. We shall deal only with those cases in which all these operators are commutative, and hence diagonal in the same complete representation $|r_j\rangle$. Let the kets $|x_j\rangle$ denote the complete set of eigenstates of a measuring operator X (thus far unspecified).

$$X|x_j\rangle = x_j|x_j\rangle. \tag{215}$$

The measurement has the result x_j labeling a state that has originated from one of the messages k. A randomized strategy is adopted to choose k, given the result x_j with probability p_{jk}. The total probability of error for equiprobable messages becomes

$$P(\mathscr{E}) = 1 - \frac{1}{M} \sum_{k=1}^{M} \sum_{j=1}^{\infty} p_{jk}\langle x_j|\rho_k|x_j\rangle. \tag{216}$$

Now denote $\langle r_j|\rho_k|r_j\rangle = r_k(j)$. Then the error probability is bounded below by

$$P(\mathscr{E}) > 1 - \frac{1}{M} \sum_{k=1}^{M} \sum_{j} \sum_{i} p_{jk} r_k(j)|\langle x_j|r_i\rangle|^2$$

$$= 1 - \frac{1}{M} \sum_{i} \max_{k} r_k(i) \sum_{k=1}^{M} p_{jk} \sum_{j} |\langle x_j|r_i\rangle|^2$$

$$= 1 - \frac{1}{M} \sum_{j} \max_{k} r_k(j) \tag{217}$$

because $|x^j\rangle$ is a complete set. This lower bound can be reached by choosing the kets $|x_j\rangle$ to be the eigenkets $|r_j\rangle$ and by using the strategy

$$p_{jk} = 1, \quad \text{if } r_k(j) \geq r_i(j), \quad i \neq k, \quad i, k = 1, \ldots, M$$

$$= 0 \text{ for all other } k.$$

(218)

Since $r_k(j) = P(x_j|\rho_k) = P(x_j|k) = P(k|x_j)P(x_j)/P(k)$, the decision rule that is adopted picks that message which gives maximum a posteriori probability to the observed state $|x_j\rangle$ (maximum-likelihood decision rule).

As shown by Liu,[26] the operator X is by no means unique. To ensure real eigenvalues it should be Hermitian, but in some cases complex operators measuring also the phase variables could be helpful. The necessary and sufficient conditions for the operator X to be optimum are that its eigenstates can be obtained from the states r_j by a unitary transformation, and that the sets $R_k = \{ |x_j\rangle$: for some i $\langle x_j|r_i\rangle \neq 0$, where $r_k(i) > r_m(i)$ for $m = 1, \ldots, k - 1$, and $r_k(i) > r_m(i)$ for $m = k + 1, \ldots, M \}$ are disjoint. Physically the last condition means that the results of the measurements (eigenvalues x_j) should belong to disjoint sets, each of which corresponds to a particular signal. These sets correspond to the usual decision regions.

The detection problem in the binary case has been discussed by Helstrom[25] for the cases of a constant signal in Gaussian noise, a constant signal with random phase in Gaussian noise, and a Gaussian signal in Gaussian noise in both the single-mode and the multimode cases. His multimode receiver is a "threshold receiver," which is optimum in the case of a very weak signal. A more extensive treatment in the case of M signals, either Gaussian or with random phase has been given by Liu.[26] We shall relate the spatial coherence to the results obtained by Liu and also consider the log-normal case.

The general idea in the treatment that follows is to obtain the likelihood functional $l_k = \ln (r_k(j)/r_o(j))$, where r_o refers to the state of the field when no signal is present.

4.3.2 Optimum Receiver for Gaussian Fields

As indicated in section 2.2 the P-representation for a Gaussian field is Gaussian. Hence the density operator for the field has the following form if the signal k was sent:

$$\rho_k = \frac{1}{|\det \underline{K}_k|} \int \cdots \int e^{-\underline{a}^T \underline{K}_k^{-1} \underline{a}^*} \prod_j |a_{jk}\rangle \langle a_{jk}| \frac{d^2 a_{jk}}{\pi},$$

(219)

where scalar index j is used instead of the vector $\underline{m}$. The covariance matrix $\underline{K}_k$ is defined as

$$\underline{K}_k = \left[\text{Tr} \left\{ \rho_k a_{jk}^+ a_{jk} \right\} \right].$$

(220)

It has been shown by Liu[26] that a unitary transformation preserves the form of (219) if the coherent states are redefined at the same time. In particular, assume that the transformation diagonalizes the matrix $\underline{K}_k$. This is equivalent to finding the Karhunen-Loève representation in the usual classical case. Under the assumptions of spatially and temporally white Gaussian noise and orthonormal mode functions and equal-energy pure "tone" signals, the density operators for the cases when the signal k is present and when no signal is present have the form

$$\rho_{1k} = \Pi_j e^{-|\beta_{jk}|^2/(N+S_j)} |\beta_{jk}\rangle \langle \beta_{jk}| \frac{d^2\beta_{jk}}{\pi(N+S_j)}$$

$$\rho_{ok} = \Pi_j e^{-|\beta_{jk}|^2/N} |\beta_{jk}\rangle \langle \beta_{jk}| \frac{d^2\beta_{jk}}{\pi N}.$$

(221)

As seen from Table 2 (line 8), the density operator ρ is diagonal in the number representation. Corresponding to state $|\{n_{jk}\}\rangle$ and signal k the diagonal components $r(\{n_{jk}\})$ become

$$r_1(\{n_{jk}\}) = \Pi_j \frac{1}{N+S_j+1} \left[\frac{N+S_j}{N+S_j+1} \right]^{n_{jk}}$$

$$r_o(\{n_{jk}\}) = \Pi_j \frac{1}{N+1} \left[\frac{N}{N+1} \right]^{n_{jk}}.$$

(222)

The quantities N and S_j are numbers related to noise and signal by relations $TN_o = hfN$, $T\lambda_j Z^2 = hfS_j$, where f refers to the frequency of the mode component and the other quantities are discussed in section 4.1. The n_{jk} are the occupation numbers telling the number of photons in state $|n_{jk}\rangle$, referring to mode j and signal frequency k.

The likelihood function with the use of (222) now becomes

$$\ell_k = \sum_j n_{jk} \ln \frac{(N+S_j)(N+1)}{(N+S_j+1)N} - \sum_j \ln \frac{N+S_j+1}{N+1}$$

$$= \sum_j n_{jk} c_j - \text{bias term.}$$

(223)

It is easy to see the correspondence to the classical case:

$$c_j = \ln\left(1 + \frac{1}{N}\right) - \ln\left(1 + \frac{1}{N + S_j}\right)$$

$$\rightarrow \frac{S_j}{N(N+S_j)} = \frac{\lambda_j Z^2}{N\left(N + \lambda_j Z^2\right)} \tag{224}$$

as the number of noise photons in a mode, N, becomes large compared with unity. The optimum quantum receiver is shown in Fig. 23. The idea is to first find the number of photons in a space-time mode of the received field. This could be done physically by using suitable reactive space-time filters and
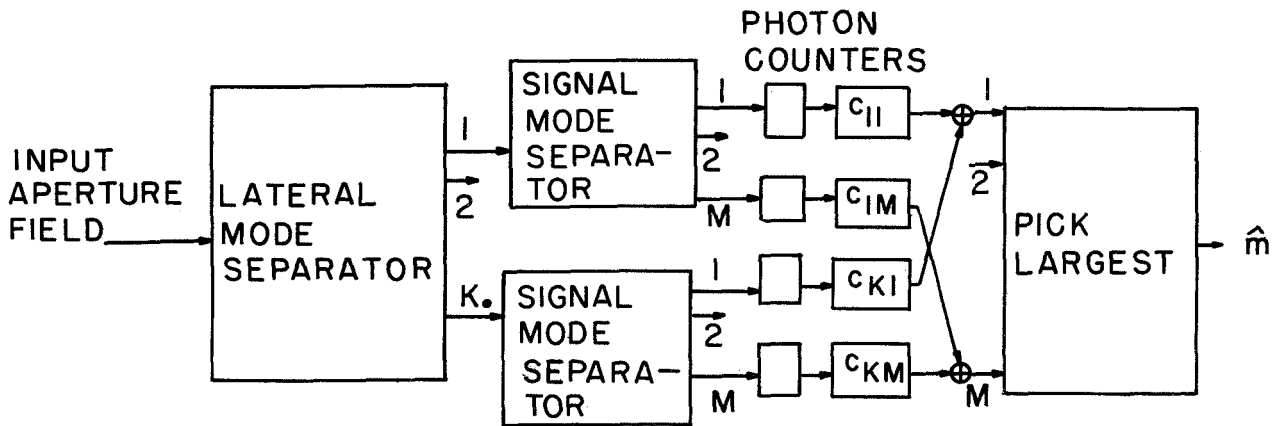

Fig. 23. Optimum quantum receiver for Gaussian fields in white Gaussian noise (diversity realization).

then using a photodetector to convert the photons into electrons. The photon counts are then weighted with c_j and summed to give the ℓ_k. Figure 24 shows the behavior of the weighting function c_j as a function of signal and noise. It is important to realize that it is no longer possible to find receiver structures similar to the estimator-correlator or filter squarer receivers. In the classical case it was possible to do the weighting either before or after the nonlinear operation, because the signal and the noise were affected similarly by the weighting. In the quantum case the weighting before photon counting reduces the level of most of the modes and hence increases the relative size of one quantum so that granularity and the total photon noise increases compared with the case in which the total number of quanta in a mode is converted into electrons, the current is amplified, and the weighting is done at macroscopical current levels.
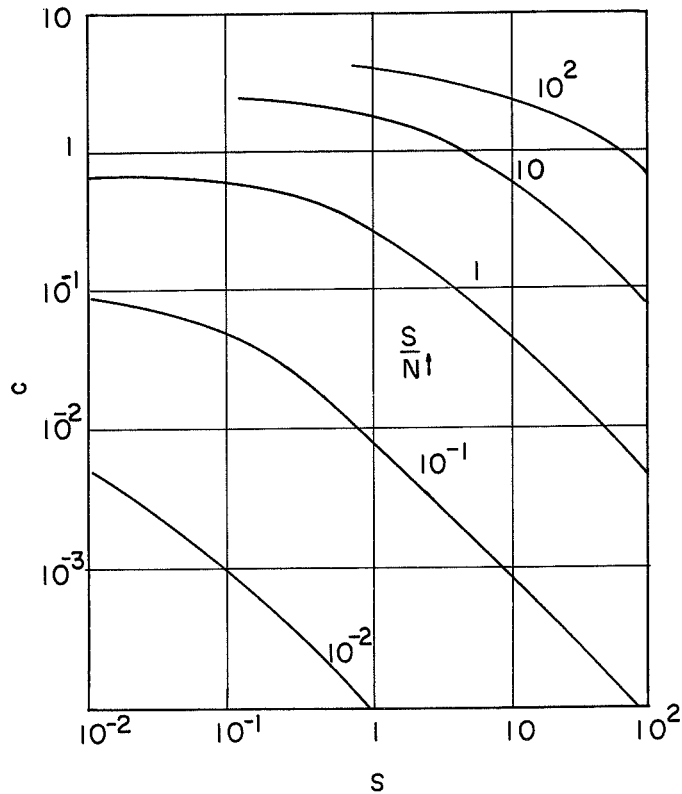
Fig. 24. Dependence of the diversity weighting coefficient c in Eq. 224 and Fig. 23 on the number of signal and noise photons in the mode, S and N.

In the discussion here single-frequency signals have been assumed. For more general orthogonal signals a similar treatment is possible by introducing more than one temporal mode on each Fourier component of the signal. To avoid crosstalk, it helps if the spectra corresponding to each signal do not overlap. Even this is unnecessary, since by Liu the field representation in terms of modes is not unique but can be subjected to any unitary transformation. For general orthogonal signals the time modes to expand the field could then be taken to be the signals themselves, and the results obtained are immediately applicable. The optimum receiver then has to contain the correlators or matched filters corresponding to the signal modes.

4.3.3 Performance of the Optimum Gaussian Receiver

The performance of the optimum quantum receiver for Gaussian fields in white noise is obtained from (218). In the single-mode case the binary error probability (M=2) can be readily evaluated:

$$P(\epsilon) = \frac{1}{(N+S+1)(N+1)} \sum_{m=0}^{\infty} \sum_{n=0}^{m} \left[\frac{N+S}{N+S+1}\right]^n \left[\frac{N}{N+1}\right]^m$$

$$= \frac{1}{2}\left[1 + \frac{S-1}{2(N+1)}\right]^{-1}. \tag{225}$$

This result has the correct classical limit (Van Trees[86]). For multimode fields and M signals bounding techniques have to be used. The expression corresponding to the error exponent $E(\rho)$ of (171) now has the following form

$$E(\rho) = -\frac{(1+\rho)}{A_r{}^{\alpha}} \ln \left[\sum_{\underline{n}} r_1^{1/(1+\rho)}(\underline{n}) \; r_o^{\rho/(1+\rho)}(\underline{n})\right]. \tag{226}$$

By using (223) and the known formula for the sum of the geometrical series, the error exponent is evaluated:

$$E(\rho) = \frac{(1+\rho)}{A_r{}^{\alpha}} \sum_j \ln \left[(N+S_j+1)^{1/(1+\rho)}(N+1)^{\rho/(1+\rho)} - (N+S_j)^{1/(1+\rho)}N^{\rho/(1+\rho)}\right]. \tag{227}$$

The classical limit as $N \gg 1$ agrees with (172).

$$E(\rho) \to \frac{(1+\rho)}{A_r{}^{\alpha}} \sum_j \ln \left[N^{\rho/(1+\rho)}(N+S_j)^{1/(1+\rho)} \frac{(1+\rho)N + \rho S_j}{(1+\rho)\,N(N+S_j)}\right]$$

$$= \frac{(1+\rho)}{A_r{}^{\alpha}} \sum_j \ln \left[\frac{1 + \rho S_j/(1+\rho)N}{(1+S_j/N)^{\rho/(1+\rho)}}\right]. \tag{228}$$

The behavior of the error exponent $E(\rho)$ has been evaluated by Liu in the case of equal eigenvalues, which is known to give the smallest error probability. For different rates there is again an optimum number of diversity paths corresponding to given signal-to-noise ratio and noise level. The optimum system reliability function has been evaluated numerically by Liu. The results for $N > .1$ are fairly close to the classical limit evaluated by Kennedy.[1] The channel capacity in the optimum case is equal to the channel capacity of the constant channel. It obviously differs from the classical capacity. The ratio of the classical and quantum mechanical capacities is

$$C_{rel} = C_{quant}/C_{class} = N \ln (1+1/N). \tag{229}$$

This ratio tends to 1 as $N \to \infty$. As $N \to 0$ the ratio tends to zero but the quantum capacity in fact tends to infinity. Because the size of a quantum is proportional to frequency,

the required power similarly tends to infinity. Because this case is a useful idealization in the realm of optical communications, the case with no background will be discussed separately.

4.3.4 Reception of Gaussian Fields in the Absence of Background Noise

When there is no background the matrix coefficient $r_o(\{n_{kj}\})$ in (222) becomes one for all $n_{kj} = 0$, and zero otherwise. The decision rule (223) now says that the message k was sent if a single one of the numbers n_{jk} is nonzero. Any receiver structure that performs an operation on n_{jk} which is zero for all $n_{jk} = 0$ and positive otherwise is an optimum receiver. Hence only temporal filtering is necessary. An error can be made only if all numbers n_{jk} are zero, even though the signal k was sent. The probability of this event is

$$P(\epsilon) = r_1(\{0\}) = \prod_j (1+S_j)^{-1}. \tag{230}$$

This probability is in no way dependent on the number of messages, M, sent. It is in this sense that the channel capacity is infinite. Using the result (178) a closed-form expression can be obtained for the error probability for large apertures.

$$-\ln P(\epsilon) = \sum_j \ln (1+S_j)$$

$$\rightarrow A_r \int\!\!\!\int_{-\infty}^{\infty} \ln \left[1 + \frac{Z^2 S(\vec{\kappa})}{hf/T} \right] d^2\vec{\kappa}/(2\pi)^2. \tag{231}$$

In the case of Gaussian field covariance (231) when (178) is applied becomes

$$P(\epsilon) = \exp\left[-\frac{D}{2} (-Li_2(-2a_p)) \right], \tag{232}$$

where $D = A_r/A_c$ is the number of inherent diversity paths, and $a_p = Z^2T/hf$ is the energy-to-quantum-noise on a diversity path. Figure 25 shows the behavior of the error probability for $D = 1$.

4.3.5 Optimum Reception of Log-normal Fields in Background Noise

For log-normal fields the sampling approach is easier in most cases than the plane-wave decomposition. The samples can be obtained from the plane-wave coefficients by a Fourier transform, which is a unitary transformation. In the field representation the coefficients of the sampling expansion can be considered as annihilation operators with
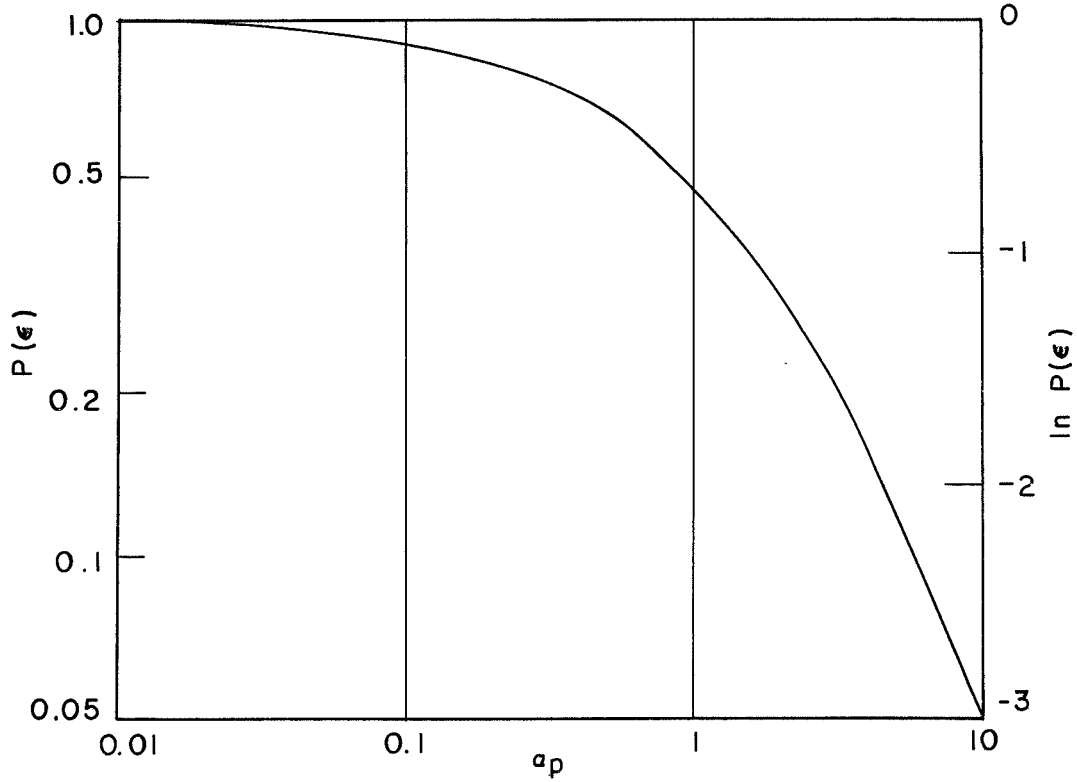
Fig. 25. Error probability of the detection of the Gaussian field with the Gaussian covariance function in the absence of background $\ln P(\epsilon) = Li_2(-2a_p)/2$, a_p = energy-to-quantum-noise ratio per diversity path.

the usual commutation relations. Hence we have the following P-representation for the log-normal field in sampling representation

$$\rho_{ik} = \int \cdots \int P_1(\{\beta_{jk}\}) \prod_j |\beta_{jk}\rangle\langle\beta_{jk}| \frac{d^2\beta_{jk}}{\pi} \tag{233}$$

with P_1 taken from (192), (196), (203), (208), (209), and (213). The P-representation cannot in general be transformed in such a way that it would only depend on the absolute values of β_{jk}. Hence the number representation is no longer diagonal. It is hard to see what other representation might be diagonal. For the case of large noise it seems reasonable to assume that the Gaussian equivalent model can be used. This leads readily into the receiver structure and performance. Some insight can be gained by considering the situation in which the samples are independent and diagonal in the number representation.

In the case of independent samples the number matrix element in the diagonal number representation is obtained by comparison with Table 1.

$$r_{ik}(\{n_{jk}\}) = \prod_j \left[\int_0^\infty \frac{e^{-u^2 S/(N+1)}}{N+1} \left[\frac{N}{N+1}\right]^{n_{jk}} L_{n_{jk}}(-S/N(N+1)) \frac{e^{-(\ln u + \sigma^2)^2/2\sigma^2}}{\sqrt{2\pi}\,\sigma u} du \right]. \tag{234}$$

92

The zero-hypothesis comes from (223). The likelihood function then becomes

$$l_k = \sum_j \ln \left[\int_0^\infty e^{-u^2 S/(N+1)} \, L_{n_{jk}}(-S/N(N+1)) \, \frac{e^{-(\ln u + \sigma^2)^2/2\sigma^2}}{\sqrt{2\pi} \, \sigma u} \, du \right]. \tag{235}$$

The classical limit of this expression can be shown to be (235) (see Helstrom[25]). The optimum receiver differs from the Gaussian receiver by the nonlinearity of the weighting, which is the complicating factor in (235).

4.3.6 Optimum Reception of Independent Log-normal Samples in the Absence of Background Noise

When the background noise is absent the matrix element r_1 has a much simpler form:

$$r_{1k}(\{n_{jk}\}) = \prod_j \left[\int_0^\infty \frac{e^{-u^2 S - (\ln u + \sigma^2)^2/2\sigma^2}}{\sqrt{2\pi} \, \sigma n_{jk}!} \, S^{n_{jk}} u^{2n_{jk}-1} \, du \right]. \tag{236}$$

Here S is the number of signal photons in a sample, and σ the log-normal standard deviation. The optimum receiver has to decide whether any photons at all came to the
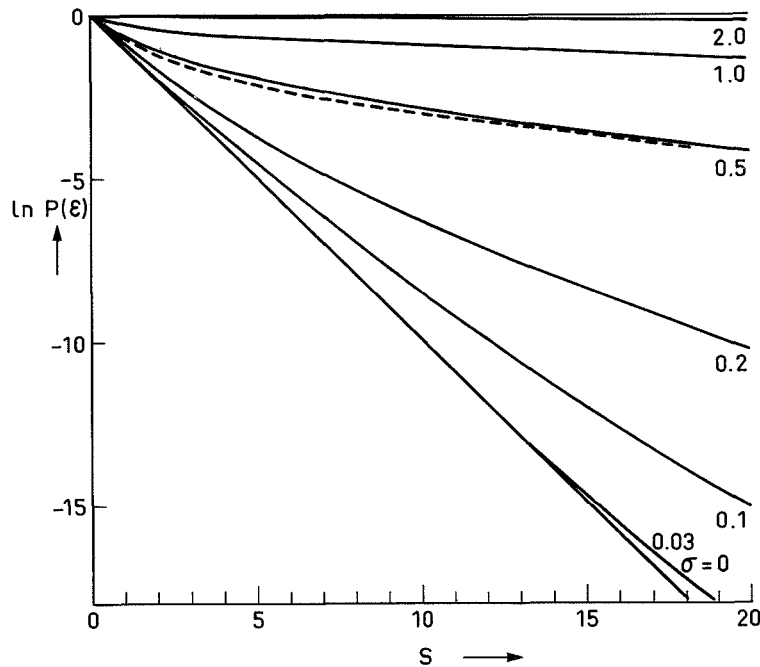
Fig. 26. Error exponent for the detection of log-normal field in the absence of background, $\ln(1/P(\epsilon)) = -D \ln Fr(S, 0; \sigma)$ for $D = 1$. Broken curve refers to a Gaussian field (cf. Fig. 25).

93

receiver in the right modes. Any of the optimum Gaussian receivers will do also for the log-normal signal.

The error probability can be evaluated numerically by substituting (234) in (227). Here the error probability will actually be determined for the case of no background noise. The error probability is then equal to

$$P(\epsilon) = \prod_j \left[\frac{e^{-u^2 S - (\ln u + \sigma^2)^2 / 2\sigma^2}}{\sqrt{2\pi}\ \sigma u} \ du \right]$$

$$= (Fr\ (S, 0; \sigma))^D, \tag{237}$$

where D is the number of independent samples. Figure 26 shows the behavior of the error exponent for D = 1.

V. CONCLUSION

5.1 SUMMARY OF RESEARCH

5.1.1 General Remarks

The purpose of this work is to relate the coherent properties of the log-normal field to the optimum detection of signals carried by the field. Spatial incoherence causes diversity in the reception. The received field can be understood to be composed of a number of diversity components that are only slightly dependent. These components may be taken to be either plane waves or just samples in the aperture. The detection problem is then formulated in terms of these components.

The optimum receiver and its performance can easily be found in certain cases. The cases of either large or small noise are best amenable to analysis. For large apertures many results are also available because Fourier integrals can be used and the Central Limit theorem is applicable to quantities that are sums over the whole aperture area.

The analysis was performed both classically and quantum-mechanically. The quantum results go over to the classical ones for large numbers of noise photons in a mode. If the total energy coming through the aperture is fixed and the number of coherent components, that is, the amount of diversity, is changed, the performance has a maximum for a certain value of energy-to-noise ratio on a diversity path. It drops for either too little or too much diversity.

5.1.2 Research on Representations

Sampling seems to be the simplest and most efficient representation of the log-normal field in a variety of cases. The moments of the samples were evaluated in the general case and expressed in terms of log-amplitude and phase-structure functions. The samples are in general dependent. The joint probability density is complicated.

The statistical properties of the plane-wave coefficients were investigated by using analytical, simulation, and experimental methods. For large apertures the coefficients were shown to converge toward a complex Gaussian variable in distribution. This is a result of the Central Limit theorem for fields. This theorem is proved by using moment methods. The field has to satisfy the strong mixing condition in order that the Central Limit theorem be valid. It is shown that the phase structure function has to grow slower than the square of the distance to satisfy the strong mixing condition. The probability density was also found for small apertures.

The speed of convergence toward a Gaussian distribution can be estimated from the results of simulations with the sums of independent log-normal variables. The simulation results agree with the analytical results of B. Levitt[87] on the convergence of the density function of the sums. The experimantal results on the distribution of the intensity samples in the focal plane agree with the theory that is presented.

We hoped that the properties of the plane-wave representation would be simpler than

they turned out to be. Our conclusion is that the plane-wave representation is much less useful for log-normal fields than for Gaussian fields, except for very strong noise or very large apertures. In the latter case the question of the joint distribution is open. It need not be Gaussian, and it cannot be exactly Gaussian because otherwise, by the well-known theorem of Cramér, the field itself would be Gaussian.

5.1.3 Detection of Classical Gaussian Fields

The detection problem was solved first for a classical Gaussian field in Gaussian white background noise. This is a useful approximation for small signal-to-noise ratios and large apertures. The spatial incoherence gives rise to inherent diversity in the channel. The receiver can be realized by using an estimator-correlator, filter-squarer, or diversity structure. It contains spatial and temporal filters, correlators, squarers and integrators in space and time. The performance of the optimum receiver was found to be very close to the upper limit of a fading dispersive channel as expressed in terms of the error exponent.

The analysis was carried through in the general case by using the Karhunen-Loève representation. In the cases of a large aperture and either long or short signals (compared with the field correlation time) the results were expressed asymptotically by using two-dimensional Fourier-transforms, wave-number spectra, and closed-form expressions. The case of short signals is interesting from the point of view of rapid communication, while the "long" signals are interesting for low-rate applications. The numerical results assume Gaussian covariance functions, but do not depend critically on the exact form of the covariance function.

5.1.4 Detection of Classical Log-normal Fields

The detection of log-normal fields in white Gaussian noise can be approached easiest by using the sampling representation and considering the limiting cases of either very strong or very weak noise. Perturbation expansions were found around these results in terms of higher moments of the field. The strong-noise case is equivalent to the Gaussian case, which is very tractable to analysis. The receiver for the weak-noise case can be found easily, but its performance cannot be expressed in any simple form. The optimum receiver does very little spatial filtering in this case. The filtering is highly nonlinear. Most of these results do not depend on log-normality but are more general. The case of independent samples can be analyzed in more detail. These results were compared with the general results for large or weak noise. A new expression for weak-noise performance is given.

5.1.5 Detection of Quantized Fields

The analysis of the optimum detection of the Gaussian field in the quantum case is quite straightforward. For large-noise photon numbers in a mode the expressions approach the corresponding classical results. The optimum receiver has no

estimator-correlator or filter-squarer realization in the quantum case. When there is no background noise the detection problem becomes degenerate because quantum noise is present only with the signal. The optimum receiver structure can be very freely chosen. The performance was evaluated. Interestingly, the channel photon capacity is infinite in this case. This is in no contradiction to the well-known expressions of channel capacity of a noiseless quantum channel because this channel usually assumes only one or limited number of modes, while the number of modes used here is unlimited.

In the log-normal quantum case the analysis is in general extremely difficult because no unitary transformation can make the modes statistically independent. The case of independent samples was analyzed. Expressions for optimum receivers and performance can be found easily in this case. The performance was evaluated explicitly for the case in which there is no background noise.

5.2 DESIGN PHILOSOPHY OF RECEIVERS

The task of the receiver discussed in this report is to detect which one of M signals was sent with the least probability of possible error. Four foes of perfect performance are obvious: fading and incoherence caused by turbulence, background noise, the quantum noise of the signal, and the device noise of the receiver. The last cause was not investigated because we have looked at the more fundamental causes of error that cannot be eliminated by better devices.

To reduce background noise, both spatial and temporal filtering are to be used. The spatial filter restricts the field of view of the receiver in a balanced way to allow most of the signal while keeping out most of the noise. The temporal filter restricts the optical bandwidth of the receiver. The research on optimum receivers shows that turbulence does not reduce the channel capacity if properly designed signals and receivers are used. The incoherence induced by the turbulence creates the possibility of a diversity receiver, for which the field modes would be separated by filtering, then envelope-detected and combined in a nonlinear weighting network. The diversity realization is also suggested by quantum detection theory.

If there is no background noise, any receiver that picks up every photon in every mode is optimal. The direct-detection receiver would be an example of this. In this case device noise should be taken into account. Direct detection certainly limits the choice of modulation methods.

The devices suggested by the optimum detection theory may be difficult to realize. For example, the desired bandwidth for available modulation frequencies is so small that comparable optical filters are very critical to the angle of arrival, that is, the spatial frequency of the field. This feature is certainly undesirable. On the other hand, large-scale integration of detection circuits on silicon chips makes it feasible to build the photodetector-amplifier-filter arrays suggested by the theory and to use heterodyning on these miniature detectors.

The detection of the log-normal field under various conditions seems to be difficult to solve to the extent that the problem of detection of the Gaussian field has been solved. This research has shown some asymptotic results, whose correction terms can be evaluated numerically by a great deal of straightforward effort.

Instead of a maximum-likelihood approach it is probably useful to try to use distribution-free methods of hypothesis testing, such as the Smirnov-Kolmogorov-test (Capon[88]). This test does not necessarily lead to the optimum receiver, but would yield a receiver that would work well for any field. The receiver structure would certainly be different, but the performance should still be acceptable.

Another general approach, which was considered but not used in this work, is to try to use the theory of multiparameter Markov processes as developed by P. Lévy. Markov processes are an extremely powerful model for stochastic processes. Most one-dimensional stochastic processes that are met in practice can at least be approximated by a Markov process. Although some of the one-dimensional results do not carry over to several dimensions, the additional structure introduced by the Markov condition may lead to new results.

As is well known, the detection and estimation problems are closely related, although estimation is in general much harder. It would be desirable to consider the estimation of parameters in a log-normal channel and see what general results could be obtained similar to the ones presented in this work.

The detection-theory formulation leads to integral equations for the optimum linear estimator (in the Gaussian case), which are similar to the ones met in connection with the optimum linear filter for stochastic processes. The solution of these integral equations is very difficult. Similar problems are met in the theory of distributed control systems. The use of grid methods is common in solving these problems, and obviously could be used in connection with the present problem. Because sampling representation seems to be the simplest in dealing with the log-normal field and probably other non-Gaussian channels as well, some research should be done on the properties of the various matrices and determinants involved. Certainly these must have some simple asymptotic forms. The importance of the discretization of the space is also enhanced by the feasibility of spatial array processors.

The approach taken by Helstrom in quantum detection theory works best if the density operators can be conveniently diagonalized in some representation. This means that modes of the field should be selected in such a way that the single-mode states would be statistically independent. Perhaps similar problems have arisen elsewhere in quantum theory. It would be very important to try to see what could be done in this respect.

Very few measurements have been made on the phase coherence relations of the optical field because phase measurements are notoriously difficult. It seems, however,

that by using the scanning techniques developed by Moldon it would be possible to improve our knowledge of phase fluctuation and field covariance functions both in the aperture and the focal plane. This would be particularly important for checking the actual behavior of the phase-structure functions. It would be very useful also to investigate the statistical dependencies of amplitude and phase beyond second-order characteristics.

Finally, work should be started toward implementing optimum receiver principles in hardware. As thesis research has already been started on optical compensation of the incoherence of the wavefront, a suggestion is made that one might try to use array detectors for heterodyning and do possible compensation electronically in baseband frequencies.

APPENDIX A

Evaluation of the Moments in the Focal Plane for a Log-normal Field with a Quadratic Structure Function

The field in the focal plane is obtained through a Fourier transform of the field in the aperture plane. For simplicity, let us look at the center point in the focal plane, for which the wave number $\vec{\kappa} = 0$. At this point call the field ζ:

$$\zeta = \int_{\mathscr{A}_r} \int z(\vec{r}) \, d^2\vec{r}, \tag{A.1}$$

where the integration is carried over the aperture area.

The real (or imaginary) part of the field in the center of the focal plane will be characterized in terms of its moments. The moments of ζ^r and ζ are related to the corresponding moments of z^r and z through linear transformations. The odd-order moments of z (and z^r) vanish, as indicated in the comment after Theorem 5. Using the same comment again, we see that by Eq. 85

$$\overline{(\zeta^r)^{2n}} = \mu_{2n} = \frac{(2n!)}{2^{2n}(n!)^2} \int\int_{\mathscr{A}_r} \overset{(4n)}{\cdots} \int K_{2n}(\vec{r}_1, \vec{r}_2, \ldots \vec{r}_{2n}) \, d^2\vec{r}_1 \ldots d^2\vec{r}_{2n}. \tag{A.2}$$

Equation A.4 is evaluated for a quadratic phase-structure function. The effect of the amplitude structure function is taken into account by using the two bounds in Eq. 87:

$$A_{2n} \int\int_{\mathscr{A}_r} \overset{(4n)}{\cdots} \int\int \exp\left[-\left|\sum_{k=1}^{n} (\vec{r}_k - \vec{r}_{k+n})\right|^2 \Big/ 2r_c^2\right] d^2\vec{r}_1 \ldots d^2\vec{r}_{2n}$$

$$\leq \mu_{2n} \leq B_{2n} \int\int_{\mathscr{A}_r} \cdots \int\int \exp\left[-\left|\sum_{k=1}^{n} (\vec{r}_k - \vec{r}_{k+n})\right|^2 \Big/ 2r_c^2\right] d^2\vec{r}_1 \ldots, \tag{A.3}$$

where

$$A_{2n} = \frac{(2n!)}{2^{2n}(n!)^2} \, e^{-n\sigma^2}, \qquad B_{2n} = \frac{(2n!)}{2^{2n}(n!)^2} \, e^{2n(n-1)\sigma^2}. \tag{A.4}$$

Evaluation of the two bounds for μ_{2n} requires the evaluation of the following integral:

$$I_{2n} = \int\int_{\mathscr{A}_r} \overset{(4n)}{\cdots} \int \exp\left[-\left|\sum_{k=1}^{n} (\vec{r}_k - \vec{r}_{k+n})\right|^2 \Big/ 2r_c^2\right] d^2\vec{r}_1 \ldots d^2\vec{r}_{2n}. \tag{A.5}$$

The aperture area is assumed to be rectangular with size a. Two observations will then be made. First, because of the symmetry of the integration domain, $-\vec{r}_{k+n}$ can be changed to $+\vec{r}_{k+n}$ without altering the value of the integral. Second, the integral factors into a product of two (2n)-dimensional integrals. Set $\vec{r}_k = (x_k, y_k)$, $k = 1, \ldots, 2n$. Then

$$I_{2n} = (I'_{2n})^2, \qquad I'_{2n} = \iint \int_{-a/2}^{+a/2} \cdots \int \exp\left[-\left[\sum_{k=1}^{2n} x_k\right]^2 \Big/ 2r_c^2\right] dx_1 \ldots dx_{2n}. \qquad (A.6)$$

Now two successive changes of variables will be made. First, notice that the integrand is a function of the sum of the x_k only. Moreover, the sign of the sum is irrelevant. By making a change of variables, we have

$$I'_{2n} = 2(na)^{2n} \int_0^1 du_{2n} \exp\left[-(na(1-u_{2n}))^2 / 2r_c^2 2n-1\right] u_{2n} \mathscr{I}_{2n}(nu_{2n}), \qquad (A.7)$$

where

$$\mathscr{I}_{2n}(nu_{2n}) = \int_{\max\left\{\substack{0\\1}\right\}-1/(nu_{2n})}^1 du_{2n-1} \, u_{2n-1} \int \cdots \int_{\max\left\{\substack{0\\1}\right\}-1/(nu_{2n}\cdots u_2)}^1 u_1^0 \, du. \qquad (A.8)$$

It can be seen from (A.5) that the function $\mathscr{I}_m(U)$ has following properties:

$$\mathscr{I}_m(U) = ((m-1)!)^{-1}, \qquad 0 \leqslant U \leqslant 1$$

$$= U^{-m+1}, \qquad m-1 \leqslant U \qquad (A.9)$$

and stays between these values for $1 \leqslant U \leqslant m-1$.

Obviously the main contribution to the integral (A.12) will arise, when u_{2n} is close to unity, or as $nu_{2n} \approx n$, which sets $\mathscr{I}_{2n}(nu_{2n}) \approx \mathscr{I}_{2n}(n)$ to an intermediate value between $((2n-1)!)^{-1}$ and $(2n-1)^{-2n+1}$. There is no simple formula for $\mathscr{I}_{2n}(n)$. It can be shown that $\mathscr{I}_2(1) = 1$, $\mathscr{I}_4(2) = 5/48$. A guess for the value of $\mathscr{I}_{2n}(n)$ could be made by taking the geometric mean of the two bounds above.

After substitution in (A.2), and assuming that u_{2n} is very close to unity on the interval, where the exponential function gives a significant contribution to I'_{2n}, we have

$$I'_{2n} \approx 2(na)^{2n-1} 2\pi r_c \mathscr{I}_{2n}(n). \qquad (A.10)$$

By further use of (A.6) and (A.5), (A.3) will be put into the following form:

$$\frac{8A_{2n}A_r^{2n}n^{4n-2}\mathscr{I}_{2n}^2(n)}{D} \leqslant \mu_{2n} \leqslant \frac{8B_{2n}A_r^{2n}n^{4n-2}\mathscr{I}_{2n}^2(n)}{D}. \qquad (A.11)$$

101

The final step will be to normalize both bounds so that the second moment equals unity. The first moment is automatically normalized to zero by the constant of Theorem 5. In (A.11) A_r = receiver aperture area = a^2, and D = number of coherent areas in the receiver aperture area = $a^2/\left(\pi r_c^2\right)$.

$$A'_{2n} D^{n-1} \leq \mu_{2n} \leq B'_{2n} D^{n-1}, \tag{A.12}$$

where by (A.4)

$$A'_{2n} = 2 \frac{2n!}{(n')^2} \left(\frac{n}{2}\right)^{4n-2} \mathscr{I}^2_{2n}(n),$$

$$B'_{2n} = 2 \frac{2n!}{(n!)^2} \left(\frac{n}{2}\right)^{4n-2} \mathscr{I}^2_{2n}(n) \, e^{2n(n-1)\sigma^2}. \tag{A.13}$$

It would be of interest to get an estimate of the asymptotic behavior of A'_{2n}. Using bounds of $\mathscr{I}_{2n}(n)$ and Stirling's formula, we get asymptotically

$$-4.188n - .5\ln n + 4.742 \leq \ln A'_{2n} \leq -.1586n - 1.5 \ln n - .092. \tag{A.14}$$

Now compare this with the characteristic function of the normalized Gaussian and log-normal variables:

$$M_{Gauss}(iv) = e^{-v^2/2} = \sum_{k=0}^{\infty} \frac{(iv)^{2k}}{k! \, 2^{2k}} \tag{A.15}$$

$$M_{\log_n}(iv) = \sum_{k=0} \frac{e^{2k(k-1)\sigma^2} (iv)^{2k}}{2^{2k}(k!)^2}, \tag{A.16}$$

while in general for a variable with vanishing odd moments

$$M(iv) = \sum_{k=0} \mu_{2k} \frac{(iv)^{2k}}{2k!}. \tag{A.17}$$

By comparing (A.17) while using (A.11)-(A.13), it is clear that as the number of coherent areas in the aperture grows, there can be no convergence in distribution toward either (A.15) or (A.16). Particularly notable is the fact that the Central Limit theorem does not hold here.

APPENDIX B

Statistical Considerations on Simulations of Sums of
Independent Log-normal Variables

We shall first give a brief discussion on generation of random numbers to be used in the simulations. Then we shall discuss the question of an appropriate sample size. The statistical method used here, as in the testing of the distribution of the sum, is the Smirnov-Kolmogorov test. The independence of two distributions is examined by using the χ^2 test. Finally, the method of simulating the field in the focal plane will be presented.

The pseudo-random numbers are most conveniently generated by using the congruence method. The algorithm is

$$z_n = az_{n-1} \ (\text{mod } M), \tag{B. 1}$$

where a is called the "seed." The M.I.T. Computation Center has provided a speeded modification "RANNO" of the I.B.M. Scientific Subroutine Package "RANDU," which is specially tailored for the I.B.M. OS-360/65 machine. The seed of this subroutine is $65539 = 2^{16} + 3$, while $M = 2^{32}$ corresponds to a single precision 4-bit integer. The cycle of repetition with this algorithm is 2^{31}, and its statistical properties are claimed to be good. We are warned that the corresponding floating-point numbers have a high probability of zeros in the trailing low-order bits, but this should not matter in the application in which the numbers will be used.

The pseudo-random numbers generated are used to generate the complex log-normal deviates used in the sums. The next step is to generate normal random deviates with given mean and variance. Here good references are Abramowitz's and Stegun's[77] Handbook or Hammersley and Handscomb.[89] The algorithm that we used was also suggested by the I.B.M. Scientific Subroutine Package for 360. It is based on an application of the Central Limit theorem:

$$w = \sigma \left(\sum_{k=1}^{12} z_k - 6.0 \right) - \sigma^2. \tag{B. 2}$$

This generated an approximately normal $(-\sigma^2, \sigma^2)$ distribution. The maximum errors in the deviates are .009 for distances $< 2\sigma$ from the mean, and .9 for distances between 2σ and 3σ from the mean. This error was considered acceptable, because of the qualitative nature of the investigations in section 3.5. The phase was similarly scaled. The log-normal deviates are then generated by taking the exponential function of the complex normal deviate. As indicated by Table 2 the distribution of the resulting deviates (K=1) is satisfactory. The error in tails that is due to the use of the approximation may accelerate the convergence toward the Central Limit theorem of the sums, but this

effect is believed to be minor.

The objective of the use of random numbers is to create a large sample of random variables, then subject them to statistical analysis. The first question was to find the distributions of the sums. The distribution of a real or imaginary part of a complex log-normal variable cannot be expressed in closed form. In fact, no data are available of these variables except their moments. Hence the distribution of the real or imaginary part of the sum of complex log-normal variables cannot be tested for its log-normality. On the other hand, the distributions of the amplitude and phase of complex log-normal variables are easy to write down. This is why we decided to test the amplitude and phase of the sum, instead of its real and imaginary parts.

What would be an appropriate number of simulations to give a reasonably stable distribution function that would be sufficiently close to the actual distribution function? The easiest test for this purpose turns out to be the Smirnov-Kolmogorov test (Fisz[90]). Assume that $F(x)$ is the distribution of the tested ensemble, $F_n(x)$ is the distribution of the tested ensemble, and $F_n(x)$ is the experimental distribution function of the sample of size n. Then the theorem of Smirnov and Kolmogorov states:

$$\lim_{n \to \infty} \Pr\left(\sqrt{n} \sup_{-\infty < x < \infty} \left| F_n(x) - F(x) \right| < y\right) = K(y), \qquad y > 0, \qquad \text{(B.3)}$$

where

$$K(y) = \sum_{k=-\infty}^{\infty} (-1)^k e^{-2k^2 y^2}. \qquad \text{(B.4)}$$

Tables of this function are available. The values of y corresponding to probabilities 10%, 1%, and .1% are 1.223, 1.628, and 1.950. This theorem does not depend on the initial statistics of the ensemble. The Smirnov-Kolmogorov test is an example of distribution-free tests. The test is uniform over the whole range of $F(x)$. This test is not very good at the tails of the distribution. There is another test that is due to Rényi,[91] which is more appropriate at the tails of the distribution. This test is more complicated than the Smirnov-Kolmogorov test. The Smirnov-Kolmogorov test is sufficient for the purposes of testing the simulations; therefore, it alone will be used.

The sample size to obtain at most 1% deviation of the actual distribution function at the probability level 1% would be 26700. We felt that this was too large in view of the large number of simulations to be performed. If, for example, K = 64, the number of random numbers to be generated would be 3.4×10^7 for a single run of simulations, thereby requiring for this purpose alone approximately 10 min of I.B.M. 360/65 computer time. More time would be needed for the nonlinear transformations, sums, sorts, etc. required by the processing of the random numbers. This was decided to be too much for the qualitative purpose of-the simulations. The sample size chosen, N = 1024, gives the following maximum deviations from the actual probability distribution at

probability levels 10%, 1%, and .1%: .038, .051, and .061. It should be remembered that, although the Smirnov-Kolmogorov theorem helps little, say at $F(x) = .03$, by using the Rényi theorem under the assumption that $F(x)$ is normal $(0, 1)$ and for $x > -1.89$, the maximum deviation at probability levels 10%, 1%, and .1%, is $.35F(x)$, $.5F(x)$, and $.62F(x)$. Hence, there is more stability in the experimental tails than predicted by the Smirnov-Kolmogorov theorem. This fact becomes intuitively clear to anyone performing the simulations.

The Smirnov-Kolmogorov test is very convenient when testing an experimental distribution against a hypothetical distribution. This method was actually used in building Tables 2-4. The parameters of the hypothesis to be tested had also to be estimated from the sample. Strictly speaking, the Smirnov-Kolmogorov theorem is no longer valid. For any sample size the confidence limits of the fitted distribution are also of the order of $n^{-1/2}$. A way out of this dilemma is to decide on the functional form of the hypothesis, test the hypothesis against the experimental distribution, and repeat the procedure for all functions belonging to the class of the hypothesis. If all tests give a probability less than the rejection level, the hypothesis has to be rejected; otherwise, it can be accepted. We found out that estimating the parameters of the hypothetical log-normal, Rayleigh or normal distributions by the maximum-likelihood method gave results that are close to the best fit to the experimental distribution. To enable easy decisions by a glance at the matter of good fit, the experimental distributions were transformed into such coordinates in terms of which the hypothetical distribution would be a straight line. The probability $F(x)$ would be transformed by using either an inverse normal probability integral or inverse Rayleigh distribution, while the variable would only be scaled if testing for Rayleigh or normal distributions, but subjected to logarithmic transformation if testing for the log-normal distribution. The experimental distribution functions were plotted by using a Calcomp graph plotter connected to the I. B. M. 360/65 machine.

Testing the independence of two random variables requires setting up a contingency table, which displays their joint histogram. Suppose the jk^{th} entry in the table happened n_{jk} times. Adding up all contributions along the row j, we obtain a number $n_{j.}$. Adding up all contributions along the column k, we obtain a number $n_{.k}$. If the total size of the sample is n, the row j and column k have experimental probabilities $p_{j.} = n_{j.}/n$ and $p_{.k} = n_{.k}/n$. The experimental probability of the entry jk is $p_{jk} = n_{jk}/n$. For independence, on the average, the requirement would be $p_{jk} \approx p_{j.}p_{.k}$. It can be shown (cf. Fisz[92]) that a good test for deciding whether there is good reason to decide in favor of or against the hypothesis of independence is the following χ^2 test:

$$\chi^2 = \sum_{j=1}^{r} \sum_{k=1}^{s} \frac{(n_{jk} - n_{j.}n_{.k}/n)^2}{(n_{j.}n_{.k}/n)}, \tag{B.5}$$

where r and s are the numbers of rows and columns of the contingency table. The number of degrees of freedom of χ^2 is $(r-1)(s-1)$.

It is clear from the heuristic discussion above that because of the asymptotic nature of the result (B. 5) each of the numbers n_{jk} should be more than 10. This did not occur in the contingency tables set up in this work because the tables were set up by finding the maximum and minimum of each random variable and dividing this range into r and s equal parts. This condition did not impair the results of the test very much, however, because the tails of the distribution do not count very much in (B.5). This kind of fudging saved plenty of time both in programming and computing.

The field in the focal plane in Fraunhofer diffraction is the Fourier transform of the field in the aperture plane. The aperture will be modelled as a set of points $r_1, \ldots, r_K$ in one dimension so that the "field" $z(r_j)$, $j = 1, \ldots, K$ is independent in each of the points. The field in the focal plane at wave number k then becomes

$$\zeta(k) = \sum_{j=1}^{K} z(r_j) \, e^{-ikr_j} \Delta r, \tag{B.6}$$

where $\Delta r = r_j - r_{j-1}$, $j = 2, \ldots, K$. Clearly, the simulations performed above probe the statistical properties of exactly this quantity. Assuming that $\overline{|z|^2} = 1$, we have the following expression for the covariance function:

$$K_2(k_1, k_2) = \overline{\zeta(k_1) \, \zeta^*(k_2)} = \sum_{j=1}^{K} \sum_{l=1}^{K} \overline{z(r_j) \, z^*(r_l)} \exp[-i(k_1 r_j - k_2 r_l)] \, \Delta r^2$$

$$= \sum_{j=1}^{K} \exp[-i(k_1 - k_2)r_j] \, \Delta r \tag{B.7}$$

$$= \frac{\sin\left((k_1 - k_2)K\Delta r/2\right)}{\sin\left((k_1 - k_2)\Delta r/2\right)} \, \Delta r,$$

where the choice $r_1 = (K-1)\Delta r/2$ was made. This is a well-known function from mathematics, physics, and electrical engineering. Its maximum value is K, while its first zero occurs at $(k_1 - k_2) = 2\pi/K\Delta r$. In the simulations the point 1 is taken at $k_1 = 0$, while $k_2 = 2\pi/K$, with $\Delta r = 1$.

Probability Density of the Log-normal Field in the

Focal Plane for Small Apertures

Within a small aperture relative to the coherent area of the field the amplitude can be considered as a randomly varying constant, while the phase front is approximately a plane with randomly varying tilt (cf. Eq. 1 for definitions):

$$z(\vec{r}) = \exp(\chi(\vec{r}_o)+i\theta(\vec{r}_o)) \ \exp(\vec{\nabla}(\chi(\vec{r}_o)+i\theta(\vec{r}_o)) \cdot (\vec{r}-\vec{r}_o))$$

$$\cdot \left(1+O\left(|\vec{r}-\vec{r}_o|^2\right)\right), \qquad \vec{r},\vec{r}_o \in \mathscr{A}_r, \tag{C.1}$$

where $\mathscr{A}_r$ is the receiving aperture, $\vec{r}_o$ is the selected center point of the aperture, and the gradients are assumed to be taken at this very point: $\vec{\nabla}\theta(\vec{r}_o)$ means $\vec{\nabla}\theta(\vec{r})$ for $\vec{r} = \vec{r}_o$. Because the amplitude coherence distance is usually much greater than the phase coherence distance, in this analysis the change of log-amplitude within the aperture is neglected. A more thorough discussion of first- and second-order approximations to the field in a small aperture has been presented by Shapiro.[93]

The field in the focal plane $\zeta(\vec{\kappa})$ is obtained by using the Fraunhofer approximation:

$$\zeta(\vec{\kappa}) = e^{\chi(\vec{r}_o)+i\theta(\vec{r}_o)-i\vec{\kappa}\cdot\vec{r}_o} \iint_{\mathscr{A}_r} \exp[-i(\vec{\kappa}-\vec{\nabla}\theta(\vec{r}_o)) \cdot (\vec{r}-\vec{r}_o)] \ d^2\vec{r}$$

$$= e^{\chi(\vec{r}_o)+i\theta(\vec{r}_o)-i\vec{\kappa}\cdot\vec{r}_o} \ \text{diff}\ (\vec{\kappa}-\vec{\nabla}\theta(\vec{r}_o)), \tag{C.2}$$

where diff $(\cdot)$ refers to the diffraction pattern in the focal plane. Physically, the interpretation of (C.2) is as follows. The field is represented by the diffraction function of the aperture which is shifted randomly around in the focal plane so that it is always centered at $\vec{\kappa} = \vec{\nabla}\theta(\vec{r}_o)$. This shifted function is multiplied by a complex log-normal random variable. Assuming, as in Section II, that the field $\chi(\vec{r}) + i\theta(\vec{r})$ is a complex normal field, the three constants in (C.2) $\chi(\vec{r}_o)$, $\theta(\vec{r}_o)$, and $\vec{\nabla}\theta(\vec{r}_o)$ are normally distributed. The nonlinear transformations of the probability densities of these three normal quantities as indicated in (C.2) need to be carried out to obtain the probability density of $\zeta(\vec{\kappa})$. Because the quantity measured in section 3.6 is intensity instead of the field itself, the transformations will be carried through for the absolute squared value of $\zeta(\vec{\kappa})$ only.

In this analysis we call $\theta(\vec{r}_o) = \vec{a}$. Then assume the following Gaussian density (see Fig. C-1a):

$$p_{\vec{a}}(\vec{a}) = \frac{e^{-|\vec{a}|^2/2b^2}}{2\pi b^2}. \tag{C.3}$$
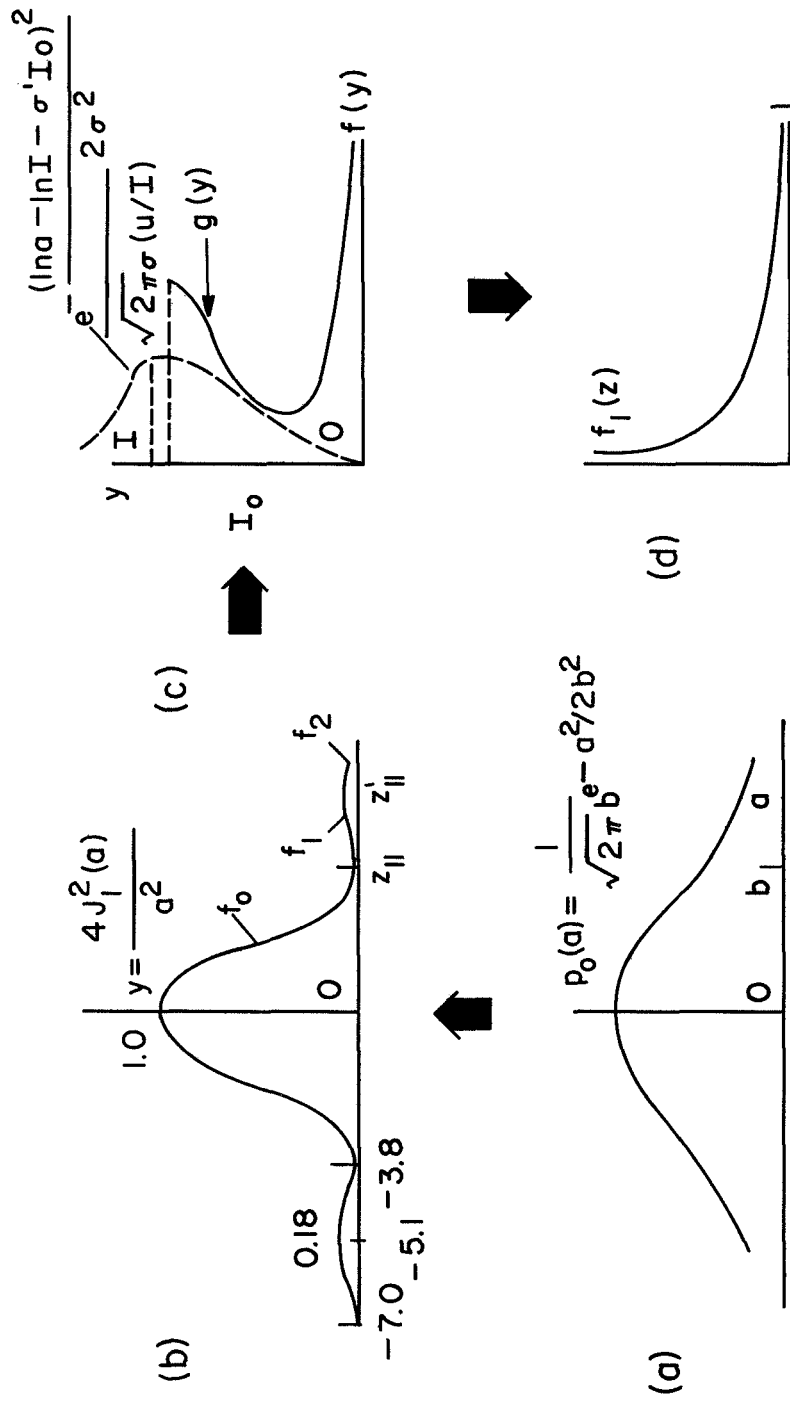
Fig. C-1. Probability density in the focal plane for small apertures is formed as a combination of the fluctuation caused by the random movement described by (a) of the diffraction pattern (b) and the log-normal fading with variance σ^2.

To be able to deal with the moving of the focal spot separately from the effects of log-normal fading we set the unfaded intensity

$$f(\vec{\kappa}-\vec{a}) = I(\vec{\kappa})/I = y. \tag{C.4}$$

In this treatment we tacitly assume independence of the phase gradient and fading. Probably the gradient and log-amplitude fields are correlated just as the phase and log-amplitude fields. Here, $f(\vec{\kappa})$ is the diffraction function, in fact, circular aperture will be assumed:

$$f(\vec{\kappa}) = (\text{diff } \vec{\kappa})^2 = 4J_1^2(|\vec{\kappa}|)/|\vec{\kappa}|^2. \tag{C.5}$$

The probability density of $y = f(\vec{\kappa}-\vec{a})$ will be evaluated in the center spot $\vec{\kappa} = 0$. Because of symmetry, $y = f(\vec{a})$. Then

$$p_y(Y) = \Pr\left\{y \leqslant Y \leqslant y+dy\right\}/dy = \iint\limits_{\substack{y \leqslant Y \leqslant y+dy \\ y=f(\vec{a})}} p_{\vec{a}}(\vec{a})\, d^2\vec{a}/dy. \tag{C.6}$$

Again, because of the symmetry of the diffraction function, polar coordinates are introduced:

$$p_y(Y) = b^{-2} \iint\limits_{\substack{y \leqslant Y \leqslant y+dy \\ y=f(\vec{a})}} a\, e^{-a^2/2b^2}\, da/dy. \tag{C.7}$$

In evaluating this integral it has to be remembered that $f^{-1}(y)$ is a many-valued function. Hence introduce a family of functions $f_k(a)$ as indicated in Fig. C-1b.

$$y = f(\vec{a}) = \sum_{k=0}^{\infty} f_k(a). \tag{C.8}$$

Here, $f(z_{1n}) = J_1(z_{1n}) = 0$, $f'(z'_{1n}) = 0$, $f(z'_{1n})$ are the local maxima or the amplitudes of the sidelobes of the diffraction pattern. Call these maxima $y_k = f(z'_{1k})$. The locations of the first four zeros are $a = 3.83,\ 7.02,\ 10.17,\ 13.32$. The locations of the first five maxima are $a = 0,\ 5.14,\ 8.42,\ 11.62,\ 14.78$. The amplitudes of these maxima are $y = 1.0,\ .018,\ .004,\ .002,\ .0007$ (cf. Fig. C-1b). The numbers come from Abramowitz and Stegun.[94] Then for $y_{k=1} < y \leqslant y_k$, $k = 0, 1, \ldots$ the inverse function of $f(a)$ is the following set:

$$f^{-1}(y) = f_l^{-1}(y), \quad l = 0, \ldots, 2k. \tag{C.9}$$

Then we see from (C.7), since $dy = f'(a)\, da$, that

$$p_y(Y) = b^{-2} \sum_{l=0}^{2k} f_l^{-1}(Y) \frac{\exp\left[-\left(f_l^{-1}(Y)\right)^2/2b^2\right]}{\left|f'\left(f_l^{-1}(Y)\right)\right|}, \qquad k = 0, 1, \ldots . \qquad (C.10)$$

When $p_y(Y)$ is known, the probability density of the intensity follows by setting, as in (C.4), $Y = I/I'$, and averaging over I' with respect to the log-normal density (cf. Eq. 5):

$$p_I(I) = \int_0^\infty p_y(I/I') \frac{e^{-(\ln I' + 2\sigma^2)^2/8\sigma^2}}{\sqrt{2\pi}\, 2\sigma I'}\, dI'. \qquad (C.11)$$

For $Y \cong 1$ and $Y \cong 0$ the expression (C.11) has a simpler asymptotic form. For intermediate values we have to resort to numerical methods to obtain results. Because the asymptotic values alone are of interest in this work, they are evaluated.

1: $Y \approx 1$, $a \approx 0$. By using Taylor-series expansions for $f(a)$ and inverting it, the following sequence of results is obtained.

$$y = f(a) = 1 - a^2/4 + 5a^4/192 - \ldots$$

$$f'(a) = -\frac{a}{2}(1 - 5a^2/24 + \ldots)$$

$$a = f^{-1}(y) = 2\,\sqrt{1 - y(1 + 5(1-y)/24 + \ldots)} \qquad (C.12)$$

$$f'(f^{-1}(y)) = -\sqrt{1 - y(1 - 5(1-y)/8 + \ldots)}$$

$$p_y(Y) = \frac{2}{b^2}\, e^{-(1-y)/b^2}\, (1 + 0(1-y)).$$

Next, $p_y(I/I')$ should be averaged according to (C.11). The most interesting part of this distribution is its tail, when $I \gg 1$. Note that in (C.11) $p_y(I/I') = 0$ for $I' < I$, since $y \leqslant 1$. The largest contribution to the integral comes when $\exp(+I/I'-1) \approx 1$: Hence $p_I(I)$ is bounded above and approximated by the following integral:

$$p_I(I) \lesssim \int_I^\infty 2b^{-2} \frac{\exp[-(\ln I' + 2\sigma^2)^2/8^2]}{\sqrt{2\pi}\, 2\sigma\, I'}\, dI' \qquad (C.13)$$

$$= 2b^{-2}\, Q\left(\frac{\ln I' + 2\sigma^2}{2\sigma}\right),$$

where $Q(\cdot)$ is the complementary normal probability integral. The upper tail of the intensity distribution of the field in the focal plane for small apertures behaves as a log-normal distribution.

2: $Y \approx 0$, $a \approx z_{1i}$, $i = 1, 2, \ldots$, where $J_1(z_{1i}) = 0$. Similarly,

$$p_y(Y) = \frac{1}{2b^2 y^{1/2}} \sum_{i=1}^{\infty} \frac{z_{1i}^2 \exp\left(-z_{1i}^2/2b^2\right)}{J_1'(z_{1i})} = y^{-1/2} C(b),$$ (C. 14)

where

$$C(b) = \sum_{i=1}^{\infty} \frac{z_{1i}^2 \exp\left(-z_{1i}^2/2b^2\right)}{2b^2 J_1'(z_{1i})}.$$ (C. 15)

It is clear that as $b \to 0$, $C(b) \to 0$. Now the time has come to use (C. 11).

$$p_I(I) = \int_0^{\infty} C(b) \left(\frac{I}{I'}\right)^{-1/2} \frac{\exp[-(\ln I' + 2\sigma^2)^2/8\sigma^2]}{\sqrt{2\pi}\, 2\sigma\, I'} dI'$$

$$= C(b)\, I^{-1/2}\, e^{-\sigma^2/2}.$$ (C. 16)

The probability density for $I \approx 0$ is a spike, which goes to infinity as $I \to 0$. If the wave-front tilt fluctuation as characterized by b is small compared with the size of the Airy disc, the radius of which is $3.832 = z_{11}$ in this analysis, $C(b)$ is small, and consequently the spike is less and less pronounced. Graphical interpretation of these analyses is shown in Fig. C-1. It is obvious that the probability distribution of the intensity in the focal plane in this case starts at the origin as a parabola with vertical slope.

The probability density $p_y(Y)$ has, in fact, a spike not only at the origin, but also for every y_k, $k = 1, 2, \ldots$, that are the maxima of the diffraction pattern $f(a)$. These spikes are much less prominent than the spike at the origin. In fact, it is easy to convince oneself that they will be leveled out by the "multiplicative convolution" operation of (C. 3), because of log-normal fading.

Acknowledgment

References

1. R. S. Kennedy, *Fading Dispersive Communication Channels* (John Wiley and Sons, Inc., New York, 1969).

2. V. I. Tatarski, *Wave Propagation in a Turbulent Medium* (McGraw-Hill Book Co., Inc., New York, 1961).

3. V. I. Tatarski, "On Strong Fluctuations of Light Wave Parameters in a Turbulent Medium," Soviet Phys. – JETP $\underline{22}$, 1083-1088 (1966).

4. D. A. de Wolf, "Saturation of Irradiance Fluctuations Due to Turbulent Atmosphere," J. Opt. Soc. Am. $\underline{58}$, 461-466 (1968).

5. E. Gehrels, "Interferometric Phase and Amplitude Fluctuation Measurements over a 7 km Atmospheric Path," Preprint, February 1969, Lincoln Laboratory, M.I.T.

6. A. S. Gurvich, M. A. Kallistratova, and N. S. Time, "Fluktuatsiya parametrov svetovoi volny ot lazera pri rasprostranenii v atmosfere" (Parameter Fluctuations of the Light Waves Coming from a Laser through the Atmosphere), Izv. vuzov ser. Radiofizika $\underline{11}$, 1360-1370 (1968).

7. L. A. Chernov, *Wave Propagation in a Random Medium* (McGraw-Hill Book Co., Inc., New York, 1960).

8. R. N. Hufnagel and N. R. Stanley, "Modulation Transfer Function Associated with Image Transmission through Turbulent Media," J. Opt. Soc. Am. $\underline{54}$, 52-61 (1964).

9. D. L. Fried, "Statistics of Geometric Representation of Wavefront Distortion," J. Opt. Soc. Am. $\underline{55}$, 1427-1435 (1965).

10. P. Beckmann, "Signal Degeneration in Laser Beams Propagated through a Turbulent Atmosphere," Radio Sci. J. Res., NBS/USNC-URSI $\underline{69D}$, 629-640 (1965).

11. E. V. Hoversten, "The Atmosphere as an Optical Communication Channel," IEEE International Convention Record, Vol. 15, Pt. 11, pp. 137-145, 1967.

12. J. W. Strohbehn, "Line-of-Sight Wave Propagation through the Turbulent Atmosphere," Proc. IEEE $\underline{56}$, 1301-1318 (1968).

13. R. J. Glauber, "The Quantum Theory of Optical Coherence," Phys. Rev. $\underline{130}$, 2529-2539 (1963).

14. L. Mandel and E. Wolf, "Coherence Properties of Optical Fields," Rev. Mod. Phys. $\underline{37}$, 231-287 (1965).

15. M. Rosenblatt, "A Central Limit Theorem and a Strong Mixing Condition," Proc. Natl. Acad. Sci. (U.S.) $\underline{42}$, 1 (1956).

16. (a) V. A. Volkonskii and Yu. A. Rozanov, "Some Limit Theorems for Random Functions I.," Theory of Probability and Its Applications $\underline{4}$, 178-197 (1959).
    (b) R. Price, "Optimum Detection of Radar Signals in Noise with Application to Scatter-Multipath Communication," IRE Trans. on Information Theory, Vol. IT-2, pp. 125-135, 1956.

17. N. T. Gaarder, "The Design of Point Detector Arrays," IEEE Trans. on Information Theory, Vol. IT-13, pp. 42-50, 1967.

18. F. Schweppe, "Sensor-Array Data Processing for Multiple-Signal Sources," IEEE Trans. on Information Theory, Vol. IT-14, pp. 294-305, 1968.

19. J. Capon, "High-Resolution Frequency-Wave Number Spectrum Analysis," Proc. IEEE $\underline{57}$, 1408-1418 (1969).

20. R. O. Harger, "Maximum-Likelihood Estimation of Focus of Gaussian Signals," IEEE Trans. on Information Theory, Vol. IT-13, pp. 318-319, 1967.

21. R. S. Kennedy, Class Notes Course 6.575, Massachusetts Institute of Technology, Spring 1968 (unpublished).

22. R. S. Kennedy and E. V. Hoversten, "On the Atmosphere as an Optical Communication Channel," IEEE Trans. on Information Theory, Vol. IT-14, pp. 716-725, 1968.

23. G. R. Heidbreder and R. L. Mitchell, "Detection Probabilities for Log-Normally Distributed Signals," IEEE Trans. on Aerospace and Electronic Systems, Vol. AES-3, pp. 5-13, 1967.

24. D. L. Fried and R. A. Schmeltzer, "The Effect of Atmospheric Scintillations on an Optical Data Channel — Laser Radar and Communications," Appl. Opt. 6, 1729-1737 (1967).

25. C. W. Helstrom, "Detection Theory and Quantum Mechanics," Inform. Contr. 10, 254-291 (1967).

26. Jane W. S. Liu, "Quantum Communication Systems," Technical Report 468, Research Laboratory of Electronics, Massachusetts Institute of Technology, Cambridge, Massachusetts, December 31, 1968.

27. J. Goldstein, P. A. Miles, and A. Chabot, "Heterodyne Measurements of Light Propagation through Atmospheric Turbulence," Proc. IEEE 53, 1172-1180 (1965).

28. S. E. Miller and L. C. Tillotson, "Optical Transmission Research," Proc. IEEE 54, 1300-1311 (1966).

29. M. Ross, Laser Receivers (John Wiley and Sons, Inc., New York, 1966).

30. B. Cooper, "Optical Communication in the Earth's Atmosphere," IEEE Spectrum 3, 83-88 (1966).

31. J. R. Kerr, "Microwave-Bandwidth Optical Receiver Systems," Proc. IEEE 55, 1686-1700 (1967).

32. E. Brookner, M. Kolker, and R. Wilmotte, "Deep-Space Optical Communications," IEEE Spectrum 4, 75-82 (1967).

33. R. T. Denton and T. S. Kinsel, "Terminals for a High-Speed Optical Pulse Code Modulation Communication System," Proc. IEEE 56, 110-154 (1968).

34. H. Cramér, Mathematical Methods of Statistics (Princeton University Press, Princeton, N.J., 1946), pp. 219-220.

35. M. E. Gracheva, "Isledovanie statisticheskikh svoistv sil'nyikh fluktuatsii intensivnosti sveta pri rasprostranenii v prizemnom sloe atmosfery" (Investigation of the Statistical Properties of Strong Intensity Fluctuations of Light Propagating in Atmosphere Close to Ground), Izv. vuzov ser. Radiofizika 10, 775-788 (1967).

36. D. L. Fried, G. E. Mevers, and M. D. Keister, "Measurements of Laser-Beam Scintillation in the Atmosphere," J. Opt. Soc. Am. 57, 787-797 (1967).

37. D. H. Höhn, "Effects of Atmospheric Turbulence on the Transmission of a Laser Beam at 6328 Å," Appl. Opt. 5, 1427-1436 (1966).

38. J. Aitchison and J. Brown, The Log-normal Distribution (Cambridge University Press, London, 1957).

39. V. I. Tatarski, Wave Propagation in a Turbulent Medium, op. cit., see Eq. (7.94).

40. Ibid., see Eq. (7.92).

41. J. W. Strohbehn, op. cit., see Fig. 8.

42. P. H. Deitz, "Optical Method for Analysis of Atmospheric Effects on Laser Beams," Proc. Symposium on Modern Optics, Vol. XVII, pp. 757-774 (Polytechnic Press, New York, 1967).

43. V. I. Tatarski, Wave Propagation in a Turbulent Medium, op. cit., see Eqs. (7.99)-(7.102).

44. J. C. Moldon, "Imaging of Objects Viewed through a Turbulent Atmosphere," Technical Report 469, Research Laboratory of Electronics, Massachusetts Institute of Technology, Cambridge, Massachusetts, March 3, 1969.

45. D. L. Fried and J. D. Cloud, "Propagation of an Infinite Plane Wave in a Randomly Inhomogeneous Medium," J. Opt. Soc. Am. $\underline{56}$, 1667-1676 (1966).

46. J. W. Strohbehn, op. cit., see Eq. (14c).

47. J. Ehrenberg, "A Study of the Effects of Atmospheric Turbulence on Intensity Properties at 6328 Å and 1.15 μ," S. M. Thesis, Department of Electrical Engineering, Massachusetts Institute of Technology, February 1968.

48. A. I. Kon and V. I. Tatarski, "Fluctuation of the Parameters of a Spatially Bounded Light Beam in a Turbulent Atmosphere," Izv. vuzov ser. Radiofizika $\underline{8}$, 870-875 (1965).

49. D. L. Fried and J. B. Seidman, "Laser Beam Scintillation in the Atmosphere," J. Opt. Soc. Am. $\underline{57}$, 181-185 (1967).

50. E. Brookner, "Communication Channel Model of the Atmosphere for Optical Frequencies," Report R68-4156, Raytheon Space and Information Systems Division, Sudbury, Massachusetts, March 12, 1968.

51. W. H. Louisell, Radiation and Noise in Quantum Electronics (McGraw-Hill Book Co., Inc., New York, 1964).

52. Ibid., see Eq. (4.179).

53. R. J. Glauber, "Coherent and Incoherent States of the Radiation Field," Phys. Rev. $\underline{131}$, 2766-2788 (1963).

54. L. D. Landau and E. M. Lifshitz, Quantum Mechanics, Nonrelativistic Theory (Pergamon Press, London, 1959).

55. G. Lachs, "Theoretical Aspects of Mixtures of Thermal and Coherent Radiation," Phys. Rev. $\underline{138}$, B1012-B1016 (1965).

56. F. Möller, "Optics of the Lower Atmosphere," Appl. Opt. $\underline{3}$, 157-166 (1964).

57. A. M. Yaglom, An Introduction to the Theory of Stationary Random Functions (Prentice-Hall, Inc., Englewood Cliffs, N. J., 1962).

58. A. Papoulis, Systems and Transforms with Applications in Optics (McGraw-Hill Book Co., Inc., New York, 1968).

59. Ibid., p. 163.

60. Ibid., pp. 197-199.

61. R. W. Blackman and J. W. Tukey, The Measurement of Power Spectra (Dover Publications, Inc., New York, 1958).

62. D. L. Fried, "Optical Heterodyne Detection of an Atmospherically Distorted Signal Wave Front," Proc. IEEE $\underline{55}$, 57-67 (1967); "Atmospheric Modulation Noise in an Optical Heterodyne Receiver," IEEE J. Quantum Electronics $\underline{QE-3}$, 213-221 (1967).

63. V. I. Tatarski, Wave Propagation in a Turbulent Medium, see Eqs. (7.97) and (7.98).

64. H. Cramér, op. cit., p. 226.

65. I. A. Ibragimov, "Some Limit Theorems for Stationary Processes," Theory of Probability and Its Applications $\underline{7}$, 361-392 (1962).

66. W. Feller, An Introduction to Probability Theory and Its Applications, Vol. II (John Wiley and Sons, Inc., New York, 1966), pp. 244-245.

67. R. L. Mitchell, "Permanence of the Log-Normal Distribution," J. Opt. Soc. Am. $\underline{58}$, 1267-1272 (1968).

68. B. K. Levitt, private communication, Research Laboratory of Electronics, M.I.T., 1969.

69. M. Ohta and T. Koizumi, "Intensity Fluctuations of Stationary Random Noise Containing an Arbitrary Signal Wave," Proc. IEEE 57, 1231-1232 (1969).

70. H. L. Van Trees, Detection, Estimation, and Modulation Theory, Vol. II (John Wiley and Sons, Inc., New York, 1969).

71. R. S. Kennedy, Fading Dispersive Communication Channels, op. cit., see Fig. 5.5.

72. J. N. Pierce, "Theoretical Limitations on Frequency and Time Diversity for Fading Binary Transmissions," IRE Trans. on Communications Systems, Vol. CS-9, pp. 186-189, 1961.

73. R. S. Kennedy, Fading Dispersive Communication Channels, op. cit., see Chap. 6.

74. R. G. Gallager, Information Theory and Reliable Communication (John Wiley and Sons, Inc., New York, 1968).

75. Ibid., see Lemma 8.5.3.

76. L. Lewin, Dilogarithm and Associated Functions (MacDonald and Co., London, 1958).

77. M. Abramowitz and I. Stegun, Handbook of Mathematical Functions (Dover Publications, Inc., New York, 1965).

78. R. S. Kennedy, Fading Dispersive Communication Channels, op. cit., see Fig. 5.8.

79. J. McDougall and E. C. Stoner, "The Computation of the Fermi-Dirac Function," Trans. Roy. Soc. (London) A237, 67-104 (1939).

80. T. Kailath, "A General Likelihood-Ratio Formula for Random Signals in Gaussian Noise," IEEE Trans. on Information Theory, Vol. IT-15, pp. 350-361, 1969.

81. H. L. Van Trees, Detection, Estimation and Modulation Theory, Vol. II, op. cit., Chap. 6, Eq. (152).

82. S. Halme, B. Levitt, and R. Orr, "Bounds and Approximations for Some Integral Expressions Involving Log-normal Statistics," Quarterly Progress Report No. 93, Research Laboratory of Electronics, M.I.T., Cambridge, Massachusetts, April 15, 1969, pp. 163-175.

83. S. L. Halme, "On Optimum Reception through a Turbulent Atmosphere," Quarterly Progress Report No. 88, Research Laboratory of Electronics, M.I.T., Cambridge, Massachusetts, January 15, 1968, pp. 247-254.

84. S. J. Halme, "Efficient Optical Communication through a Turbulent Atmosphere," Quarterly Progress Report No. 91, Research Laboratory of Electronics, M.I.T., Cambridge, Massachusetts, October 15, 1968, pp. 191-201.

85. A. Papoulis, op. cit., pp. 30, 35.

86. H. L. Van Trees, Detection, Estimation, and Modulation Theory, Vol. I (John Wiley and Sons, Inc., New York, 1968), p. 357.

87. B. K. Levitt, "Some Relevant Statistics for Optical Communication through the Turbulent Atmosphere" (unpublished).

88. J. Capon, "A Non-parametric Technique for the Detection of a Constant Signal in Additive White Noise," WESCON Convention Record, Part 4, pp. 92-104, 1959.

89. J. M. Hammersley and D. C. Handscomb, Monte Carlo Methods (Methuen and Co. Ltd., London, 1964).

90. M. Fisz, Probability Theory and Mathematical Statistics (John Wiley and Sons, Inc., New York, 1963), pp. 445-449.

91. A. Rényi, Wahrscheinlichkeitsrechnung (VEB Deutsch. Vlg. Wiss., Berlin, 1962).

92. M. Fisz, op. cit., pp. 456-460.

93. J. H. Shapiro, "A Plane Wave Model for a Turbulence Corrupted Laser Beam," S. M. Thesis, Department of Electrical Engineering, Massachusetts Institute of Technology, September 1968.

94. M. Abramowitz and I. Stegun, op. cit., see Tables 9.5 and 9.7.

Department of Defense

Asst Director/Research (Rm 3C128)
Office of the Secretary of Defense
Pentagon
Washington, D.C. 20301

Technical Library
DDR&E
Room 3C-122, The Pentagon
Washington, D.C. 20301

Director For Materials Sciences
Advanced Research Projects Agency
Room 3D179, Pentagon
Washington, D.C. 20301

Chief, R&D Division (340)
Defense Communications Agency
Washington, D.C. 20305

Defense Documentation Center
Attn: DDC-TCA
Cameron Station
Alexandria, Virginia 22314

Dr Alvin D. Schnitzler
Institute For Defense Analyses
Science and Technology Division
400 Army-Navy Drive
Arlington, Virginia 22202

Central Intelligence Agency
Attn: CRS/ADD/PUBLICATIONS
Washington, D.C. 20505

M. A. Rothenberg (STEPD-SC(S))
Scientific Director
Deseret Test Center
Bldg 100, Soldiers' Circle
Fort Douglas, Utah 84113

Department of the Air Force

Hq USAF (AFRDDD)
The Pentagon
Washington, D.C. 20330

Hq USAF (AFRDDG)
The Pentagon
Washington, D.C. 20330

Hq USAF (AFRDSD)
The Pentagon
Washington, D.C. 20330
Attn: LTC C. M. Waespy

Colonel E. P. Gaines, Jr.
ACDA/FO
1901 Pennsylvania Avenue N. W.
Washington, D.C. 20451

LTC H. W. Jackson (SREE)
Chief, Electronics Division
Directorate of Engineering Sciences
Air Force Office of Scientific Research
Arlington, Virginia 22209

Mr I. R. Mirman
Hq AFSC (SGGP)
Andrews Air Force Base
Washington, D.C. 20331

Rome Air Development Center
Attn: Documents Library (EMTLD)
Griffiss Air Force Base, New York 13440

Mr H. E. Webb, Jr (EMBIS)
Rome Air Development Center
Griffiss Air Force Base, New York 13440

Dr L. M. Hollingsworth
AFCRL (CRN)
L. G. Hanscom Field
Bedford, Massachusetts 01730

Hq ESD (ESTI)
L. G. Hanscom Field
Bedford, Massachusetts 01730

Professor R. E. Fontana, Head
Dept of Electrical Engineering
Air Force Institute of Technology
Wright-Patterson Air Force Base,
Ohio 45433

AFAL (AVT) Dr H. V. Noble, Chief
Electronics Technology Division
Air Force Avionics Laboratory
Wright-Patterson Air Force Base,
Ohio 45433

Director
Air Force Avionics Laboratory
Wright-Patterson Air Force Base,
Ohio 45433

AFAL (AVTA/R. D. Larson)
Wright-Patterson Air Force Base,
Ohio 45433

Director of Faculty Research
Department of the Air Force
U.S. Air Force Academy
Colorado 80840

Academy Library (DFSLB)
USAF Academy, Colorado 80840

Director of Aerospace Mechanics Sciences
Frank J. Seiler Research Laboratory (OAR)
USAF Academy, Colorado 80840

Major Richard J. Gowen
Tenure Associate Professor
Dept of Electrical Engineering
USAF Academy, Colorado 80840

Director, USAF PROJECT RAND
Via: Air Force Liaison Office
The RAND Corporation
Attn: Library D
1700 Main Street
Santa Monica, California 90406

Hq SAMSO (SMTAE/Lt Belate)
Air Force Unit Post Office
Los Angeles, California 90045

AUL3T-9663
Maxwell Air Force Base, Alabama 36112

AFETR Technical Library
(ETV, MU-135)
Patrick Air Force Base, Florida 32925

ADTC (ADBPS-12)
Eglin Air Force Base, Florida 32542

Mr B. R. Locke
Technical Adviser, Requirements
USAF Security Service
Kelly Air Force Base, Texas 78241

Hq AMD (AMR)
Brooks Air Force Base, Texas 78235

USAFSAM (SMKOR)
Brooks Air Force Base, Texas 78235

Commanding General
Attn: STEWS-RE-L, Technical Library
White Sands Missile Range,
New Mexico 88002

Hq AEDC (AETS)
Arnold Air Force Station, Tennessee 37389

USAF European Office of
        Aerospace Research
APO New York 09667

Electromagnetic Compatibility Analysis
        Center (ECAC) Attn: ACOAT
North Severn
Annapolis, Maryland 21402

VELA Seismological Center
300 North Washington Street
Alexandria, Virginia 22314

Capt C. E. Baum
AFWL (WLRE)
Kirtland Air Force Base, New Mexico 87117

Department of the Army

Director
Physical & Engineering Sciences Division
3045 Columbia Pike
Arlington, Virginia 22204

Commanding General
U.S. Army Security Agency
Attn: IARD-T
Arlington Hall Station
Arlington, Virginia 22212

Commanding General
U.S. Army Materiel Command
Attn: AMCRD-TP
Washington, D.C. 20315

Director
Advanced Materiel Concepts Agency
Washington, D.C. 20315

Commanding General
USACDC Institute of Land Combat
Attn: Technical Library, Rm 636
2461 Eisenhower Avenue
Alexandria, Virginia 22314

Commanding Officer
Harry Diamond Laboratories
Attn: Dr Berthold Altman (AMXDO-TI)
Connecticut Avenue and
        Van Ness Street N. W.
Washington, D.C. 20438

Commanding Officer (AMXRO-BAT)
U.S. Army Ballistic Research Laboratory
Aberdeen Proving Ground
Aberdeen, Maryland 21005

Technical Director
U.S. Army Limited War Laboratory
Aberdeen Proving Ground
Aberdeen, Maryland 21005

U.S. Army Munitions Command
Attn: Science & Technology Information
    Branch, Bldg 59
Picatinny Arsenal, SMUPA-RT-S
Dover, New Jersey 07801

U.S. Army Mobility Equipment Research
    and Development Center
Attn: Technical Documents Center, Bldg 315
Fort Belvoir, Virginia 22060

Commanding Officer
U.S. Army Engineer Topographic
    Laboratories
Attn: STINFO Center
Fort Belvoir, Virginia 22060

Dr Herman Robl
Deputy Chief Scientist
U.S. Army Research Office (Durham)
Box CM, Duke Station
Durham, North Carolina 27706

Richard O. Ulsh (CRDARD-IP)
U.S. Army Research Office (Durham)
Box CM, Duke Station
Durham, North Carolina 27706

Technical Director (SMUFA-A2000-107-1)
Frankford Arsenal
Philadelphia, Pennsylvania 19137

Redstone Scientific Information Center
Attn: Chief, Document Section
U.S. Army Missile Command
Redstone Arsenal, Alabama 35809

Commanding General
U.S. Army Missile Command
Attn: AMSMI-RR
Redstone Arsenal, Alabama 35809

Commanding General
U.S. Army Strategic Communications
    Command
Attn: SCC-CG-SAE
Fort Huachuca, Arizona 85613

Commanding Officer
Army Materials and Mechanics
    Research Center
Attn: Dr H. Priest
Watertown Arsenal
Watertown, Massachusetts 02172

Commandant
U.S. Army Air Defense School
Attn: Missile Science Division, C&S Dept
P. O. Box 9390
Fort Bliss, Texas 79916

Commandant
U.S. Army Command and General
    Staff College
Attn: Acquisitions, Lib Div
Fort Leavenworth, Kansas 66027

Mr Norman J. Field, AMSEL-RD-S
Chief, Science and Technology Division
Research and Development Directorate
U.S. Army Electronics Command
Fort Monmouth, New Jersey 07703

Mr Robert O. Parker, AMSEL-RD-S
Executive Secretary, TAC/JSEP
U.S. Army Electronics Command
Fort Monmouth, New Jersey 07703

Commanding General
U.S. Army Electronics Command
Fort Monmouth, New Jersey 07703
Attn: AMSEL-SC
                DL
                GG-DD
                XL-D
                XL-DT
                BL-FM-P
                CT-D
                CT-R
                CT-S
                CT-L (Dr W.S. McAfee)
                CT-O
                CT-I
                CT-A
                NL-D (Dr H. Bennett)
                NL-A
                NL-C
                NL-P
                NL-P-2
                NL-R
                NL-S
                KL-D
                KL-I
                KL-E
                KL-S
                KL-SM
                KL-T
                VL-D
                VL-F
                WL-D

Director (NV-D)
Night Vision Laboratory, USAECOM
Fort Belvoir, Virginia 22060

Commanding Officer
Atmospheric Sciences Laboratory
U.S. Army Electronics Command
White Sands Missile Range,
New Mexico 88002

Commanding Officer (AMSEL-BL-WS-R)
Atmospheric Sciences Laboratory
U.S. Army Electronics Command
White Sands Missile Range,
New Mexico 88002

Chief
Missile Electronic Warfare Tech
    Area (AMSEL-WL-M)
U.S. Army Electronics Command
White Sands Missile Range,
New Mexico 88002

Product Manager NAVCON
Attn: AMCPM-NS-TM, Bldg 439
    (H. H. Bahr)
Fort Monmouth, New Jersey 07703

Department of the Navy

Director, Electronic Programs
Attn: Code 427
Department of the Navy
Washington, D.C. 20360

Commander
Naval Security Group Command
Naval Security Group Headquarters
Attn: Technical Library (G43)
3801 Nebraska Avenue, N. W.
Washington, D.C. 20390

Director
Naval Research Laboratory
Washington, D.C. 20390
Attn: Code 2027
    Dr W. C. Hall, Code 7000
    Mr A. Brodzinsky, Supt,
    Electronics Div

Code 8050
Maury Center Library
Naval Research Laboratory
Washington, D.C. 20390

Dr G. M. R. Winkler
Director, Time Service Division
U.S. Naval Observatory
Washington, D.C. 20390

Naval Air Systems Command
AIR 03
Washington, D.C. 20360

Naval Ship Systems Command
Ship 031
Washington, D.C. 20360

Naval Ship Systems Command
Ship 035
Washington, D.C. 20360

U.S. Naval Weapons Laboratory
Dahlgren, Virginia 22448

Naval Electronic Systems Command
ELEX 03, Rm 2534 Main Navy Bldg
Department of the Navy
Washington, D.C. 20360

Commander
U.S. Naval Ordnance Laboratory
Attn: Librarian
White Oak, Maryland 20910

Director
Office of Naval Research
Boston Branch
495 Summer Street
Boston, Massachusetts 02210

Commander (ADL)
Naval Air Development Center
Attn: NADC Library
Johnsville, Warminster,
Pennsylvania 18974

Commander (Code 753)
Naval Weapons Center
Attn: Technical Library
China Lake, California 93555

Commanding Officer
Naval Weapons Center
Corona Laboratories
Attn: Library
Corona, California 91720

Commanding Officer (56322)
Naval Missile Center
Point Mugu, California 93041

W. A. Eberspacher, Associate Head
Systems Integration Division, Code 5340A
U.S. Naval Missile Center
Point Mugu, California 93041

Commander
Naval Electronics Laboratory Center
Attn: Library
San Diego, California 92152

Deputy Director and Chief Scientist
Office of Naval Research Branch Office
1030 East Green Street
Pasadena, California 91101

Library (Code 2124)
Technical Report Section
Naval Postgraduate School
Monterey, California 93940

Glen A. Myers (Code 52 Mv)
Assoc Professor of Electrical Engineering
Naval Postgraduate School
Monterey, California 93940

Commanding Officer (Code 2064)
Navy Underwater Sound Laboratory
Fort Trumbull
New London, Connecticut 06320

Commanding Officer
Naval Avionics Facility
Indianapolis, Indiana 46241

Director
Naval Research Laboratory
Attn: Library, Code 2039 (ONRL)
Washington, D.C. 20390

Commanding Officer
Naval Training Device Center
Orlando, Florida 32813

Other Government Agencies

Dr H. Harrison, Code RRE
Chief, Electrophysics Branch
National Aeronautics and
        Space Administration
Washington, D.C. 20546

NASA Lewis Research Center
Attn: Library
21000 Brookpark Road
Cleveland, Ohio 44135

Los Alamos Scientific Laboratory
Attn: Reports Library
P. O. Box 1663
Los Alamos, New Mexico 87544

Mr M. Zane Thornton, Chief
Network Engineering, Communications
        and Operations Branch
Lister Hill National Center for
        Biomedical Communications
8600 Rockville Pike
Bethesda, Maryland 20014

U.S. Post Office Department
Library - Room 6012
12th & Pennsylvania Ave. N. W.
Washington, D.C. 20260

Non-Government Agencies

Director
Research Laboratory of Electronics
Massachusetts Institute of Technology
Cambridge, Massachusetts 02139

Mr Jerome Fox, Research Coordinator
Polytechnic Institute of Brooklyn
333 Jay Street
Brooklyn, New York 11201

Director
Columbia Radiation Laboratory
Columbia University
538 West 120th Street
New York, New York 10027

Director
Coordinated Science Laboratory
University of Illinois
Urbana, Illinois 61801

Director
Stanford Electronics Laboratory
Stanford University
Stanford, California 94305

Director
Microwave Laboratory
Stanford University
Stanford, California 94305

Director
Electronics Research Laboratory
University of California
Berkeley, California 94720

Director
Electronics Sciences Laboratory
University of Southern California
Los Angeles, California 90007

Director
Electronics Research Center
The University of Texas at Austin
Engineering-Science Bldg 110
Austin, Texas 78712

Division of Engineering and
      Applied Physics
210 Pierce Hall
Harvard University
Cambridge, Massachusetts 02138

Dr G. J. Murphy
The Technological Institute
Northwestern University
Evanston, Illinois 60201

Dr John C. Hancock, Head
School of Electrical Engineering
Purdue University
Lafayette, Indiana 47907

Dept of Electrical Engineering
Texas Technological University
Lubbock, Texas 79409

Aerospace Corporation
P. O. Box 95085
Attn: Library Acquisitions Group
Los Angeles, California 90045

Airborne Instruments Laboratory
Deerpark, New York 11729

The University of Arizona
Department of Electrical Engineering
Tucson, Arizona 85721

Chairman, Electrical Engineering
Arizona State University
Tempe, Arizona 85281

Engineering and Mathematical
      Sciences Library
University of California at Los Angeles
405 Hilgred Avenue
Los Angeles, California 90024

Sciences-Engineering Library
University of California
Santa Barbara, California 93106

Professor Nicholas George
California Institute of Technology
Pasadena, California 91109

Aeronautics Library
Graduate Aeronautical Laboratories
California Institute of Technology
1201 E. California Boulevard
Pasadena, California 91109

Hunt Library
Carnegie-Mellon University
Schenley Park
Pittsburgh, Pennsylvania 15213

Dr A. G. Jordan
Head of Dept of Electrical Engineering
Carnegie-Mellon University
Pittsburg, Pennsylvania 15213

Case Institute of Technology
Engineering Division
University Circle
Cleveland, Ohio 44106

Hollander Associates
Attn: Librarian
P. O. Box 2276
Fullerton, California 92633

Dr Sheldon J. Welles
Electronic Properties Information Center
Mail Station E-175
Hughes Aircraft Company
Culver City, California 90230

Illinois Institute of Technology
Department of Electrical Engineering
Chicago, Illinois 60616

Government Documents Department
University of Iowa Libraries
Iowa City, Iowa 52240

The Johns Hopkins University
Applied Physics Laboratory
Attn: Document Librarian
8621 Georgia Avenue
Silver Spring, Maryland 20910

Lehigh University
Department of Electrical Engineering
Bethlehem, Pennsylvania 18015

Mr E. K. Peterson
Lenkurt Electric Co. Inc.
1105 County Road
San Carlos, California 94070

MIT Lincoln Laboratory
Attn: Library A-082
P. O. Box 73
Lexington, Massachusetts 02173

Miss R. Joyce Harman
Project MAC, Room 810
545 Main Street
Cambridge, Massachusetts 02139

Professor R. H. Rediker
Electrical Engineering, Professor
Massachusetts Institute of Technology
Building 13-3050
Cambridge, Massachusetts 02139

Professor Joseph E. Rowe
Chairman, Dept of Electrical Engineering
The University of Michigan
Ann Arbor, Michigan 48104

Dr John R. Ragazzini, Dean
School of Engineering and Science
New York University
University Heights
Bronx, New York 10453

Professor James A. Cadzow
Department of Electrical Engineering
State University of New York at Buffalo
Buffalo, New York 14214

Department of Electrical Engineering
Clippinger Laboratory
Ohio University
Athens, Ohio 45701

Raytheon Company
Research Division Library
28 Seyon Street
Waltham, Massachusetts 02154

Rice University
Department of Electrical Engineering
Houston, Texas 77001

Dr Leo Young, Program Manager
Stanford Research Institute
Menlo Park, California 94025

Sylvania Electronic Systems
Applied Research Laboratory
Attn: Documents Librarian
40 Sylvan Road
Waltham, Massachusetts 02154

Dr W. R. LePage, Chairman
Department of Electrical Engineering
Syracuse University
Syracuse, New York 13210

Dr F. R. Charvat
Union Carbide Corporation
Materials Systems Division
Crystal Products Department
8888 Balboa Avenue
P. O. Box 23017
San Diego, California 92123

Utah State University
Department of Electrical Engineering
Logan, Utah 84321

Research Laboratories for the
        Engineering Sciences
School of Engineering and Applied Science
University of Virginia
Charlottesville, Virginia 22903

Department of Engineering and
        Applied Science
Yale University
New Haven, Connecticut 06520

DOCUMENT CONTROL DATA - R & D

(Security classification of title, body of abstract and indexing annotation must be entered when the overall report is classified)

1. ORIGINATING ACTIVITY *(Corporate author)*	2a. REPORT SECURITY CLASSIFICATION
Research Laboratory of Electronics Massachusetts Institute of Technology Cambridge, Massachusetts 02139	Unclassified
	2b. GROUP None

3. REPORT TITLE

Efficient Optical Communication in a Turbulent Atmosphere

4. DESCRIPTIVE NOTES *(Type of report and inclusive dates)*

Technical Report

5. AUTHOR(S) *(First name, middle initial, last name)*

Seppo J. Halme

6. REPORT DATE	7a. TOTAL NO. OF PAGES	7b. NO. OF REFS
April 1, 1970	134	94

8a. CONTRACT OR GRANT NO. DA 28-043-AMC-02536(E) b. PROJECT NO. 20061102B31F c. NASA Grant NGL 22-009-013 d.	9a. ORIGINATOR'S REPORT NUMBER(S) Technical Report 474 9b. OTHER REPORT NO(S) *(Any other numbers that may be assigned this report)* None

10. DISTRIBUTION STATEMENT

This document has been approved for public release and sale; its distribution is unlimited.

11. SUPPLEMENTARY NOTES	12. SPONSORING MILITARY ACTIVITY Joint Services Electronics Program Through U. S. Army Electronics Command

13. ABSTRACT

Given a transmitter that radiates an electromagnetic light field, we assume that the resulting field at the plane of the receiver aperture is log-normal with some coherence properties. Various representations of the field are discussed: aperture sampling, plane-wave decomposition, and Karhunen-Loève expansion. The statistical properties of the coefficients in these representations are investigated by analytical, simulation, and experimental methods. Based on these representations the problem of optimum detection of an orthogonal signal set, subject to distortion and noise in the atmosphere, is investigated. The optimum receiver and its performance are evaluated and discussed in the cases of log-normal and Gaussian statistics, classical and quantum models, large and small apertures, and strong, weak or absent background noise.

14. KEY WORDS	LINK A		LINK B		LINK C	
	ROLE	WT	ROLE	WT	ROLE	WT
Detection of Random Fields						
Information Theory						
Laser Communication						
Optical Communication						
Optimum Receivers						